LASER-PRODUCTION OF ALKALI HYDRIDE PARTICLES

by
Takashi SATO

September 1982

Kyoto University
Kyoto, Japan

LASER–PRODUCTION OF ALKALI HYDRIDE PARTICLES

by
Takashi SATO

September 1982

Kyoto University
Kyoto, Japan

ACKNOWLEDGEMENTS

The author would like to express his sincere appreciation to Professor Toru Ogawa for his continuous guidance, many stimulating suggestions, and valuable discussions throughout the present work. The author is much indebted to Dr. Tsutomu Yabuzaki for many helpful and encouraging discussions, and for his critical reading of the manuscript.

The author also wishes to express his gratitude to Professor Susumu Kato and Professor Iwane Kimura for their valuable comments and suggestions.

The author wishes to acknowledge the encouragements of Professor Ryozo Hihara and Professor Takeo Omori and other staffs of Electrical Engineering of Niigata University.

It is a pleasure to acknowledge the help and the encouragements of Mr. Masao Kitano and other staffs of Radio Atmospheric Science Center and Professor Kimura's group.

The author wishes to acknowledge the assistance of Mr. Daiji Okuda and Mr. Takashi Kurosu during much of this work, and of Mr. Masanobu Watanabe and Mr. Sadao Mori during the early stages. He is also indebted to Dr. Taisuke Endo and Dr. Takeshi Manabe for their valuable advices in the early stages.

Numerical calculations in this work were performed at the Data Processing Center of Kyoto University.

ABSTRACT

This thesis deals with studies on the laser-production of alkali hydride particles, which can be observed when alkali atoms or molecules are excited in hydrogen gas. These particles are called "laser snow", because they are white crystals when the gas temperature is relatively low and fall down from a laser beam through gravity.

The laser-production of such particles was first observed by Tam *et al.* in 1975 when cesium atoms mixed with hydrogen molecules are excited by a laser beam. We have extended the work in this direction, and found firstly that the alkali hydride particles are also produced by exciting alkali molecules. Some possible chemical reactions have been proposed for the production of alkali hydride molecules, from which the larger particles are considered to be produced by condensation in the initial stage. The first measurements of the size distribution of the particles have been made, without perturbing the production, by using light scattering method, and the precise temporal changes of the size distribution during the growth of particles have been obtained. Until the present work, such measurements of the temporal changes had not been reported even for the production of many other particles, although they are known to be very important to reveal the particle-growth.

In general laser radiation can induce selective photochemical reactions which are applicable to the isotope separation, microfabrication of integrated circuits, and so on. This is because lasers have the following advantages compared with conventional light sources: i) high power, ii) high directivity, iii) narrow pulse width, and iv) high monochromaticity.

The first half of this thesis is devoted to the studies of the laser-production of alkali hydride particles, giving a particular attention to the first observation of sodium hydride particles which are produced by exciting sodium atoms and also by exciting sodium molecules. Among the laser-produced alkali hydride molecules and particles, we are particularly interested in sodium hydride, because, in the study of the planetary atmosphere, relatively large amounts of sodium and hydrogen are known to exist in the upper atmosphere of the earth and the atmosphere of Io, the satellite of Jupiter, under the relatively strong solar radiation suitable to excite sodium atoms.

In the case of sodium hydride, particle formation is observed by exciting sodium atoms to the 3P states by a dye laser beam tuned to the one of sodium D lines, and also by exciting sodium dimers (Na_2 molecules) to the $B^1\Pi_u$ state by an Ar^+ laser beam. Since Na atoms in the 3P states have not energies enough to produce directly NaH molecules, two possible processes to produce NaH molecules are proposed in this thesis. One is that the collisions between two 3P state atoms excite one of those atoms to highly excited states, which react with H_2 molecules,

and the other is that the energies of the 3P states are used to excite H_2 molecules to highly vibrational states, which react then with the 3P state Na atoms and produce NaH molecules. Both of these processes can explain the experimental fact that the threshold laser power for producing NaH particles is inversely proportional to the density of Na atoms, in other words, when the density of Na atoms in the 3P states exceeds a critical value for the particle formation, NaH particles begin to be produced. In the case of the excitation of Na_2 molecules, it is shown experimentally that the threshold laser power for production of NaH particles is inversely proportional to the density of Na_2 molecules. This means that the density of Na_2 in the $B\,^1\Pi_u$ state has a critical value for NaH particle formation. From this fact, we find the importance of the reaction of the excited Na_2 molecules in the $B\,^1\Pi_u$ state with H_2 molecules in production of NaH molecules, which is energetically possible. The first experimental evidence of the dissociation of the produced NaH particles by the collisions with Na atoms in the 3P states are also reported here.

In the first half of this thesis, we describe also our experiments on the production of CsH molecules and particles, under various conditions of the exciting laser beam and of gases. We could ascertain that the small particles are initially produced by condensation of CsH molecules, from the experimental fact that a large amount of these molecules are produced by the laser beam.

In the latter part of this thesis, we report on the first measurement of the size distribution of the laser-produced CsH particles, with a particular attention given to its temporal changes. The measurement of the size distribution is made by using the wavelength- and polarization-dependences of the light scattering by the laser-produced particles, and its temporal changes are measured. In the calculation of the size distribution, the Mie theory is used for the light scattering by each particle, by assuming that the laser-produced particles are spherical. To approximate the shape of size distribution, the distribution functions of Gauss, Stevenson, and Junge are used as test functions, each having three parameters. The best-fit test function and its parameters are determined at each moment after the beginning of the laser-irradiation, by comparing theoretical and experimental scattered light intensities. By using obtained size distributions, the changes of number density, mean radius, and mean volume are calculated, and then two growth mechanisms of particles under several experimental conditions are shown. One is the growth by coalescence of particles, which is observed in the relatively high temperature ($T = 330°C$), and the other is the growth by condensation of molecules, which is observed in the relatively low temperature ($T = 300°C$) and in the high laser power density case.

CONTENTS

Fig. 3.18 A photograph of the typical CsH laser snow. The experimental conditions were $T = 261°C$, $\lambda = 584.5$ nm, and laser power was 70 mW. (See page 70.)

Fig. 3.20 A photograph of the white light scattering by CsH laser snow produced by the Ar^+ laser 457.9 nm line. The white light beam diameter was about 10 mm and the Ar^+ laser beam diameter was about 15 mm. The cell temperature was 334°C and the Ar^+ laser power was 210 mW. In this figure, we can see both the stripes of the scattered light intensity and the changes of color or wavelength. This means that there are spatial distributions of both the particle density and the particle size. (See pages 75 and 134.)

CHAPTER I

GENERAL INTRODUCTION

I. 1 Introduction

The laser-production of alkali hydride particles was first reported by Tam *et al.*[1] in 1975 for CsH and RbH. This is an example of laser-photochemistry (or simply laser-chemistry) and is considered to be applicable for an isotope separation and a systematic investigation of photochemistry, photonucleation, and so on. However, the size distribution of laser-produced particles has not been measured yet. The measurements of size distribution, especially its temporal changes, are expected to give important informations about the nucleation and particle growth mechanisms. This thesis is concerned with our studies of the laser-production of alkali hydride particles and of their growth mechanisms which are investigated by observing the temporal changes in their size distribution.

Since the first report on the laser-production of alkali hydride particles by Tam *et al.*,[1] the laser-production of CsH particles have been discussed in several reports.[2-5] However, the laser-production of NaH particles had not been discussed until our study was reported in 1980.[6] On the other hand, there are also several reports on the

laser-production of particles other than alkali hydride,[7-9] on the laser-induced chemical reactions,[10] and on the light-induced particle formation by using conventional light.[11-16] The photochemical reaction and photonucleation processes of the laser-production of alkali hydride particles observed in the present work will be discussed by relating with these studies. Regarding the particle growth mechanisms of the laser-produced alkali hydride particles, few have been understood. We then investigated them by observing the white light scattering from the laser-produced CsH particles, and we could reveal the growth mechanisms of particles under several experimental conditions.

I. 2 Laser and Laser Snow

The invention of a laser in 1960[17] has given us new possibilities for many fields, one of which is the photochemistry. In general lasers have following characteristics: i) high power, ii) high directivity, iii) narrow pulse width, and iv) high monochromaticity. These characteristics are useful in chemistry for controlling chemical reactions and for inducing new photochemical reactions. Especially much progress in spreading the range of laser wavelengths and in developing the tuning and stabilization of laser frequency has made possible the further systematic investigation of selective chemical reactions.

On the other hand, since Tyndall's first report on the light-induced particle formation in "nitrite of butyl" in 1869,[11] numerous light-induced particle formations have been reported. Such particle formations have been observed under the light from a conventional light source and the sun light, but the experiments using a laser light as a light source have been quite few. This phenomenon has been not only investigated from a photochemical point of view[12-14] but also utilized to the fundamental studies of particle growth mechanisms.[15,16]

The alkali hydride particles which will be described in this thesis is an example of laser-produced particles. The laser-production of alkali hydride particles was firstly observed by Tam *et al.* in 1975.[1] They observed that crystalline particles of μm size were produced when a laser beam was applied to Cs vapor mixed with H_2 gas to excite Cs atoms to the 7P states. This was the first report of light-induced particle formation in metal vapors. They considered that production of small crystalline particles are due to the condensation of laser-produced CsH molecules, because the presence of gaseous hydrogen and cesium is necessary for particle formation and, in proper conditions, a progression of doublet fluorescence lines of CsH molecules from the laser-excited CsH $A^1\Sigma^+$ state can be observed. Two possible mechanisms to produce CsH molecules have been proposed. Tam *et al.*[1] considered that CsH molecules are produced by the direct photochemical reactions of the excited Cs atoms with H_2 molecules in the ground electronic state. On the

other hand, Sayer *et al.*[10] proposed recently the other reactions in which the excited Cs atoms react indirectly with H_2 molecules. Namely, energies of excited Cs atoms are transferred to H_2 molecules by collisions, and H_2 molecules are excited to highly vibrational states, which react with ground state Cs atoms to produce CsH molecules.

These photochemically produced particles or laser-produced alkali hydride particles were named "laser snow" because they are white crystals and fall down through gravity. Moreover these particles are expected to be cold like ordinary snow. This is because the heat of decomposition is taken away when they are decomposed into cesium and hydrogen after they fall out of the laser beam.[2,6] Since the first experiment by Tam *et al.*,[1] there have been reports on the experiments of CsH or CsD laser snow[2-4] and on simple explanation about laser snow formation.[5] But laser snow of other alkali hydrides has not been reported except for brief description about observation of RbH laser snow in the first report of Tam *et al.*[1]

In 1978 we observed also the CsH laser snow formation and made some experiments described later. Among the laser-produced alkali hydride molecules and particles, we were particularly interested in sodium hydride since relatively large amount of sodium and hydrogen are known to exist in the upper atmosphere of the earth and in the planetary atmospheres under the existence of strong radiation suitable to excite sodium atoms to highly excited states. For this reason, we tried to produce NaH laser snow using a CW dye laser whose frequency was tuned by means of a Fabry-Pelot etalon, and we could observe it firstly in 1979.

We found that the NaH laser snow is produced not only when Na atoms are excited to their excited states by the dye laser tuned to one of the D lines, but also when Na_2 molecules are excited to the $B^1\Pi_u$ state by an Ar^+ laser. We proposed a new chemical reaction to produce NaH molecules between excited Na_2 molecules and ground state hydrogen molecules. We found also that NaH laser snow is not only produced by exciting Na atoms but also decomposed by the collisions with the 3P state atoms. We reported these effects in 1980[6] and this was the first report on the production of NaH laser snow.

I. 3 Particle Growth and Its Observation

There are many kinds of small particles in the natural world. The size distributions of meteorological particles, such as raindrops, clouds and fogs, are comparatively well investigated. The size distribution of the particles have been measured by using two methods: one is to collect the particles and measure the size through a microscope, and the other is to utilize the light scattering from particles. According to works reported so far, the size distribution of raindrops can be approximated by the Gauss distribution[18] and the size distribution of clouds can be approximated by the modified gamma distribution.[19,20] Aerosols, especially in the stratosphere, can be expressed by the Junge distribution or the exponential distribution function.[21] Since the size distributions of these particles vary temporally and also

spatially, it is difficult to measure their changes continuously. A few measurements of the temporal changes of the size distributions of raindrops and clouds[22-24] have been reported, although they are not continuous.

Some experimental studies on the size distribution of particles and its temporal changes have been made in a cloud chamber or in a diffusion cloud chamber.[25] For example by measuring the falling velocity of water drops, Sinnarwalla *et al.*[26] reported the measurement of the growth rate. Ferrara *et al.*[27] also reported the measurement of size distribution which is based on the observation of the light scattering from particles in a cloud chamber. By using the CCl_4 as the filling gas in a diffusion cloud chamber, Cordier *et al.*[8] reported the laser-production of particles but did not measure the size distribution.

There are several theoretical reports[28-31] on particle growth by condensation and/or coalescence. However, the theories which are based on simplified models have not explained well with the experimental results.

In this thesis we describe our experimental studies on the size distribution and its temporal changes of CsH laser snow in order to reveal the mechanisms of nucleation and particle growth of CsH laser snow. Since the conditions for production of laser snow can easily be controlled, we study on the size distribution and its temporal changes of CsH laser snow under the different experimental conditions, which are found to give us important informations of the growth mechanisms of CsH particles.

I. 4 Outline of the Present Work

Chapter II is devoted to the historical back ground of laser-induced chemical reaction. At first we describe the principal difference of the laser from the conventional light sources, from the point of view of its chemical and spectroscopic uses. Especially monochromaticity and stability of tunable laser wavelength are emphasized because these are important in use of lasers to state-selective chemical reactions. Next, we mention a photochemical reaction and relations between laser and photochemistry, such as laser isotope separation, laser uses in microfabrication of integrated circuits and chemical lasers. Then we review the works on the laser-production of particles other than alkali hydrides.

In chapter III we study the production of alkali hydride laser snow. First of all, we mention the properties of alkali atoms, molecules, and hydrides. Since alkali atoms have only one unpaired electron, they easily react with many elements and make compounds. The spectroscopic properties of alkali atoms are the simplest ones in all elements except for hydrogen. This is also due to their electronic structure. In our experiments, we control the number densities of alkali atoms and molecules by controlling cell temperature. Therfore the relations between the number densities of alkali atoms or molecules and temperature are described. The physical and chemical properties of alkali hydrides are also described. Next, we present the energies of several states of alkali atoms, molecules, and hydrides, which will

be used in the energetical discussions of proposed chemical reactions, are shown here. Next, we describe several fundamental experiments relating with the production of CsH laser snow: for example, the excitation of Cs atoms or molecules by lasers, quenching collisions of excited Cs atoms with H_2 molecules, and spectroscopy of CsH molecules. Here, we describe also our experiments of the production of CsH laser snow, under the various conditions of the exciting laser beam and gases, and then we discuss two chemical reaction mechanisms which have been proposed to produce CsH molecules.

Then we describe the experiments on production of NaH laser snow. At first, we mention about the preliminary experiment with respect to excitation of Na atoms or molecules by lasers. Using results, we discuss about the mechanisms of the excitations and chemical reactions. Through the experiments described in this chapter, we find that the NaH laser snow is produced from the excited Na_2 molecules directly, which is confirmed from the obtained fact that the threshold laser power for production of particles is inversely proportional to the densities of Na_2 molecules. Furthermore, we find that the NaH laser snow is produced also from the excited Na atoms. Especially, in this subsection, the energy relations between NaH molecules, H_2 molecules, and excited Na atoms are discussed. The first excited state 3P, to which we excited Na atoms by laser light, dose not have enough energy required for the reaction with H_2 molecules. We find that the reaction of Na atoms in highly excited states with ground state H_2

molecules and the reaction of Na atoms in the 3P states with vibrationally excited H_2 molecules are important in production of NaH molecules from the measured relation of the threshold laser power vs. the density of Na atoms. The dissociation of NaH laser snow is also discussed. Finally, we summarize the experiments of laser snow and compare alkali hydride laser snow with other laser-production of particles.

In chapter IV, we study the temporal changes in size distribution of CsH laser snow and its growth mechanisms. First of all, we describe the principle of measurements of size distribution. We use the wavelength- and polarization-dependences of light scattering from the laser-produced particles. We review the Mie theory, which is the basic theory of light scattering by a spherical single particle. The Mie theory gives us the scattered light intensity as functions of wavelength, polarization, scattered angle, and particle radius. When a size distribution is assumed, we can calculate the scattered light intensities as functions of wavelength and polarization. To approximate the shape of size distribution, we use distribution functions, Gauss, Stevenson, and Junge, as test functions, each having three parameters. By finding the approximate size distribution function which minimizes the mean-square deviation between the calculated scattered light intensities and the observed ones at five different wavelengths and two orthogonal polarizations, we determine the best-fit distribution function.

Next, we describe about the experiments and analyses. In the

experiment we applied the white light, and measured the wavelength- and polarization-dependences of scattered light intensities from the laser-produced CsH particles. By comparing the experimental results with theory, we obtain the size distribution as a function of time after the beginning of production of CsH molecules. From obtained size distribution, we calculate the temporal changes of number density, total radius, total volume, mean radius, and mean volume of particles, and then we discuss the growth mechanisms of the produced particles. In the last part of this chapter, we summarize the growth mechanisms of CsH laser snow and we also discuss the decomposition of particles. It is known that particles are charged in the early stage of particle growth. We discuss on the neutralization of the charges, in the course of the particle decomposition.

In chapter V, the general conclusions of this thesis are presented.

CHAPTER II

LASER-INDUCED CHEMICAL REACTION

II. 1 Introduction

In the history of chemistry, man has been aiming at controlling chemical reactions and separating the elementary processes from a chemical reaction which is composed of many processes. These have been done so far by changing and controlling temperature, concentrations, catalysts, etc., particularly in organic chemistry. However, the invention of a laser in 1960[17] gave us new possibility for a systematic investigation of the control of selective chemical reactions. This is because lasers have several advantages compared with conventional light sources used in photochemistry: i) high power, ii) high directivity, iii) narrow pulse width, and iv) high monochromaticity.

In recent years much progress has been made in spreading the range of laser wavelength and in developing the tuning and stabilization of laser frequency. This has made possible the further systematic investigation of selective chemical reactions. Especially the tunable laser is the most promising laser from the chemist's point

of view.

In section II.2, we describe the characteristics of lasers as tools for controlling chemical reactions. We describe also on the wavelength-stabilization of tunable lasers. In section II.3, we present some applications of lasers to photochemistry. In section II.4, we describe on the laser-production of particles.

II. 2 Lasers

II. 2. 1 Characteristics of Lasers in Chemical and Spectroscopic Uses

Many photochemical experiments that cannot be achieved with a conventional light source are often possible with a laser because of its high power, high monochromaticity, etc.[32,33] In this section we describe the characteristics of lasers which have been used and will be used in photochemistry.

(1) High power

Generally speaking, laser power is high enough to induce photochemical reactions even if it is about few mW. This is relevant to the directivity and monochromaticity of laser which will be described later. In other words, laser power density with respect to both of volume and frequency is, in many cases, sufficient to induce photochemical reactions. We cannot tell, however, that it is always

true for any photochemical experiments. In fact, when one has to excite atoms or molecules to their highly excited states by two or more photon absorption, much higher laser power is required.

(2) Directivity

Directivity is related with spatial coherence of lasers. Since laser light has usually high directivity, it is possible to focus it in an extremely small area and to get high power density. So, when the laser light focussed in a small area induces a chemical reaction, one can say that the high spatial coherence of a laser is used. However, there are quite few applications of self-interferences (a unique characteristics of coherence) of laser light to chemical reactions.

(3) Narrow pulse widths

Extremely short pulses of laser light can now be obtained by using such techniques as mode-locking. The narrow laser pulses have been used mainly for diagonostics of chemical reactions. In other words, one can spectroscopically detect intermediate products (or reaction intermediates) with a very short lifetime, which plays, in many cases, very important roles in chemical reaction.

(4) High monochromaticity

Monochromaticity is related with temporal coherence of lasers. Generally speaking, laser light has high monochromaticity comparing with conventional light. The light from a gaseous laser has extremely high monochromaticity, but its wavelengths are so

restricted. So, when we use gaseous laser light in atomic or molecular spectroscopy, one has to expect the accidental coincidence of absorption lines and laser lines. This restriction of wavelengths has been disadvantages from the point of view of controlling many chemical reactions. However, the tunable lasers such as dye lasers can remove these disadvantages, so that they will be powerful light sources in photochemistry.

II. 2. 2 Wavelength-Stabilization of Tunable Lasers

In recent years, much progress has been made in tunable lasers. Dye Lasers are well investigated lasers in tunable lasers. Dye lasers [34] have the widest tunable range compared with other types of lasers. This wide tunability, however, results in poor stability of the wavelength, and hence the stabilization of the wavelength is often required for the use of dye lasers in chemical and other applications. The stabilization of the wavelength of the dye lasers can be made by inserting wavelength selective elements into the dye laser cavity. The methods of wavelength-stabilization, which have been developed so far, can broadly be classified into following two types:

(a) A method using prisms, diffraction gratings, Fabry-Pelot etalons, Lyot filters, and combinations of these elements as intracavity

wavelength-selective elements. The tuning of the wavelength is made mechanically by controlling positions, angles, and tilts of these elements.

(b) A method using the spectral lines of atoms or molecules, such as a Doppler-broadened absorption line, a very sharp saturated absorption signal, the Faraday effect, etc. This method has advantages that a high stability can be achieved by only one optical element and that the laser wavelength is always stabilized within a spectral line.

In order to get the state-selective or isotope selective chemical reactions, we need the laser light with a sharp spectrum, whose frequency can be tuned finely to absorption lines of atoms or molecules. Therefore the method (b) is considered to be simpler and more useful for chemical uses compared with the method (a). We investigated also the stabilization of the dye laser wavelength by using the method (b). By using a Faraday filter as a wavelength-selective element, the frequency of a CW dye laser could locked at the center of the sodium D lines [35] and at absorption lines of neon.[36] In our laboratory, this frequency-locked CW dye laser by a Faraday filter has practically been used to study the relaxation and transfer of multipole moments of excited atoms by the anisotropic collisions,[37] but we have not applied it to control chemical reactions. In the experiments to be described in this thesis, we used the more conventional method (a), because we did not need an extremely sharp spectrum and high frequency-stability. As

mentioned later, the absorption lines of alkali vapor were not sharp due to the collisional broadening but they were well separated from the adjoining lines.

In recent years, much progress has also been made in diode lasers. They are very small tunable lasers, whose output amplitude and frequency can be modulated directly at a high frequency (~GHz).[38,39] Although oscillation wavelengths are now restricted to wavelengths longer than about 650 nm,[40] and the output power is less than about 10 mW in CW operation, it is also expected that they will become powerful light sources in chemistry and spectroscopy. The stabilization of the diode laser wavelength at the D_2 line of Cs (852.1 nm) has recently been performed in our laboratory,[41] by using a Doppler-free saturated absorption signal. We consider that the wavelength-stabilized diode laser can be used in photochemical production of CsH and RbH particles, which are studied in this thesis by using other lasers (Ar^+ laser and dye laser).

II. 3 Laser and Photochemical Reaction

In this section we review some important works made so far on the laser-induced chemical reactions occuring in gas phase.

II. 3. 1 Photchemical Reaction

We consider a reaction between hydrogen and chlorine as an example of photochemical reactions. The reaction is usually represented as

$$H_2 + Cl_2 + h\nu \rightarrow 2HCl, \tag{2.1}$$

but when we consider it in detail, we know that this is a series of reactions as follows:[42)]

$$Cl_2 + h\nu \rightarrow 2Cl, \tag{2.2}$$

$$Cl + H_2 \rightarrow HCl + H, \tag{2.3}$$

$$H + Cl_2 \rightarrow HCl + Cl, \tag{2.4}$$

where only the process (2.2) is directly related to light. This kind of process is called photolysis or photodissociation. To control chemical reactions by using light (including lasers), we must consider not only whether the process (2.2) is possible or not but also how the other processes occur, because they will determine the rate of whole reaction.

We have briefly shown an example of the photochemical reaction resulted from photlysis, but, of course, there are other types of photochemical reactions due to photoexcitation and photoionization. We describe some examples of these types in the next subsection.

II. 3. 2 Laser and Chemical Reaction

There are many reports of photochemical reactions induced by photoexcitation and photoionization by laser light [see review papers [32,33]]. An example of the chemical reactions induced by photoexcitation is shown in (2.5), whose reaction rate was measured by Odiorne *et al.*[43]

$$HCl(\nu = 0,1) + K \rightarrow KCl + H. \qquad (2.5)$$

A pulse HCl chemical laser was used to excite HCl molecules to $\nu = 1$, which has energy 8.3 kcal/mol higher than that of the ground vibrational states $\nu = 0$. They found that HCl(ν=1) reacts approximately 100 times faster than HCl(ν=0).

Photoionization by laser has been applied to isotope separation:[44]

$$A + h\nu \rightarrow A^* \rightarrow A^+ + e^-, \qquad (2.6)$$

where A represents an isotope. Ionized isotopes are collected by applying electric field. Up to date, the isotope separation using this scheme has been reported for ^{40}Ca,[45] ^{85}Rb,[46] ^{235}U,[47] and ^{6}Li.[48]

The conditions to induce a selective chemical reaction are as follows.

1) High monochromaticity of the exciting radiation with a necessary power level at a given frequency. This makes possible the sufficient

excitation of particular atoms or molecules to the desired excited state.

2) Existence of a narrow absorption line without overlapping with adjoining lines.

3) Conservation of the selectivity even in subsequent physical and chemical processes.

The first condition is the condition of light source, which has been described already. The second condition can be fulfilled with a dilute substance in the gas phase which has discrete energy levels, and hence the selective excitation to an electronic or vibrational state is possible. It is much more complicated problem to satisfy the third conditions, since the selectivity obtained as a result of the primary photochemical process can easily be lost after many subsequent processes, such as thermal relaxation and resonant transfer of excitation. Therefore two principal ways can be considered to induce a selective chemical reaction. One is, of course, to make the primary chemical reaction fast and the other is to use the ionization or dissociation of excited atoms or molecules. These two ways have possibilities to induce a selective chemical reaction faster than the other subsequent processes which lose the selectivity.

The laser isotope separation[49-51] is an application of such selective photochemical reactions. The best result was obtained by Mayer *et al*,[51] with a mixture of methanol and completely deuterated methanol (CD_3OD). By irradiating a 2.7 μm hydrogen fluoride laser,

CH_3OH molecules are excited to vibrationally excited states and react selectively with Br_2. The laser isotope separations by using photoionization, photodissociation, and photoexcitation have also been studied extensively.

Recently, laser-induced chemical reactions have been applied to the microfabrication of integrated-circuits etc. by Ehrlich *et al.*[52-58] This technique makes use of gas-phase reactions initiated by a visible or UV laser. An important attribute of this technique is that high-spatial-resolution deposition,[52] etching,[53,54] or doping[55-58] can be accomplished by "direct writing", that is, without use of photolithography. Deutsch *et al.*[52] demonstrated laser photodeposition by using a UV laser and the metal alkyl compounds, such as trimethylaluminum, $Al(CH_3)_3$. In their experiments molecular bonds were broken directly by UV laser photons, and free metal atoms were produced and then condensed on a substrate. UV laser photoetching was demonstrated by Ehrlich *et al.*[53] UV laser photolysis of methyl-halides was used to produce halogen atoms, Cl, Br, or I. These halogen atoms are chemisorbed onto the surface and erode the surface. Ehrlich *et al.*[55] demonstrated also the process of direct or one-step doping of semeiconductors by using photodeposition of metals and laser-induced surface heating. The deposited metals incorporate well with semiconductors when their surface are heated by a laser.

Finally, it must be noted that chemical reactions have been applied to get new kinds of lasers or chemical lasers. The hydrogen fluoride laser is an typical example.[59] The population inversion in hydrogen fluoride molecules is attained through the chemical reaction as

$$F + H_2 \rightarrow H + HF^{\dagger}. \qquad (2.7)$$

The induced fluorescence is due to

$$HF^{\dagger} \rightarrow HF + h\nu, \qquad (2.8)$$

where $HF^{\dagger}$ represents a vibrationally excited HF molecule. The oscillation wavelength of the chemical laser is directly related to chemical reactions involved.

II . 4 Laser-Production of Particles

Numerous light-induced particle formations have been reported since the first report of Tyndall in 1869.[11] However, mechanisms of these phenomena have not been well understood yet, although some of these phenomena have been well investigated.[12-16]

On the other hand, in recent years, lasers have been used in the work on the photochemical productions of particles of μm size. The alkali hydrides, which are described in detail in this thesis, have been observed in a mixture of alkali vapor and hydrogen gas.[1-4,6] The production of particles in gaseous NO_2 - SO_2 mixtures[7] and in super-saturatated CCl_4 and impurity Cl_2 mixtures[8] has also been observed. Furthermore, it has also been reported that the UF_5 particles can be produced in UF_6 and H_2 mixtures,[9] which is expected to be applicable to isotope separation of ^{235}U. Such particle production is clearly due to the laser-induced chemical reaction of producing nonvolatile matter and from the subsequent nucleation. The particle formation described above have not been observed when one uses light from a conventional light source. As mentioned already, the advantages of the use of laser light are i) high efficiency and selectivity for chemical reactions because of its monochromaticity, ii) the ability of producing particles in a small space because of its directivity, and iii) the ability to cause strongly endothermic reactions, which result in nucleation of their products at even low temperature without any catalyst, because of its high intensity.

Let us mention some of above works in more detail, since the particle formation observed in these works are analogous to that of alkali hydrides studied in this thesis. In 1978 Iwamoto *et al.*[7] reported the particle formation in gaseous NO_2 - SO_2 mixtures irradiated by a laser beam from an Ar^+ laser at 488.0 nm and with intensities between 0.02 - 0.1 W. The particles were produced in a few tens of seconds after the beginning of laser-irradiation. They found that the produced particles are aggregates of composition $(SO_3)_2N_2O_3$, which is produced by reaction of photoexcited NO_2 with SO_2. The constitution is however uncertain [$SO_3SO_2(NO)_2$, $(SO_3)_2NO_2NO$, etc.]. In 1981 Cordier *et al.*[8] reported the photonucleation in supersaturated CCl_4 and impurity Cl_2 mixtures, which are irradiated by an Ar^+ laser light. They observed the first falling of the produced droplet typically at 25 - 150 sec after the beginning of laser-irradiation. Since the nucleation was dependent largely on the presence of Cl_2, they concluded that the phenomenon of photonucleation was initiated by the photodecomposition of Cl_2 into two atoms. In 1977 Ronn *et al.*[9] reported the production of UF_5 particles in the cell containing UF_6 and H_2, under the irradiation of infrared laser beam ($\lambda = 10.6$ μm). The dielectric breakdown induced by nonresonant laser beam was found to induce the reaction

$$2UF_6 + H_2 \rightarrow 2UF_5 + 2HF. \qquad (2.9)$$

Since produced UF_5 particles can easily be collected, one can apply this

process for laser isotope separation of ^{235}U.

II. 5 Summary and Conclusions

The invention of lasers, especially the progress in tunable lasers, has brought new possibilities for controlling chemical reactions and for obtaining much knowledge about chemical reactions. The laser isotope separation is a typical application of controlling chemical reactions. The laser-induced chemical reactions have recently been applied to the microfabrication of integrated-circuits etc. Although photochemical production of particles has a long history, studies using a laser have been quite few yet. This must be mainly because the lasers suitable for the particle formations have not been so many and the chemical reactions associated with the particle formation have not been well known.

CHAPTER III

ALKALI HYDRIDE LASER SNOW

III. 1 Introduction

In 1975 Tam *et al.*[1] discovered the laser-production of CsH crystalline particles of μm size when a laser beam was applied to Cs vapor mixed with H_2 gas to excite Cs atoms to the 7P states. This is the first report of light-induced particle formation in metal vapors. The particles were named "laser snow" and were considered to be formed through condensation of CsH molecules produced by laser-induced chemical reactions. The CsH molecules are considered to be produced by the reactions as

$$Cs(7P) + H_2 \rightarrow CsH + H, \qquad (3.1)$$

$$Cs(6S) + H + X \rightarrow CsH + X, \qquad (3.2)$$

where X represents any atom or molecule in the ground electronic state. In stead of (3.1), Sayer *et al.*[10] proposed recently the other reactions to produce CsH molecules as

$$Cs(7P) + H_2 \rightarrow Cs(6S) + H_2(\nu), \qquad (3.3)$$

$$Cs(6S) + H_2(\nu) \rightarrow CsH + H, \qquad (3.4)$$

where ν represents some vibronic excited state in the ground electronic state of H_2 molecules.

Since the first experiment by Tam *et al.*,[1] there have been some reports on CsH or CsD laser snow,[2-5] but there have been no reports on NaH laser snow. In 1978 we also observed the CsH laser snow formation and made some experiments described later. Next, we tried to produce NaH laser snow, which is more interesting from the points of geophysics and planetary science, and succeeded in the first observation of NaH particle formation in 1979. We found that the NaH laser snow is not only produced when Na atoms are excited to their excited states but also when Na_2 molecules are excited to the $B^1\Pi_u$ state. The possible reaction to produce NaH molecules from excited Na_2 molecules is

$$Na_2(B^1\Pi_u) + H_2 \rightarrow 2NaH. \qquad (3.5)$$

We found also that NaH laser snow is not only produced by exciting Na atoms but also decomposed by the collision with Na atoms in the 3P states. In 1980[6] we reported on the first observation of NaH laser snow, its dissociation, and laser snow production from the excitation of alkali diatomic molecules.

In this chapter we describe the production of CsH and NaH laser snow. First of all, since the produced particles are made of alkali hydrides, we have to describe properties of alkali atoms, alkali dimers (alkali molecules), and alkali hydrides. Secondly, we describe the spectroscopic studies of Cs and CsH and the experiment of CsH laser snow formation. Thirdly, we describe the spectroscopic studies of Na and Na_2 and the experiment of NaH laser snow formation. Next, we summarize the alkali hydride laser snow.

III. 2 Properties of Alkali Atoms, Molecules, and Hydrides

Because alkali metals have highly reactive nature, none of elements in the group is found in nature around us as the free metal. But, in the planetary atmosphere (including the atmosphere of some satellites), alkali atoms can be found as a single atom. For example, sodium can be observed in the sodium layer in the upper atmosphere of the earth and in the atmosphere of Io,[60-63] the innermost of the four Galilean satellites of Jupiter. In the planetary atmosphere, there exist also hydrogen and intense light so that the photochemical reactions to be described in this thesis are expected to occur more or less.

In this section, we describe physical and chemical properties of alkali atoms, molecules, and hydrides and their spectroscopic properties.

Table 3.1 Physical properties of Na, K, Rb, and Cs. (See Ref. 64)

	Na	K	Rb	Cs
Atomic number	11	19	37	55
Atomic weight	22.9898	39.102	85.47	132.905
Melting point (°C)	97.82	63.2	39.0	28.5
Boiling point (°C)	881.4	756.5	688	705
Atomic radius (Å)	1.896	2.349	2.48	2.67
Ionic radius (Å)	0.95	1.33	1.48	1.69
Atomic volume (c.c./g·atom)	23.7	45.3	55.9	70.0
Ionization potential (eV)	5.12	4.32	4.16	3.87
Electron work function (eV)	2.28	2.24	2.09	1.81
Electron emission wavelength (μm)	0.60	0.65	0.73	0.80
Electron resistivity (micro-ohm-cm)(0°C)	4.48	6.1	11.6	18
Density, solid, 20°C	0.968	0.856	1.532	1.90
Heat of fusion (cal/g)	27.05	14.17	6.1	3.766
Heat of vaporization (cal/g), b.p.	925.6	496	212	146
Important spectral lines (nm)	588.995	404.414	420.185	455.536
	589.592	766.491	421.556	459.318
	819.481	769.898	780.023	852.110
			794.760	894.350

III. 2. 1 Physical and Chemical Properties

Physical properties of sodium, potassium, rubidium, and cesium metals or ions are shown in Table 3.1.[64] Most of the alkali metals are low-melting and soft materials except for cesium, which is liquid at ordinary temperatures. Their thermal and electrical conductivities are among the highest of all known materials. Ionization potentials are the lowest of all groups in the periodic chart. All of the alkali metals are paramagnetic, due to a single unpaired s electron.

The chemistry and chemical properties of the alkali atoms are also explained from the electronic structure of the atoms.[64] The metals of this group have the low ionization potentials, the low electron work functions, and the high position in the electromotive series. Rubidium and cesium metals are both photosensitive, which indicates that ordinary light is sufficiently energetic to liberate the valence electrons. The strongly electro-positive nature of these elements dictates their chemical reactivities in both metallic and combined states. In the metallic state, the elements are among the strongest reducing agents known and react to form compounds with a very high degree of ionic bonding: in the combined state, the metal ions are the most stable of all cations.

In our experiments, we control the number densities of alkali atoms and molecules in vapor by controlling the cell temperature and so it is necessary to know the relations between temperature and

pressures or number densities of alkali atoms and molecules. Pressures and number densities of these alkali atoms and molecules at several temperatures are listed in Table 3.2.[65,66]

All the alkali hydrides[67] have face-centered cubic colorless crystal structures analogous to the structure of sodium chloride. Alkali hydrides have therefore similar properties to alkali halides, for example, high melting points, a high degree of thermal stability, and they are able to conduct electricity if they are melted. The alkali hydrides are prepared by the direct reaction of metallic alkali with elemental hydrogen at elevated temperatures. The ambient pressure of hydrogen must be higher than the dissociation pressure of alkali hydride since reaction is reversible.

Most of alkali hydrides[67] are used as the photosensitive elements in photocells. Sodium hydride is also used for descaling metals and for reduction agent in organic reactions. Alkali hydrides, especially sodium hydrides, may be of importance in the planetary atmosphere where relatively large amount of alkali, especially sodium, and hydrogen are known to exist under the existence of intense radiation. Because, under such conditions, large amount of alkali hydrides are expected to be produced through the photochemical reactions which will be described in this thesis.

Since the dissociation of alkali hydrides will be important in our experiments, it is worthwhile to show the dissociation pressures of

Table 3.2 Pressures and densities of alkali atoms and molecules.[65,66]

(a) Sodium

	Na atom[a]			Na_2 molecule	
T(K)	P(Torr)	$n(cm^{-3})$	T(K)	P(Torr)	$n(cm^{-3})$
325	1.16E-09	3.45E+07	325	5.75E-14	1.71E+03
350	1.79E-08	4.93E+08	350	2.62E-12	7.22E+04
375	1.92E-07	4.95E+09	375	5.37E-11	1.38E+06
400	1.54E-06	3.72E+10	400	8.14E-10	1.97E+07
425	9.72E-06	2.21E+11	425	8.85E-09	2.01E+08
450	5.01E-05	1.07E+12	450	7.25E-08	1.56E+09
475	2.18E-04	4.43E+12	475	4.70E-07	9.55E+09
500	8.20E-04	1.58E+13	500	2.50E-06	4.83E+10
550	8.15E-03	1.43E+14	550	4.41E-05	7.74E+11
600	5.56E-02	8.96E+14	600	4.75E-04	7.65E+12
650	2.85E-01	4.23E+15	650	3.51E-03	5.22E+13
700	1.16E+00	1.60E+16	700	1.93E-02	2.67E+14

(b) Cesium

	Cs atom			Cs_2 molecule	
T(K)	P(Torr)	$n(cm^{-3})$	T(K)	P(Torr)	$n(cm^{-3})$
300	1.67E-06	5.38E+10	300	3.12E-11	1.01E+06
325	1.60E-05	4.75E+11	325	8.10E-10	2.41E+07
350	1.17E-04	3.23E+12	350	1.37E-09	3.78E+07
375	6.55E-04	1.69E+13	375	1.56E-07	4.02E+09
400	2.92E-03	7.05E+13	400	1.29E-06	3.11E+10
425	1.08E-02	2.45E+14	425	8.23E-06	1.87E+11
475	1.07E-01	2.18E+15	475	1.79E-04	3.64E+12
500	2.40E-01	4.64E+15	500	6.50E-04	1.26E+13
550	1.29E+00	2.27E+16	550	5.94E-03	1.04E+14
600	4.32E+00	6.95E+16	600	3.69E-02	5.94E+14
650	1.30E+01	1.93E+17	650	1.71E-01	2.54E+15
700	3.31E+01	4.57E+17	700	6.25E-01	8.62E+15

a) Ref. 66.

Table 3.2 (Continued)

(c) Pottasium

	K atom		K_2 molecule	
T(K)	P(Torr)	n(cm^{-3})	P(Torr)	n(cm^{-3})
325	1.90E-07	5.63E+09	4.15E-12	1.23E+05
350	2.74E-06	7.57E+10	1.08E-10	2.98E+06
375	1.89E-05	4.87E+11	1.78E-09	4.58E+07
400	1.17E-04	2.82E+12	2.00E-08	4.83E+08
425	5.49E-04	1.25E+13	1.71E-07	3.89E+09
450	2.09E-03	4.49E+13	1.13E-06	2.43E+10
475	6.84E-03	1.39E+14	6.03E-06	1.23E+11
500	2.06E-02	3.97E+14	2.71E-05	5.23E+11
550	1.32E-01	2.32E+15	3.58E-04	6.29E+12
600	6.19E-01	9.96E+15	3.01E-03	4.85E+13
650	2.27E+00	3.37E+16	1.79E-02	2.66E+14
700	8.88E+00	1.22E+17	8.10E-02	1.12E+15
750	1.79E+01	2.30E+17	2.97E-01	3.82E+15

(d) Rubidium

	Rb atom		Rb_2 molecule	
T(K)	P(Torr)	n(cm^{-3})	P(Torr)	n(cm^{-3})
325	4.16E-06	1.24E+11	2.23E-10	6.63E+06
350	3.42E-05	9.43E+11	4.22E-09	1.16E+08
375	2.12E-04	5.46E+12	5.29E-08	1.36E+09
400	1.03E-03	2.49E+13	4.77E-07	1.15E+10
425	4.10E-03	9.31E+13	3.37E-06	7.66E+10
450	1.39E-02	2.98E+14	1.83E-05	3.93E+11
475	3.91E-02	7.94E+14	8.11E-05	1.65E+12
500	1.10E-01	2.12E+15	3.06E-04	5.91E+12
550	5.88E-01	1.03E+16	3.04E-03	5.34E+13
600	2.37E+00	3.81E+16	2.09E-02	3.37E+14
650	7.62E+00	1.13E+17	1.06E-01	1.57E+15
700	2.06E+01	2.85E+17	3.96E-01	5.47E+15
750	5.01E+01	6.45E+17	1.13E+00	1.46E+16

Table 3.3 Dissociation pressures of alkali hydrides and deutrides (see Ref. 64).

P: Pressure (Torr) T: Temperature (K)

NaD:	$\log P = 13.1994 - 6915.00(1/T)$
NaH:	$\log P = 11.9250 - 6318.41(1/T)$
KD:	$\log P = 12.1977 - 6318.68(1/T)$
KH:	$\log P = 11.6535 - 6185.57(1/T)$
RbD:	$\log P = 6.07 - 2664.0\ (1/T)$
RbH:	$\log P = 9.20 - 4533.5\ (1/T)$
CsD:	$\log P = 8.68 - 2695.5\ (1/T)$
CsH:	$\log P = 7.50 - 3475.5\ (1/T)$

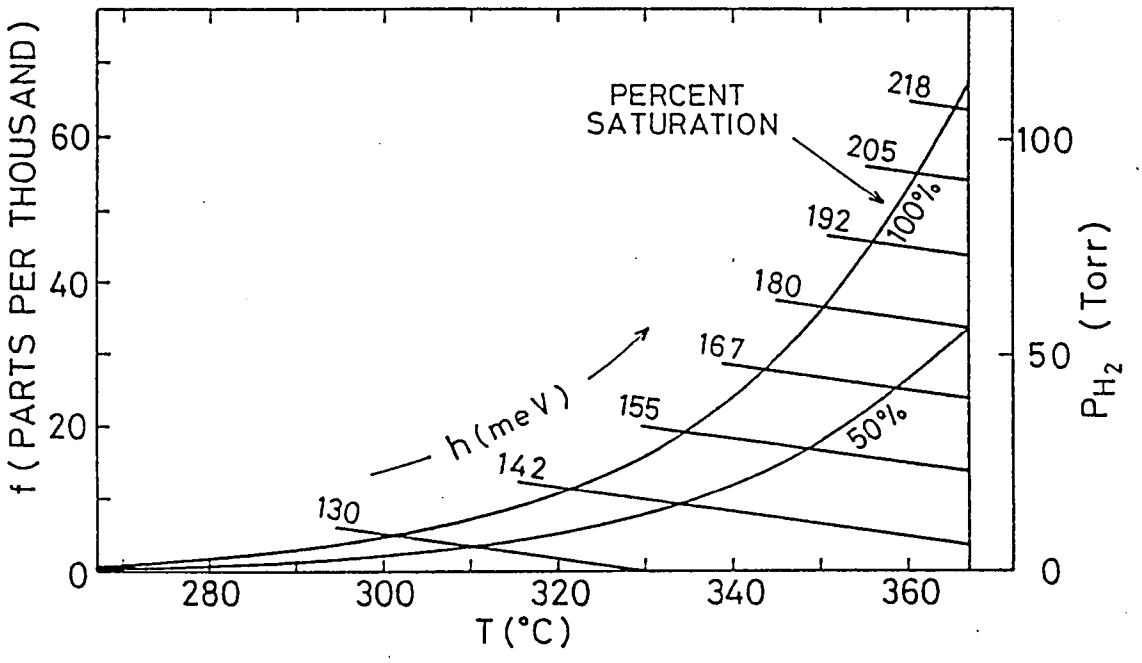

Fig. 3.1 Psychrometric chart of NaH.[2] Two curves show the hydrogen pressure vs. temperature at two relative humidities of hydrogen, where relative humidities of hydrogen are computed from the dissociation pressure of NaH, which is 100 % humidity of hydrogen. Approximately linear lines show the fraction, f, defined by $f = n_{H_2} / n_{He}$ at several gas-phase enthalpy, h, where $n_{He} = 2.69 \times 10^{19}$ cm^{-3} (the density of gas at 0°C at 1 atm) in this figure.

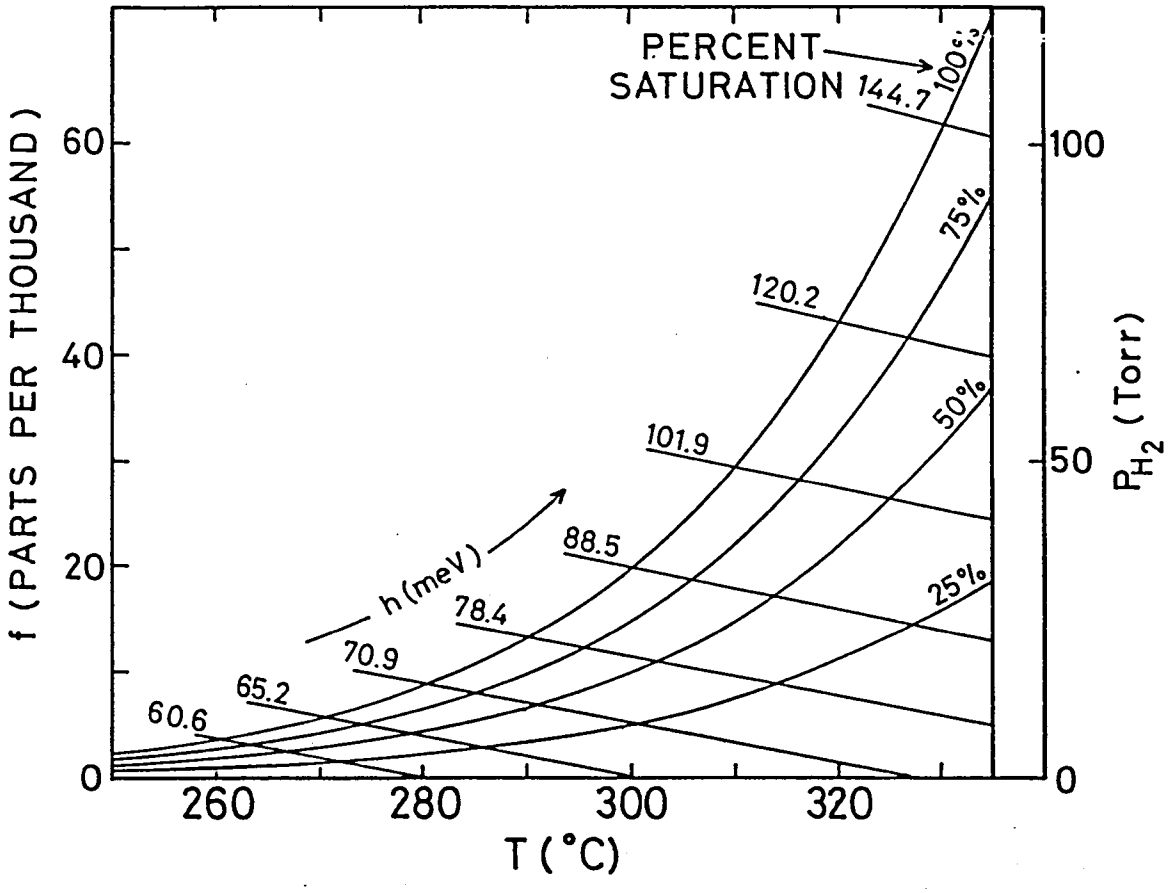

Fig. 3.2 Psychrometric chart of CsH.[2] Four curves show the hydrogen pressure vs. temperature at four relative humidities of hydrogen, where relative humidities of hydrogen are computed from the dissociation pressure of CsH, which is 100 % humidity of hydrogen. Approximately linear lines show the fraction, f, defined by $f = n_{H_2} / n_{He}$ at several gas-phase enthalpy, h, where $n_{He} = 2.69 \times 10^{19} cm^{-3}$ (the density of gas at 0 ℃ at 1 atm) in this figure.

alkali hydrides and deutrides as functions of temperature T in Table 3.3.[64] Since the dissociation of sodium hydride and cesium hydride are especially important for the present work, we show their psychrometric charts in Figs. 3.1 and 3.2.[2]

These psychrometric charts[2] are composed of two kinds of lines. One is the curve of the hydrogen pressure vs. temperature at several relative humidities of hydrogen, where relative humidities of hydrogen are computed from the dissociation pressure of alkali hydrides, which is 100 % humidity of hydrogen. The other is the fraction, f, defined by $f = n_{H_2} / n_{He}$ as a function of temperature, where n_{H_2} and n_{He} represent the densities of H_2 and He, respectively, and in our calculation, the density 2.69×10^{19} cm^{-3} (the density of gas at 0°C at 1 atm) is used as n_{He}, because relatively high pressure of He gas was used as a buffer gas in our experiment. From Eq. (3.6) shown below, when the gas-phase enthalpy, h, is constant, the fraction, f, becomes approximately a linear function of temperature as shown in Figs. 3.1 and 3.2. The gas-phase enthalpy, h, is calculated from the enthalpy for a helium atom, h(He), which is given by a heat capacity at constant pressure, and that of hydogen gas per H_2 molecule, $h(H_2)$, which is obtained from the thermodynamic properties of the alkali-hydrogen system.[68] In the sodium-hydrogen system, the gas-phase enthalpy, h, are given by

$$\begin{aligned} h &= h(He) + f\, h(H_2) \\ &= 5.92 \times 10^{-2} + 2.17 \times 10^{-4} T + f(1.256 - 8.02 \times 10^{-4} T) \end{aligned} \qquad (3.6)$$

where T is a temperature in °C. Because of the low heat capacity of condensed CsH crystals compared with the heat of decomposition of the crystal, h remains very nearly constant during the decomposition, so that h may be given by the enthalpy of the dry gas before the crystals have decomposed. Consider, as an example, a sodium cell containing hydrogen gas of about 1 Torr and helium gas of 760 Torr at 0°C. The fraction f is 1.3 parts per thousand in this case. Suppose that the cell is maintained at 325°C where, according to Fig. 3.1, the relative humidity is about 10 %. When the NaH crystal begins to evaporate into surrounding buffer gas, the temperature decreases along the line of constant gas-phase enthalpy i.e. the line of the fraction, f, which is a function of temperature, until the H_2 pressure reaches its saturation value. In this case we see from Fig. 3.1 that the gas temperature will drop to 300°C, so that the total cooling is about 25°C.

In Fig. 3.3, we show the energy diagram of sodium-hydrogen system and cesium-hydrogen system. These energies[64,67,69-72] of sodium-hydrogen system and cesium-hydrogen system will be used in the following sections. Here, it is important that the alkali hydride gas (MH) has the higher energy position than that of the alkali vapor (M) and the hydrogen gas (H_2) mixture system, in other words, we must give energies at least more than 0.2 eV for NaH and 0.4 eV for CsH to the M + H_2 system for producing MH molecules.

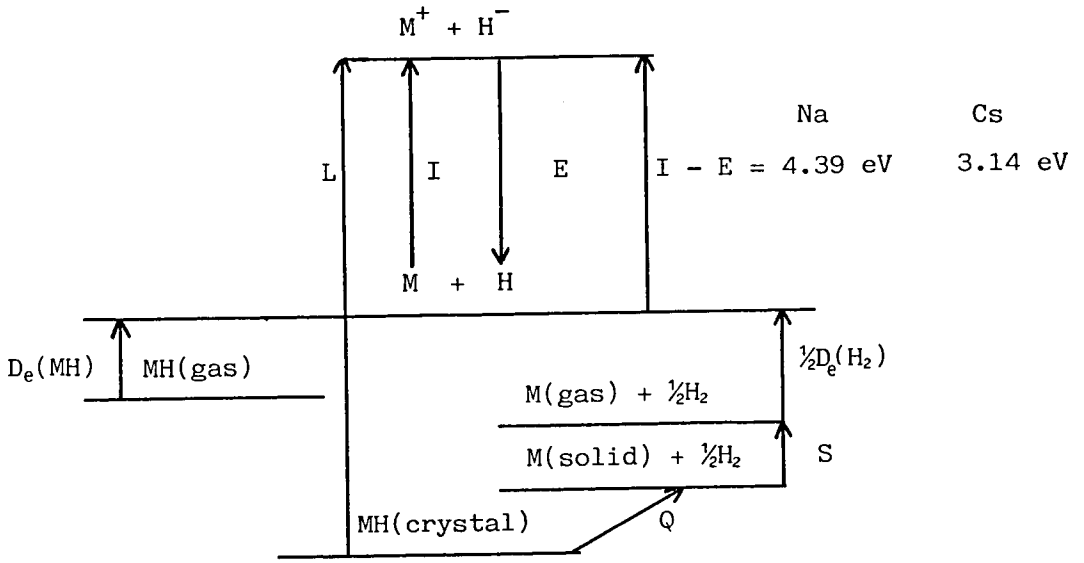

Fig. 3.3 Energy diagram of alkali-hydrogen system. The symbols used in the figure and their values are as follows.

I : Ionization energy	I(Na) = 5.14 eV,[a]	I(Cs) = 3.89 eV,[a]
D_e : Dissociation energy	D_e(NaH) = 2.02 eV,[b]	D_e(CsH) = 1.86 eV,[c]
	$D_e(H_2)$ = 4.745 eV,[d]	
S : Heat of vaporization (at b.p.)	S(Na) = 0.92 eV,[e]	S(Cs) = 0.84 eV,[e]
Q : Heat of formation (25°C)	Q(NaH) = 0.60 eV,[f]	Q(CsH) = 0.86 eV,[f]
L : Lattice energy	L(NaH) = 8.76 eV,[e]	L(CsH) = 7.03 eV,[e]
E : Electron affinity of hydrogen atom		E(H) = 0.754 eV,[a]

It must be noted that some of these values have relatively large differences in different references, such as the dissociation energies of NaH and CsH, which will be described later.

a) Ref. 69, b) Ref. 71, c) Ref. 72, d) Ref. 70, e) Ref. 64, f) Ref. 67

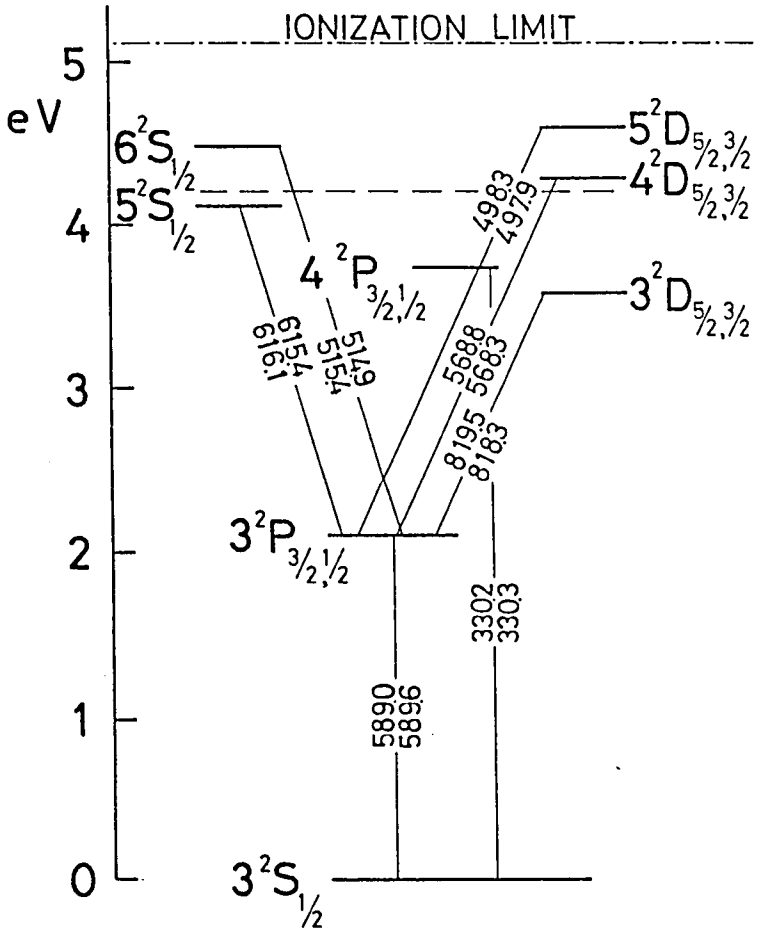

Fig. 3.4 Energy diagram of Na.[73] The ionization limit is 5.14 eV. The wavelengths (nm) which correspond to the transitions between some energy levels are also shown in this figure. The 589.6 nm and 589.0 nm lines correspond to the transitions between $3S_{1/2} - 3P_{1/2}$ and $3S_{1/2} - 3P_{3/2}$, which are called D_1 and D_2 lines, respectively. The sum of the electronic energy of two 3P excited atoms is marked by the dashed line.

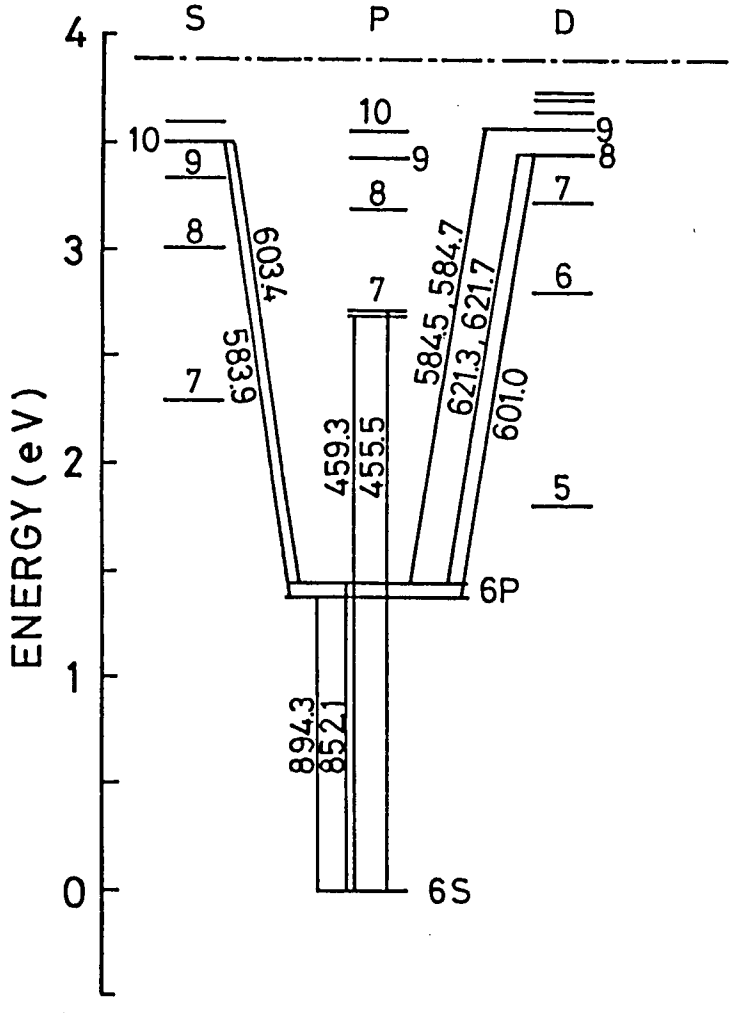

Fig. 3.5 Energy diagram of Cs.[74,75] The ionization limit is 3.87 eV. The wavelengths (nm) which correspond to the transitions between some energy levels are also shown in this figure. Cesium D lines are 894.3 nm and 852.1 nm lines which correspond to the transitions between $6S_{1/2} - 6P_{1/2,3/2}$.

III. 2. 2 Spectroscopic Properties

We show in Figs. 3.4 - 3.8 the spectroscopic data and energy diagrams of Na, Cs, Na_2, Cs_2, and H_2.

In Fig. 3.4, we show the energy diagram of Na.[73] The most important lines for our experiment are 589.6 nm and 589.0 nm lines. The 589.6 nm and 589.0 nm lines correspond to the transitions between $3S_{1/2} - 3P_{1/2}$ and $3S_{1/2} - 3P_{3/2}$, which are called D_1 and D_2 lines, respectively.

In Fig. 3.5, we show the energy diagram of Cs.[74,75] Cesium D lines are 894.3 nm and 952.1 nm lines, which correspond to the transitions between $6S_{1/2} - 6P_{1/2,3/2}$. We used other lines 583.9 nm, 601.0 nm, and 621.3 nm for the laser excitation, which correspond to the transitions between $6P_{1/2} - 10S_{1/2}$, $6P_{1/2} - 8D_{3/2}$, and $6P_{3/2} - 8D_{5/2}$. We used also the Ar^+ laser 457.9 nm line , which can be absorbed by the pressure broadened 459.3 nm and 455.5 nm lines (the transition between $6S_{1/2} - 7P_{1/2,3/2}$), for excitation of Cs atoms.

In Fig. 3.6, we show the potential curves for Na_2.[76] The dissociation energy of the ground electronic state of Na_2 ($D_0(Na_2)$) is 0.73 eV or 5890 cm^{-1}.[70] This value will be used in our analysis of chemical reactions. Since Na_2 absorbs well the most lines of Ar^+ laser, such as the line of 488.0 nm, molecular constants and spectroscopic properties of Na_2 can well be studied by using the laser-induced fluorescence techniques.

In Fig. 3.7, we show the potential curves for Cs_2.[78] The dissociation energy of the ground electronic state of Cs_2 ($D_e(Cs_2)$) is 0.396 eV or 3197 cm^{-1}.

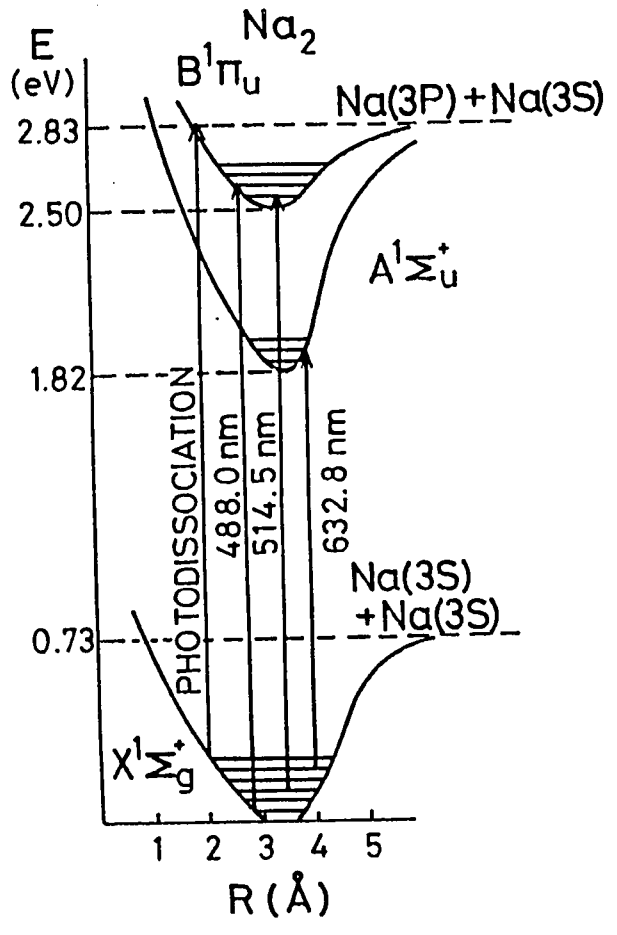

Fig. 3.6 Potential curves for Na_2.[76] The dissociation energy of the ground electronic state of $Na_2(D_0(Na_2))$ is 0.73 eV or 5890 cm^{-1}.[70] Na_2 molecules absorb well the most lines of Ar^+ laser, such as the line at 488.0 nm.

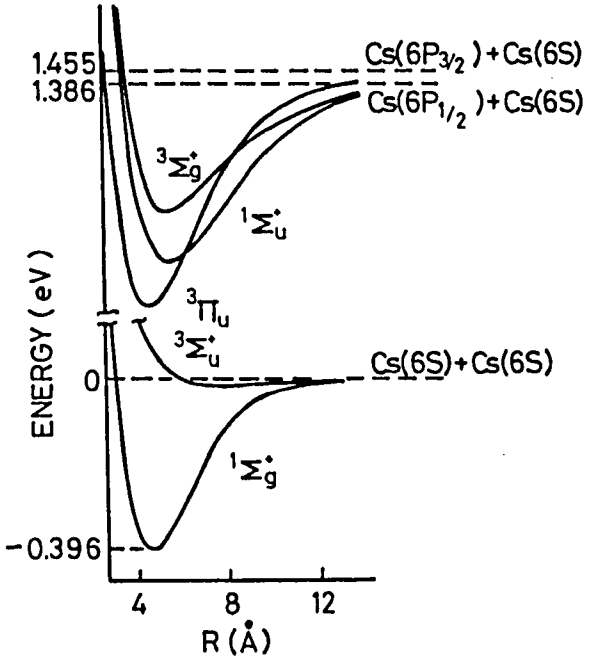

Fig. 3.7 Potential curves for Cs_2.[78] The dissociation energy of the ground electronic state of Cs_2 ($D_e(Cs_2)$) is 0.396 eV or 3197 cm^{-1}.

In Fig. 3.8, we show the potential curve of the H_2 ground state with the vibrational levels.[70] The dissociation energy*) of the ground electronic state of H_2 ($D_0(H_2)$) is 4.476 eV or 36101 cm^{-1} ($D_e(H_2)$ = 4.745 eV or 38269 cm^{-1}). This value will be also used in our analysis of chemical reactions.

The lifetimes of excited states of atoms and molecules are important factors to determine the rate of the laser-induced chemical reaction. We list the typical values of these lifetimes of alkali atoms,[79] molecules,[80] and hydrides[81,82] in Table 3.4. We list also in Table 3.4 the Einstein's A coefficient, which is correlated to the lifetime. The broadening of spectrum due to the buffer gas pressure and Doppler effect must also be considered in our experiment. The pressure broadening of Na D lines are shown in Table 3.5.[83] The Doppler broadening Δ_D (full-width at half-maximum) is represented as follows

$$\Delta_D = \frac{2\nu_0}{c}\sqrt{\frac{2\ln 2\, k_B T}{M}}\,(\mathrm{Hz}), \qquad (3.7)$$

where M is atomic weight, ν_0 is the center frequency, k_B is the Boltzmann

*) D_0; The dissociation energy which is designated as the height of the asymptote (the beginning of the continuum) above the lowest vibrational level.

D_e; The dissociation energy which is designated as the height of the asymptote above the minimum of potential energy curve.

These dissociation energies are shown in Fig. 3.8.

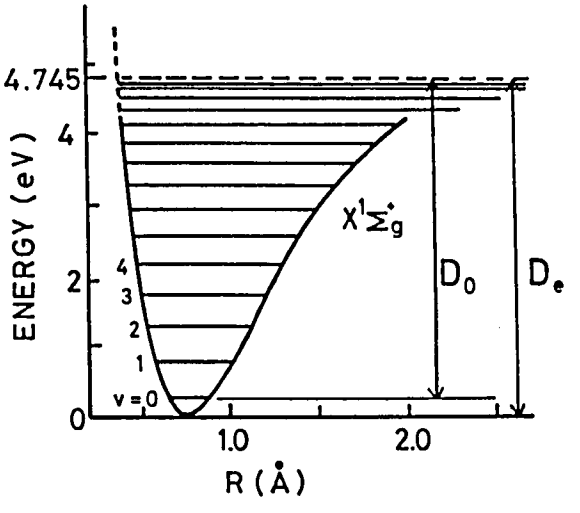

Fig. 3.8 Potential curve of H_2 ground state with the vibrational levels.[70] The dissociation energy of the ground electronic state of H_2 ($D_0(H_2)$) is 4.476 eV or 36101 cm^{-1}. ($D_e(H_2)$ = 4.745 eV or 38269 cm^{-1})

Table 3.4 (a) Lifetimes and total A coefficients of alkali atoms.

(See Ref. 79)

(1) Sodium

State	$\sum A$ ($\times 10^{-6}$ sec^{-1})	Lifetime ($\times 10^{-8}$ sec)
$3P_{1/2}$	58.9	1.70
$3P_{3/2}$	59.1	1.69
$4S_{1/2}$	24.7	4.05
$3D_{3/2}$	49.6	2.02
$3D_{5/2}$	49.5	2.02
$4P_{1/2}$	9.44	10.6
$4P_{3/2}$	9.48	10.6
$5S_{1/2}$	11.9	8.4

(2) Rubidium

State	$\sum A$ ($\times 10^{-6}$ sec^{-1})	Lifetime ($\times 10^{-8}$ sec)
$5P_{1/2}$	35.6	2.81
$5P_{3/2}$	37.5	2.67
$4D_{3/2}$	12.7	7.87
$4D_{5/2}$	11.9	8.40
$6S_{1/2}$	19.5	5.13
$6P_{1/2}$	9.13	11.0
$6P_{3/2}$	9.16	10.9

(3) Cesium

State	$\sum A$ ($\times 10^{-6}$ sec^{-1})	Lifetime ($\times 10^{-8}$ sec)
$6P_{1/2}$	28.6	3.50
$6P_{3/2}$	32.4	3.09
$5D_{3/2}$	1.05	95.2
$5D_{5/2}$	0.73	137
$7S_{1/2}$	17.6	5.68
$7P_{1/2}$	7.23	13.8
$7P_{3/2}$	8.25	12.1

Table 3.4 (b) Lifetimes of alkali molecules and hydrides.

Molecule	Lifetime (10^{-9} sec)
$Na_2(B^1\Pi)$	~ 7 [a]
$K_2(B^1\Pi)$	~ 10 [a]
$Rb_2(B^1\Pi)$	~ 20 [a]
Cs_2	~ 10 [a]
(not yet analysed electronic states)	
$CsH(A^1\Sigma)$	~ 85 [b]
$LiH(A^1\Sigma)$	~ 30 [c]
$NaH(A^1\Sigma)$	~ 23 [c]

a) Ref. 80 b) Ref. 82 c) Ref. 81

Table 3.5 Pressure broadening constant γ (full-width) of Na D lines by rare gases. (See Ref. 83)

	γ (10^{-9}rad sec^{-1} cm^{-3})
He D_1	3.55 ± 0.09
D_2	4.30 ± 0.03
Ne D_1	2.79 ± 0.05
D_2	2.53 ± 0.03
Ar D_1	5.56 ± 0.04
D_2	4.22 ± 0.11
Kr D_1	4.83 ± 0.09
D_2	4.73 ± 0.11
Xe D_1	5.83 ± 0.12
D_2	4.94 ± 0.11

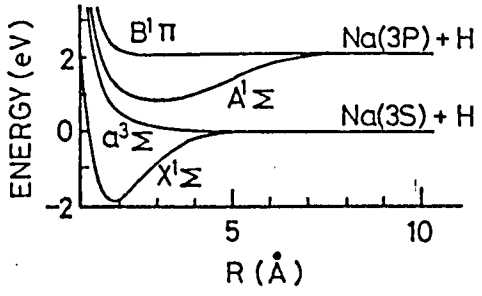

Fig. 3.9 Potential curves for NaH.[85] The dissociation energy of the ground electronic state of NaH (D_e(NaH)) is 1.92 eV[85] (calculation) or 2.02 eV[71] (experimental extrapolation).

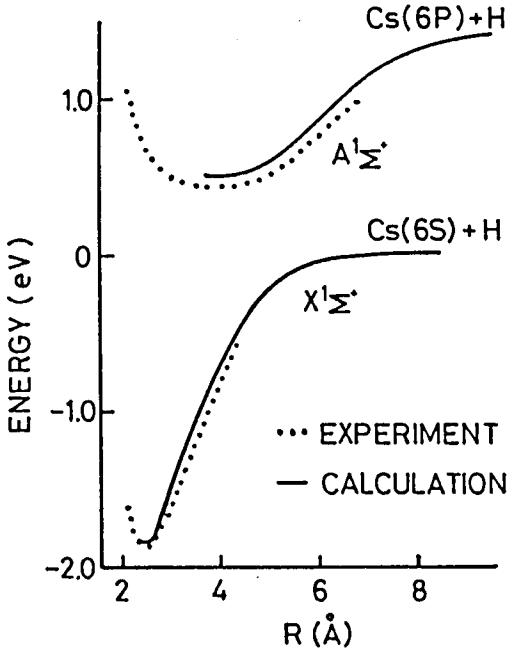

Fig. 3.10 Potential curves for CsH.[91] The calculated and experimentally obtained results of the low lying states are shown. The dissociation energy of the ground electronic state of CsH (D_e(CsH)) is 1.85 eV[91] (calculation) or 1.86 eV[72] (experimental extrapolation).

constant, c is the velocity of light, and T is the temperature of the Na vapor in Kelvin.

Many spectroscopic properties of alkali hydrides (for example NaH,[84-88] CsH,[89-91] and RbH[92,93]) have been reported since the first report on NaH by Hori 1930.[94] However, the values of the dissociation energy of ground electronic state of alkali hydrides have not been determined precisely yet, although they are the most important quantity in chemical reactions. For example, the dissociation energy of NaH (D_e(NaH)) has been calculated to be 1.88 eV[87] or 1.79 eV[86] in multiconfiguration self-consistent-field (MCSCF) method and to be 1.92 eV in configuration-interaction (CI) method,[85] whereas the extrapolation of the measured ground state vibrational levels suggests 2.12 eV[95] or 2.02 eV.[71]

Since small differences of the dissociation energy of alkali hydrides would result in the large differences of rate of the chemical reaction to produce alkali hydride molecules, the uncertainty of the dissociation energy makes our detailed discussion difficult. In this thesis, we use the latest results of NaH and CsH, which are shown in Fig. 3.9[71] and Fig. 3.10.[91]

In Fig. 3.9, we show the calculated results of low-lying molecular states of NaH.[85] We use the values 1.92 eV (calculation)[85] or 2.02 eV (experimental extrapolation)[71] as the dissociation energy (D_e(NaH)) of the ground electronic state.

In Fig. 3.10, we show the calculated results and experimentally obtained results of the low-lying states of CsH.[91] We use the values 1.85 eV (calculation)[91] or 1.86 eV (experimental extrapolation)[72] as the dissociation energy (D_e(CsH)) of the ground electronic state.

In our experiment, not only the excitation of alkali atoms and molecules but also the excitation of H_2 molecules must be considered. However, the excitation of H_2 molecules to the high electronic states by visible light is energetically impossible and the excitation to the high vibrational states in the ground electronic state by light does not occur because of the selection rule. Therefore only the collisional excitation of H_2 molecules to the high vibrational states with excited alkali atoms or molecules are possible. Here, the vibrationally excited H_2 molecule has long lifetime[96] about 8×10^{-5} sec in 10 Torr of H_2 gas and about 5×10^{-5} sec in 500 Torr of He buffer gas. These lifetimes are longer than that of alkali atoms and molecules in the excited electronic states of about $10^{-8\sim-7}$ sec (see Table 3.4). This long lifetime of the vibrationally excited H_2 molecules will be discussed again in consideration about chemical reaction processes, because the reaction through the vibrational excitation of H_2 molecules is expected to occur under the high density of H_2 molecules.

III. 3 CsH Laser Snow

III. 3. 1 Excitation of Cs Atoms and Molecules by Lasers

The laser excitation of Cs atoms or molecules is necessary for producing CsH particles. We investigate experimentally the excitation mechanisms of Cs atoms and molecules in this subsection.

The experimental setup is shown in Fig. 3.11. The cell used was cylindrical with a 3 cm i.d. and a 5 cm length, which was made of alkali-resistant aluminosilicate (Corning 1720) glass. The cell was baked at 650 ℃ in a vacuum of 10^{-6} Torr before filling with Cs vapor and 27 Torr of H_2 (We will call this cell "C-1" hereafter. See Table 3.6 at page 68.).

The cell was placed inside an oven, in which the cell temperature was set about 340°C or changed from 250°C to 360°C, corresponding Cs density being 9.12×10^{16} cm^{-3} or from 1.1×10^{16} to 1.4×10^{17} cm^{-3}.

We used an Ar^+ laser pumped dye laser and an Ar^+ laser as exciting light sources.

(a) The dye laser: The wavelength was tuned at the transitions between the 6P states and the $8D_{3/2}$ or $9D_{5/2}$ states of Cs, i.e., 601.0 nm ($6P_{1/2} - 8D_{3/2}$) or 584.5 nm ($6P_{3/2} - 9D_{5/2}$). The laser power was less than 70 mW.

(b) The Ar^+ laser: Without an intracavity prism, the Ar^+ laser oscillates at several lines simultaneously. (multi-line operation) The major components of these laser wavelengths are 457.9, 476.5, 488.0, 496.5, 501.7, and 514.5 nm. Selective single-line oscillation among these lines is possible by introducing the intracavity prism. (single-

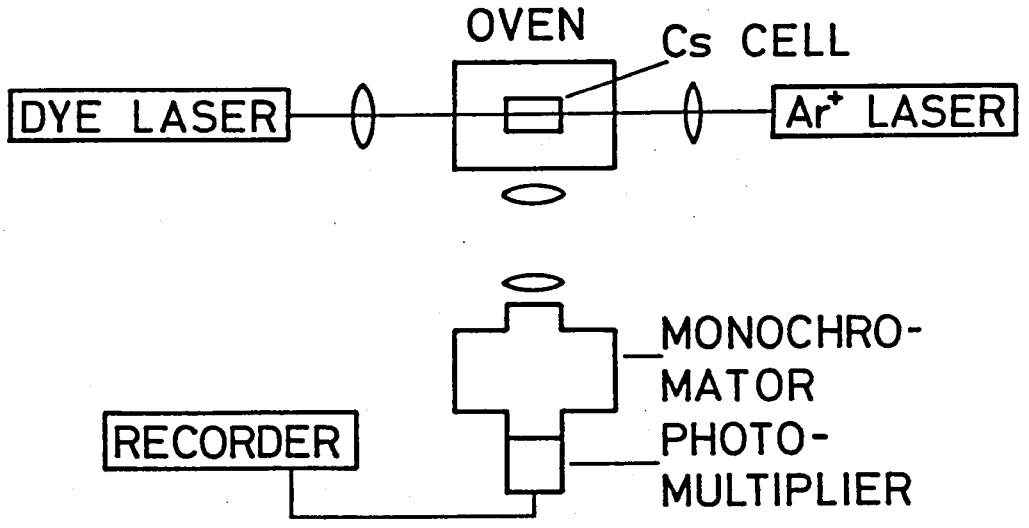

Fig. 3.11 Experimental setup of excitation of Cs atoms and molecules. Cs atoms and molecules are excited by the Ar^+ laser and/or the dye laser beams. The laser-induced fluorescence from Cs atoms or molecules is detected at right angles from laser beams by a photomultiplier through a monochromator.

line operation) The laser power was less than 600 mW for multi-line and was less than 50 mW for single-line oscillation.

We set the two laser beams colinearly so that the simultaneous irradiation was possible. We used some combinations of the dye laser and the Ar^+ laser wavelengths. These laser beams were focussed and applied to the cell, and their beam diameters at the cell were about 1 mm.

The laser-induced fluorescence from Cs atoms or molecules was detected at right angles from laser beams by a photomultiplier through a monochromator. The resolving power of the monochromator was about 1 nm. Figure 3.12 (a) and (b) show the observed spectra for the excitation by the dye laser beams at 601.0 nm and 584.5 nm, respectively. We could see the fluorescence from some highly excited states which are not excited by the dye laser beam directly.

The observed spectra excited by the multi-line Ar^+ laser beam are shown in Fig. 3.13. We could also find that the fluorescence from highly excited atoms was increased in the experiment of the simultaneous irradiation both of the dye laser and Ar^+ laser beams when two beams were overlapped within the cell.

These observed results can be explained by the following mechanisms of the excitation.

The mechanism of the excitation by the dye laser tuned at 601.0 nm has been reported already by Tam *et al.*[3,74,75] and Yabuzaki *et al.*[97] The laser wavelength must be finely tuned to the line center, for

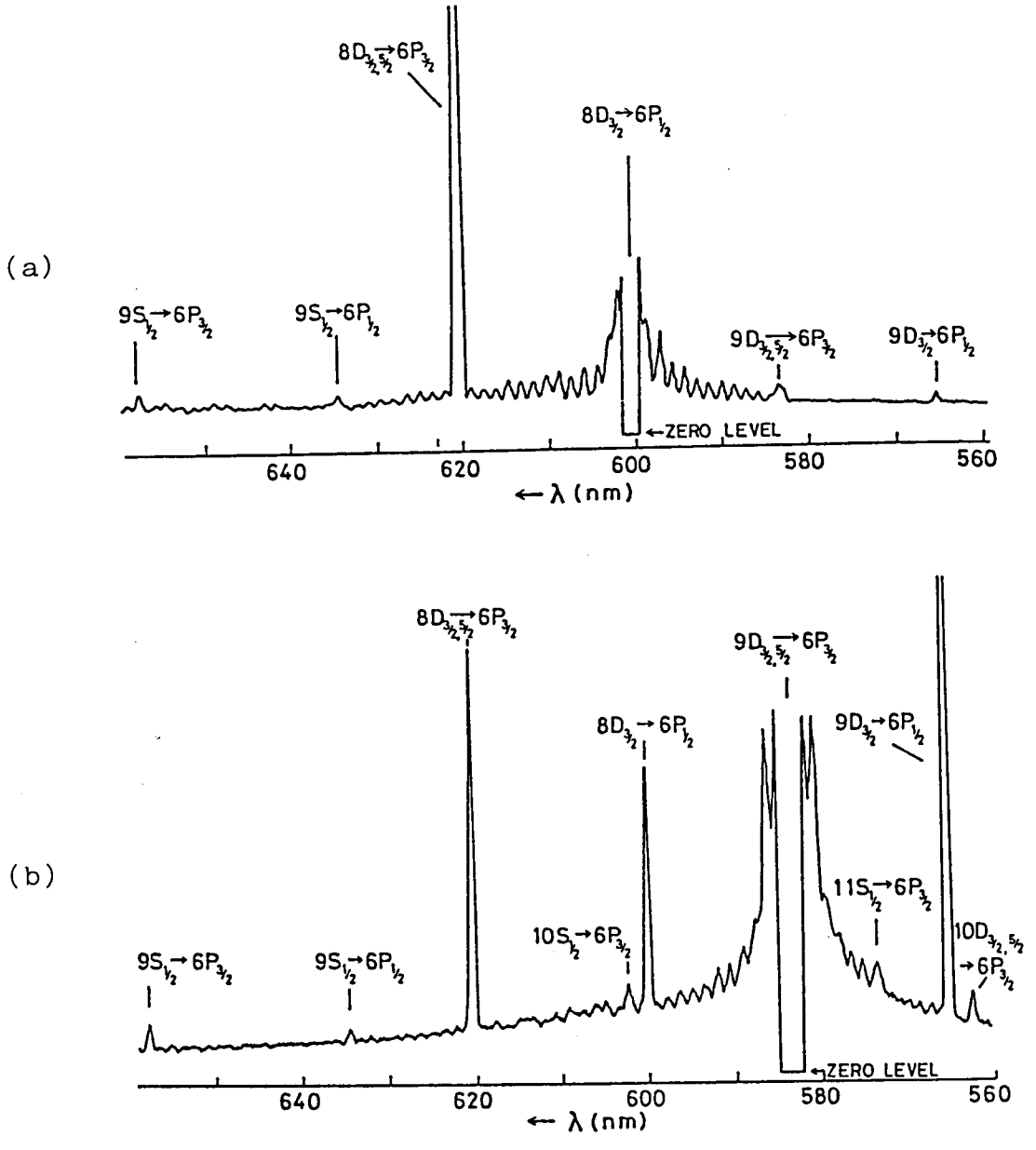

Fig. 3.12 The observed spectra of the fluorescence from highly excited states of Cs atoms excited by the dye laser beam. The dye laser wavelength is tuned to (a) 601.0 nm ($6P_{1/2} - 8D_{3/2}$) and (b) 584.5 nm ($6P_{3/2} - 9D_{5/2}$). The cell temperature is about 340°C.

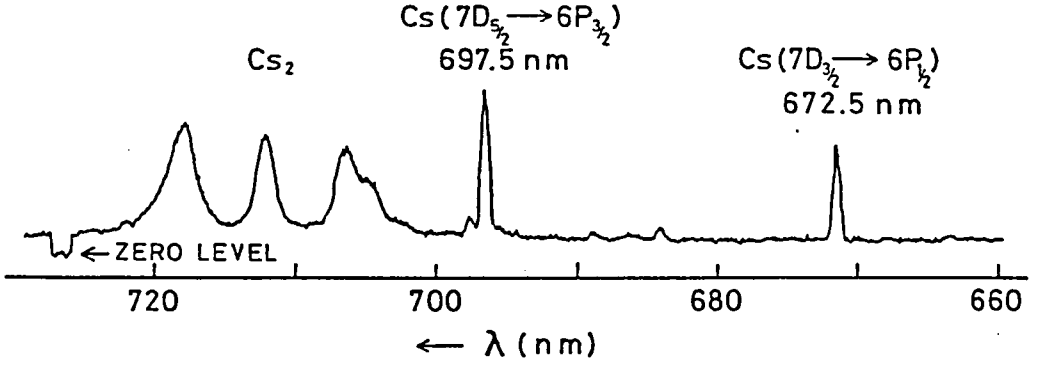

Fig. 3.13 The observed spectra of the fluorescence from Cs_2^* and Cs(7D) excited by the multi-line oscillating Ar^+ laser beam at the cell temperature about 340°C.

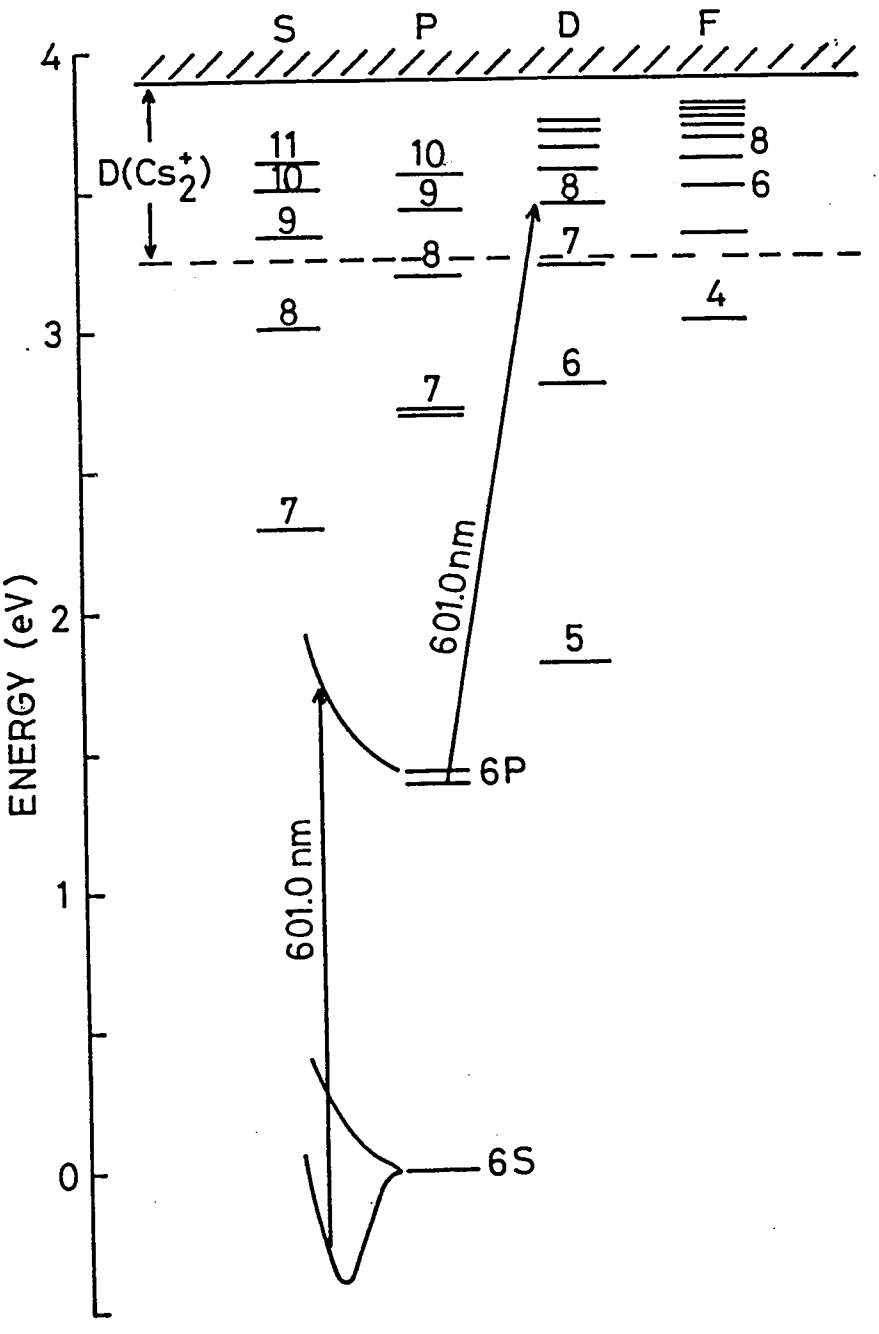

Fig. 3.14 Energy level diagram of Cs.[75] The mechanism of the excitation to the $8D_{3/2}$ state by the dye laser beam at $\lambda = 601.0$ nm is also shown.

example at 601.0 nm, to observe the fluorescence from highly excited Cs atoms,[74,97] the particle formation,[3] and the plasma formation.[75] The laser beam tuned at 601.0 nm can excite Cs atoms from the $6P_{1/2}$ state to the $8D_{3/2}$ state, but cannot excite Cs atoms in the ground state to $6P_{1/2}$ state. So, we must seek some mechanism to produce relatively high density of $6P_{1/2}$ atoms by the laser beam. Tam *et al.*[74] produced that the high population of $Cs(6P_{1/2})$ atoms is produced by dissociative optical excitation from the ground singlet and/or triplet state of Cs_2 to a repulsive excited Cs_2 state, which produces Cs(6P) atoms by direct dissociation (Fig. 3.14), and also by the excitation to the bound state of Cs_2 and the succeeding collisional energy transfer. It is known that the Cs_2 molecule has a structureless broad absorption band in the region between 550 and 620 nm through which such dissociative Cs_2 excitations are possible.[127] Tam *et al.*[3] proposed also that the accumulation of atoms in the $6P_{1/2}$ state is facilitated by strong trapping of the atomic resonance radiation and that laser-produced $Cs(6P_{1/2})$ atoms are further excited to the $8D_{3/2}$ state by the 601.0 nm laser light. They also observed the fluorescence not only from $8D_{3/2}$ state but also from neighbouring states, *e.g.* 7D, which were considered to be produced by collisional transfer or cascades from the $8D_{3/2}$.

As described previously, we excited Cs atoms by the laser beam tuned at 601.0 nm ($6P_{1/2} - 8D_{3/2}$) or 584.5 nm ($6P_{3/2} - 9D_{5/2}$), and we observed the laser-induced fluorescence from the $8D_{3/2}$ or the $9D_{5/2}$ and also from the neighbouring states and confirmed the existence of atoms in these

highly excited states. Possible excitation mechanisms to these highly excited states are as follows:

$$Cs_2 + h\nu \rightarrow Cs_2^*, \tag{3.8}$$

$$Cs_2^* \rightarrow Cs(6P) + Cs(6S), \tag{3.9}$$

$$Cs_2^* + Cs(6S) \rightarrow Cs_2 + Cs(6P), \tag{3.10}$$

$$Cs(6P) + h\nu \rightarrow Cs(n\,L), \tag{3.11}$$

$$Cs(n\,L) + X \rightarrow Cs(n'L') + X, \tag{3.12}$$

where nL is a highly excited state $8D_{3/2}$ or $9D_{5/2}$, n'L' is a highly excited state except for $8D_{3/2}$ and $9D_{5/2}$, such as , 7D, 8S, 9S, etc., and X represents any atom or molecule in the ground electronic state. Process (3.8) is the laser-excitation of Cs_2 molecules from the ground electronic state. Process (3.9) is the dissociation of the excited state Cs_2 molecules, as illustrated in Fig. 3.14. Process (3.10) is collisional energy transfer between Cs atom and excited Cs_2 molecule. Process (3.11) is the laser-excitation of Cs atom from the 6P state to the highly excited state. For this process, it is required to tune the dye laser to the corresponding atomic transition wavelength, *e.g.* 601.0 nm, within about ±0.01 nm or ±10 GHz of the line center. Process (3.12) is the collisional energy transfer between the excited Cs atom and any atom

or molecule in the ground state.

The mechanism of the excitation by the Ar^+ laser beam at 457.9 nm was also reported by Tam *et al.*[1] Under the presence of H_2 at the pressure higher than 50 Torr, the pressure broadenings of the second resonance lines at 455.5 nm ($6S_{1/2} - 7P_{3/2}$) and 459.3 nm ($6S_{1/2} - 7P_{1/2}$) are not so large but it is enough to excite Cs atoms to the 7P states by the 457.9 nm line of Ar^+ laser. The mechanisms of excitation by the other Ar^+ laser lines at 488.0, 476.5, 514.5 nm, etc. were reported by McClintock *et al.*[98] Although there is no atomic absorption close to the wavelength of these laser lines, many atomic fluorescence lines were observed. The intensities of atomic fluorescence from the 6P and 5D states were found to be linearly dependent on the laser intensity. According to McClintock *et al.*, the possible process is

$$Cs_2(^1\Pi) + Cs \rightarrow Cs(6P \text{ or } 5D) + Cs_2(X \text{ vib.}). \qquad (3.13)$$

This process needs single-photon for the excitation to $Cs_2(^1\Pi)$. On the other hand, the atomic fluorescence lines from 7D, 8D, 8S, etc. were found to have more than quadratic dependence on laser intensity. Then they proposed the following two excitation processes. One is the dissociative excitation as

$$Cs_2(^1\Pi) + h\nu \rightarrow Cs(6P) + Cs(7D), \qquad (3.14)$$

and the other is recombination of ionized atoms, which are ionized via collisions between 6P atoms and excited Cs_2 molecules as

$$Cs_2(^1\Pi) + Cs(6P) \rightarrow Cs_2(X^1\Sigma) + Cs^+ + e^-. \quad (3.15)$$

If there are many excited atoms, the collisional excitation as

$$Cs^* + Cs^* \rightarrow Cs^{**} + Cs(6S) + \Delta E, \quad (3.16)$$

is possible, where Cs* represents a Cs atom in the excited state 6P, 5D, or 7S, and Cs** represents a highly excited Cs atom. The quantity ΔE is the energy excess for the reaction.

The excitation by the Ar^+ laser operating on multi-lines is considered to be accomplished through both of atomic and molecular absorption processes mentioned above. We found that the intensities of atomic fluorescence (I_F) at 672.5 nm ($6P_{1/2} \rightarrow 7D_{3/2}$) and 697.5 nm ($6P_{3/2} \rightarrow 7D_{5/2}$) have quadratic dependence on intensity (I_L) of the Ar^+ laser operating on multi-lines in the blue-green region, as shown in Fig. 3.15. We thought that the density of highly excited state Cs atoms, such as Cs(7D), is not simply related to the density of Cs atoms nor molecules in the ground states, because of their complicated excitation processes, such as Processes (3.13) – (3.16). But, as shown in Fig. 3.16 (a) and (b), intensities of the fluorescence at 672.5 nm and 697.5 nm show that the density of Cs(7D) has the quadratic and linear dependences on the density of Cs atoms and molecules, respectively, in the low density region. However, in the high density region, we see that the density of Cs(7D) is insensitive to the change of the densities of Cs atoms nor molecules. This result can not be explained from only

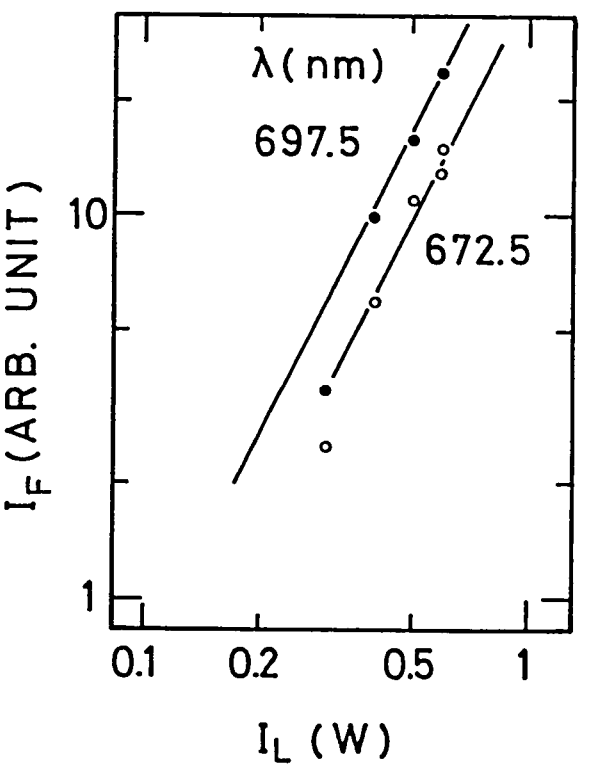

Fig. 3.15 The intensities of Cs atomic fluorescence (I_F) at 672.5 nm ($6P_{1/2} \leftarrow 7D_{3/2}$) and 697.5 nm ($6P_{3/2} \leftarrow 7D_{5/2}$) vs. the intensity ($I_L$) of the Ar^+ laser operating on multi-lines. The cell temperature was 300°C. The linear lines in the figure have a slope 2. This means that the fluorescence (I_F) has a quadratic dependence on the Ar^+ laser intensity (I_L).

(a)

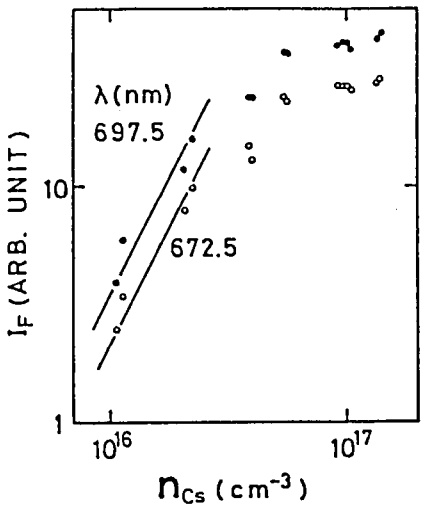

(b)

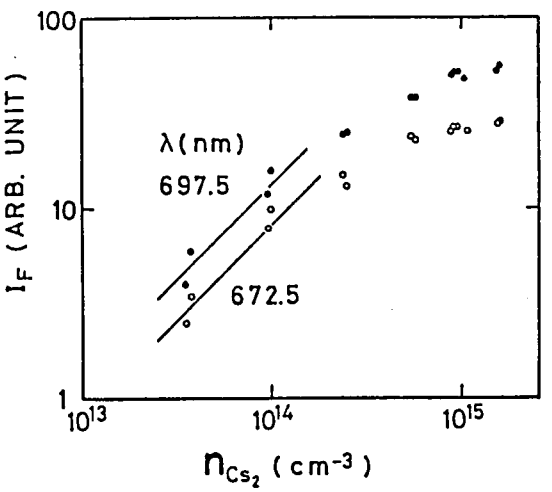

Fig. 3.16 The intensities of Cs atomic fluorescence (I_F) at 672.5 nm ($6P_{1/2} \leftarrow 7D_{3/2}$) and 697.5 nm ($6P_{3/2} \leftarrow 7D_{5/2}$) vs. the densities of (a) Cs and (b) Cs_2. In the low density region, the fluorescence shows (a) the quadratic dependence on the density of Cs and (b) the linear dependence on the density of Cs_2. But, in the high density region, the fluorescence becomes insensitive to the change of the densities of Cs and Cs_2

the Processes (3.13) - (3.16). We think, therefore, that these results come mainly from the quenching processes of Cs(7D) by H_2, which involve the energy transfer processes both with and without chemical reactions, because we used the Cs cell containing H_2 at about 27 Torr. The detailed quenching mechanisms will be discussed in the next subsection.

The simultaneous excitation by the dye laser and the Ar^+ laser beams must induce both mechanisms mentioned above. The excitation by the Ar^+ laser beam produces Cs(6P) atoms and the dye laser beam excites Cs(6P) atoms to Cs(8D) or Cs(9D). The highly excited Cs atoms, such as the 7D states, are produced by the energy transfer collisions of the Cs atoms in the 8D or 9D states with atoms or molecules in the ground state (Process (3.12)). Therefore the atomic fluorescence from highly excited Cs atoms, such as Cs in the 7D state, becomes large when the Cs vapor is simultaneously excited to the 8D or 9D states by the dye laser and the Ar^+ laser beams.

III. 3. 2 Quenching Collisions of Excited Cs Atoms with H_2 Molecules

We consider the effects of quenching collisions of excited Cs atoms with H_2 molecules on the population of excited states of Cs atoms or the intensities of fluorescence originating from these states. For simplicity, we restrict our consideration to the direct excitation of Cs(6S) atoms to Cs* atoms and the following collisional excitation

$$Cs^* + Cs^* \rightarrow Cs^{**} + Cs(6S) + \Delta E, \qquad (3.17)$$

where Cs* represents a Cs atom in the 6P, 7P, 5D, or 7S state and Cs** represents a highly excited Cs atom in the state such as 7D, 8D, or 9D. There are two quenching processes as

$$Cs^*(\text{or } Cs^{**}) + H_2 \rightarrow Cs + H_2(\nu) + \Delta E, \qquad (3.18)$$

$$Cs^*(\text{or } Cs^{**}) + H_2 \rightarrow CsH + H + \Delta E, \qquad (3.19)$$

where $H_2(\nu)$ represents the vibrationally excited H_2 molecule. Process (3.18) represents the energy transfer from electronic to vibrational and/or to translational energies, and Process (3.19) represents the collision leading to a chemical reaction. We have to consider both of Processes (3.18) and (3.19) as quenching processes. Therefore the whole processes, which will be considered here, are as follows:

$$\left.\begin{array}{l} \text{(a)}\ Cs + h\nu \rightarrow Cs^*, \\ \text{(b)}\ Cs^* + Cs^* \xrightarrow{k_b} Cs^{**} + Cs, \\ \text{(c)}\ Cs^* + H_2 \begin{cases} \xrightarrow{k_c} Cs + H_2(\nu), \\ \rightarrow CsH + H, \end{cases} \\ \text{(d)}\ Cs^{**} + H_2 \begin{cases} \xrightarrow{k_d} Cs + H_2(\nu), \\ \rightarrow CsH + H, \end{cases} \end{array}\right\} \qquad (3.20)$$

where k_b, k_c, and k_d are rate constants of the processes.

The density of Cs** is determined by the following rate equations in this case.

$$\frac{dn_{Cs^*}}{dt} = Bn_{Cs} I - A_{Cs^*} n_{Cs^*} - k_b n_{Cs^*}^2 - k_c n_{Cs^*} n_{H_2}, \tag{3.21}$$

$$\frac{dn_{Cs^{**}}}{dt} = k_b n_{Cs^*}^2 - A_{Cs^{**}} n_{Cs^{**}} - k_d n_{Cs^{**}} n_{H_2}, \tag{3.22}$$

where n_{Cs}, n_{Cs^*}, $n_{Cs^{**}}$, and n_{H_2} are densities of Cs, Cs*, Cs**, and H_2, respectively, B is an Einstein's B coefficient, A_{Cs^*} and $A_{Cs^{**}}$ are Einstein's A coefficients for Cs* and Cs**, respectively, and I is the energy density of light per unit volume and unit frequency. In the steady state, Eqs. (3.21) and (3.22) are reduced to

$$k_b n_{Cs^*}^2 + (A_{Cs^*} + k_c n_{H_2}) n_{Cs^*} - Bn_{Cs} I = 0, \tag{3.23}$$

$$n_{Cs^{**}} (A_{Cs^{**}} + k_d n_{H_2}) = k_b n_{Cs^*}^2, \tag{3.24}$$

If the density of H_2 is much higher than that of Cs* ($n_{H_2} >> n_{Cs^*}$) and k_b is about the same order of magnitude as k_c, we can ignore $k_b n_{Cs^*}^2$ in Eq. (3.23). In such a case Eqs. (3.23) and (3.24) become

$$n_{Cs^*} = \frac{Bn_{Cs} I}{A_{Cs^*} + k_c n_{H_2}}, \tag{3.25}$$

$$n_{Cs^{**}} = \frac{k_b B^2 n_{Cs}^2 I^2}{(A_{Cs^{**}} + k_d n_{H_2})(A_{Cs^*} + k_c n_{H_2})^2}, \qquad (3.26)$$

When the rate constants and the density of H_2 are constant, the density of Cs** has a quadratic dependence on the density of Cs and the light intensity. In expeiments the densities of Cs and Cs_2, i.e. n_{Cs} and n_{Cs_2}, can be varied by changing the cell temperature. It must be noted that the density of H_2 and rate constants have also temperature dependences. The change of the density of H_2 can be estimated from the psychrometric chart described in section III.2, but the rate constants can not easily be estimated. Therefore it is difficult to discuss the dependence of atomic fluorescence from Cs** (in the 7D state in our experiment) on n_{Cs}, n_{H_2}, and the rate constants, quantitatively. However, we can discuss it qualitatively as follows. The density of Cs atoms increases with temperature. The density of H_2 molecules and the rate constants also increase with temperature. Therefore, from Relation (3.26), we can suppose that $n_{Cs^{**}}$ is proportional to n_{Cs}^2 only in the low temperature range ($A_{Cs^{**}} \gg k_d n_{H_2}$ and $A_{Cs^*} \gg k_c n_{H_2}$), but $n_{Cs^{**}}$ might not be proportional to n_{Cs}^2 in the high temperature range ($A_{Cs^{**}} \sim k_d n_{H_2}$ and $A_{Cs^*} \sim k_c n_{H_2}$).

When there are no H_2 molecules in the Cs cell, it is apparent from Relation (3.26) that $n_{Cs^{**}}$ is proportional to n_{Cs}^2. Therefore, if the deviation from the quadratic dependence of $n_{Cs^{**}}$ on n_{Cs} is large, such as in our experiment described above, it can be said that the CsH or $H_2(v)$ molecules are produced by Reactions (3.20) (c) and (d).

III. 3. 3 CsH Particle Formation by Lasers

As described already, the first observation of alkali hydride particle formation by a laser beam was reported by Tam *et al.*[1] in 1975, where they used the Ar^+ laser 457.9 nm line as the exciting light. Since then several observations of laser-production of CsH particles have been reported,[2-4] in which the excitation schemes of Cs atoms or molecules are different from the first experiment. In 1977 Tam *et al.*[3] reported that the CsD particle formation was observed when Cs vapor was excited by dye laser tuned at 601.0 nm. In 1980 Picqué *et al.*[4] reported the production of CsH particles by the excitation at 455.5 nm and 459.3 nm, which correspond to the second resonance lines of Cs atom from the ground state $6S_{1/2}$ to the $7P_{3/2}$ and $7P_{1/2}$ states. In 1978 we also observed the CsH particle formation in the experiment where the dye laser beam tuned at 601.0 nm was applied to the Cs cell containing H_2 gas. Since then we have changed the laser wavelength and observed the particle formation by exciting Cs atoms to the 8D, 9D, and 10S states by means of a dye laser beam. We found also that the particles are produced by the excitation using the Ar^+ laser lines at 457.9, 476.5, 488.0, and 496.5 nm. In this subsection we describe our experiments of laser-production of CsH particles.

Our experimental setup is very simple and it is shown schematically in Fig. 3.17. The cell used was cylindrical with a 3 cm i.d. and a 6 cm length, which was made of alkali-resistant aluminosilicate

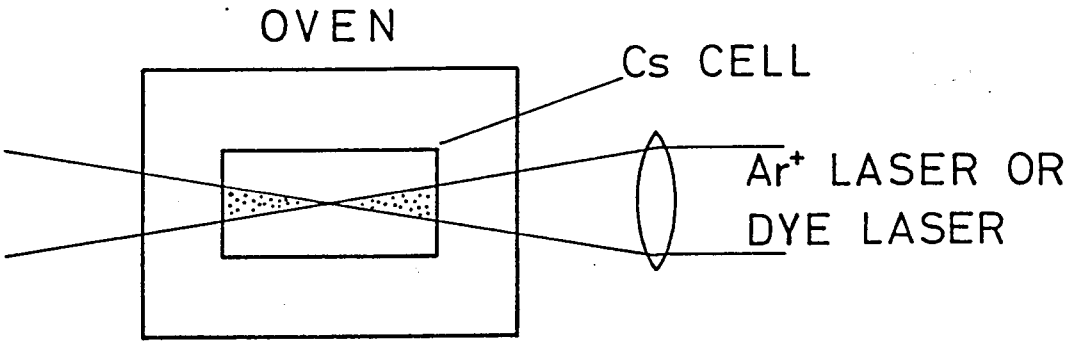

Fig. 3.17 Experimental setup of CsH laser snow formation. The cell used was made of alkali-resistant aluminosilicate (Corning 1720) glass.

Table 3.6 Conditions of Cs cells used in our experiment and results of experiment of particle formation.
The symbol "o" indicates that particle formation was observed, and the symbol "x" indicates that it has not been observed.

Cell No.	P_{H_2} (Torr)	P_{He} (Torr)	Exciting light source	
			Ar^+ laser	Dye laser
C-1	27	0	x	o
C-2	4	550	o	o

(Corning 1720) glass and baked at 650°C in a vacuum of 10^{-6} Torr before filling with Cs vapor. We used two cells; one containing Cs with 27 Torr of H_2 (cell No. C-1) and the other containing Cs with 4 Torr of H_2 and 550 Torr of He (cell No. C-2). Here, 550 Torr of He was used as a buffer gas. In Table 3.6, we show the conditions of these cells and the results of the experiment of particle formation. When the baking was not sufficient, we could not observe the particle formation. This must be due to the presence of Na_2O on the surface of the walls, which reacts quickly with H_2, resulting in a considerable decrease of H_2 pressure.

The cell was placed inside an oven and the cell temperature was changed from room temperature up to about 340°C, corresponding Cs density is from 5×10^{10} to 9×10^{16} cm^{-3}. In the experiment, a particular attention was paid on the temperature distribution to avoid the convection within the cell. When we increase the density of the Cs atoms by raising the cell temperature and/or when we increase the power density of the incident laser beam, the small particles become visible. As mechanisms of the particle formation are different for different excitation schemes, we have to discuss the particle formation for each case.

When we used the dye laser beam as an exciting light, we could observe the particle formation only if the dye laser wavelength was tuned at 601.0 nm ($6P_{1/2} - 8D_{3/2}$), 621.3 nm ($6P_{3/2} - 8D_{5/2}$), 584.5 nm ($6P_{3/2} - 9D_{5/2}$), 583.9 nm ($6P_{1/2} - 10S_{1/2}$), and 603.4 nm ($6P_{3/2} - 10S_{1/2}$), finely. We used

the Ar^+ laser pumped dye laser (Rhodamine 6G), whose oscillating wavelength range was from 570 to 645 nm. The spectral width (full-width at half-maximum) of this dye laser was less than 40 GHz; presumably, about 10 GHz at 100 mW of output power.

We have observed the particle formation at the temperature higher than 175°C by using the Cs cell C-2 containing H_2 at 4 Torr and He at 550 Torr. The wavelength and the power of the dye laser beam were 601.0 nm and about 100 mW, respectively. We have also observed the particle formation by using the dye laser tuned at 621.3, 584.5, 583.9, and 603.4 nm at temperature of about 260°C. Figure 3.18 shows the photograph showing the scattering of the laser beam from the produced particles. The experimental conditions were $T = 261°C$, $\lambda = 584.5$ nm, and $P = 70$ mW. As the tuning of the dye laser at these wavelengths is necessary for producing particles, there is no doubt that the particle formation is related to the transition from the 6P states to the highly excited states of a Cs atom. When we used the cell C-1 ($P_{H_2} = 27$ Torr), the particle formation was also observed when the temperature was about 300°C and at the laser power about 250 mW. Finer tuning to the transition wavelengths than the case of the cell C-2 was required. These results are explained as follows. As there are less pressure broadening of spectral lines of a Cs atom in the cell C-1, the finer tuning of the dye laser is necessary to excite Cs atoms to highly excited states. Moreover, as excited Cs atoms and produced CsH molecules diffuse from laser beam rapidly in the low buffer gas

pressure condition, it is necessary to produce more Cs* and CsH than those required in the higher buffer gas pressure. It has been also observed with the naked eye that the particles in C-1 was moving faster than those in C-2.

When we used the Ar^+ laser beam at 457.9 nm line, we could also observe the particle formation in the cell C-2 at temperature of 240°C and at the laser power of about 50 mW even if the laser beam was expanded to about 15 mm in diameter. However, we have not observed the particle formation in the cell C-1 yet at $T \lesssim 350$°C and at about 200 mW of the Ar^+ laser power even if the laser beam has been focussed by a lens. As described in III.3.1, the excitation of Cs atoms by the Ar^+ laser 457.9 nm line is made through the far wing of the pressure broadened lines at 455.5 nm ($6S_{1/2} - 7P_{3/2}$) and 459.3 nm ($6S_{1/2} - 7P_{1/2}$), the rate of the excitation of Cs atoms becomes extremely low in the cell without buffer gas. This is one of the reasons why the particle formation has not been observed in the cell C-1. The other reason is that the faster diffusion of excited atoms and produced CsH molecules in the cell without buffer gas. These two effects require more Cs* and CsH to be produced in order to produce CsH particles as described above.

The particle formation in the cell C-2 by the dye laser and Ar^+ laser beams have different threshold laser power densities. We can observe the particle formation by broad Ar^+ laser beam at 457.9 nm, whereas we must focus the dye laser beam to observe the particle formation. This is because the highly excited Cs atoms, which react with H_2 and

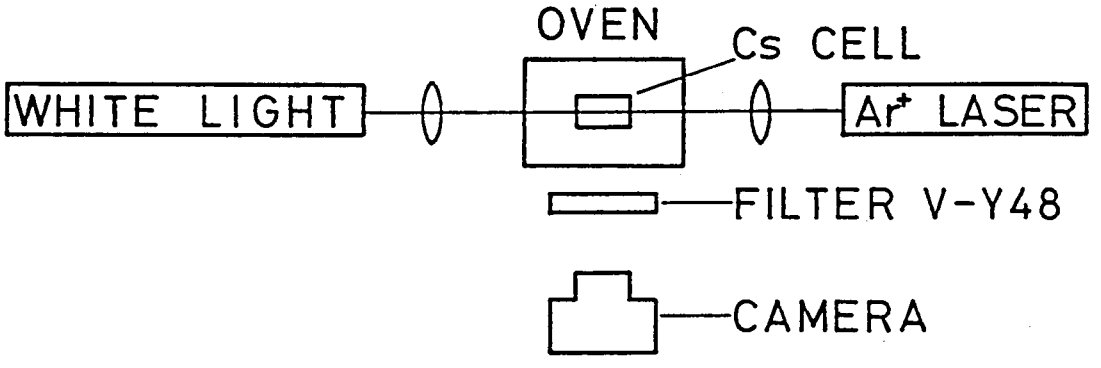

Fig. 3.19 Observation setup of white light scattering by CsH laser snow produced by the Ar^+ laser 457.9 nm line.

produce CsH molecules, are produced by the single-photon absorption in the case of the Ar^+ laser 457.9 nm line and by the step-wise excitation (two-photon process) in the case of the dye laser beam.

As a large number of particles are produced by the Ar^+ laser 457.9 nm line, we can observe it under the illumination of a white light and photographs of the scattering of the white light can be taken. As shown in Fig. 3.19, the white light beam was applied to the cell from the opposite direction to the Ar^+ laser beam, which overlapped to each other within the cell. A filter V-Y48, omitting the wavelengths shorter than 480 nm, was used to eliminate the Ar^+ laser 457.9 nm line. A photograph of the particles is shown in Fig. 3.20. The diameter of the white light beam was about 10 mm and that of the Ar^+ laser beam was about 15 mm. The cell temperature was 334°C and the Ar^+ laser power was 210 mW.

We can see the stripes in the cell from Fig. 3.20. These stripes move downwards about 1 mm/sec, and cause the oscillation of the scattered light intensity. This phenomenon was observed also by Tam *et al.*[3] as an oscillation of the scattered light intensities from the CsD particles produced by the dye laser 601.0 nm line. The oscillation is now understood as follows. The density of laser produced CsH (or CsD) molecules builds up rapidly in the vicinity of the laser beam until the supersaturation of CsH (or CsD) molecules leads to nucleation of CsH (or CsD) crystals. When sufficient CsH (or CsD) crystal

nuclei are formed, they act as efficient sinks for the laser-produced CsH (or CsD) molecules, and depress the CsH (or CsD) molecular density enough to prevent further formation of nuclei. The nuclei grow rapidly due to accretion of laser-produced CsH (or CsD) molecules and they begin to fall down from the laser beam. The density of CsH (or CsD) molecules builds up rapidly and nucleation of CsH (or CsD) crystals may take place again. This leads to the oscillation in production of particles.

When we used the Ar^+ laser operating at 476.5, 488.0, and 496.5 nm, we could also observe the particle formation in the cell C-2 at the temperature 240°C and at the laser power of 800 mW. This is because these lines can excite Cs_2 molecules and produce the highly excited states of atoms and molecules through collisional excitation or ionization. But as the absorption coefficients of Cs_2 at the 514.5 nm line are low, particles were not produced even at 1.5 W at 240°C.

III. 3. 4 Spectroscopy of CsH Molecules

As mentioned already, the laser-produced particles described in this section are considered to be CsH crystals. According to Tam *et al.*[1] the reasons are as follows:

(1) The presence of gaseous hydrogen is necessary for particle formation, and gettering it out results in no particle formation.

(2) A white deposit forms on the cell wall in a vertical line just below the point of exit of the laser beam.

(3) If a cell containing about 100 Torr of hydrogen is excited with the 457.9 nm line of the Ar^+ laser, one can see a progression of doublet fluorescent lines of the CsH.

Picqué *et al.*[4] and Sayer *et al.*[10] also reported that they observed the emission lines of the CsH by using the dye laser beams at 455.5 and 459.3 nm. We also observed the emission lines of the CsH excited by the Ar^+ laser 457.9 nm line. The experimental setup is shown in Fig. 3.21. The cells used were C-1 (P_{H_2} = 27 Torr) and C-2 (P_{H_2} = 4 Torr, P_{He} = 550 Torr), which we mentioned before. The low pass filter V-Y48 was used in order to eliminate the strong scattered light of 457.9 nm laser line by the produced particles. The other instruments were the same as described before. The cell temperature was 300°C - 360°C in this experiment. The observed laser-induced fluorescence of CsH and Cs_2 in C-1 are shown in Fig. 3.22. As there was a little back ground light, we subtracted the back ground from detected signal and obtained the molecular fluorescence of CsH and Cs_2. The fluorescence of CsH at λ = 499.12 nm and λ = 496.48 nm shown in Fig. 3.22 correspond to the transitions of $A^1\Sigma^+$ (ν' = 19, J' = 10) → $X^1\Sigma^+$ (ν'' = 2, J'' = 11) and $A^1\Sigma^+$ (ν' = 19, J' = 10) → $X^1\Sigma^+$ (ν'' = 2, J'' = 9), respectively. The laser power dependence of the observed laser-induced fluorescence is shown in Fig. 3.23, where

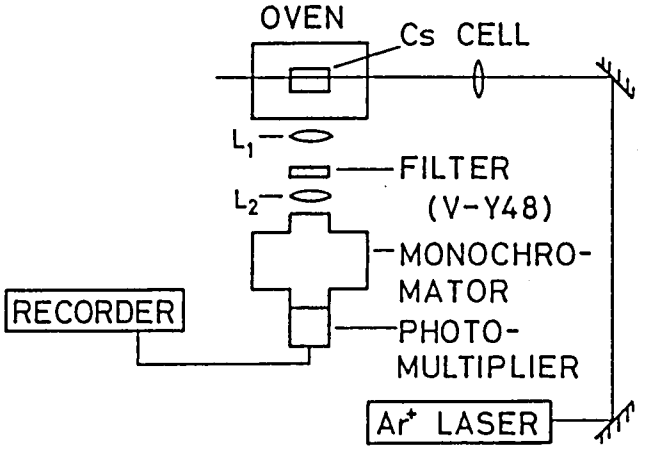

Fig. 3.21 Observation system of CsH fluorescence. Under conditions where particles were formed, the low pass filter V-Y48 was used in order to eliminate the strong scattered light of 457.9 nm laser line by the produced particles.

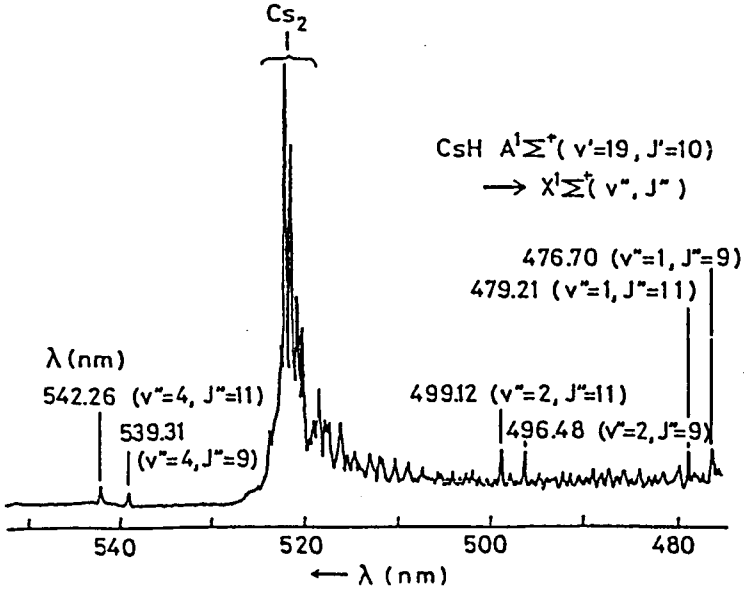

Fig. 3.22 Observed laser-induced fluorescence of CsH and Cs_2 excited by the Ar^+ laser 457.9 nm line at 200 mW. The cell C-1 (P_{H_2} = 27 Torr) was used and the cell temperature was 360°C.

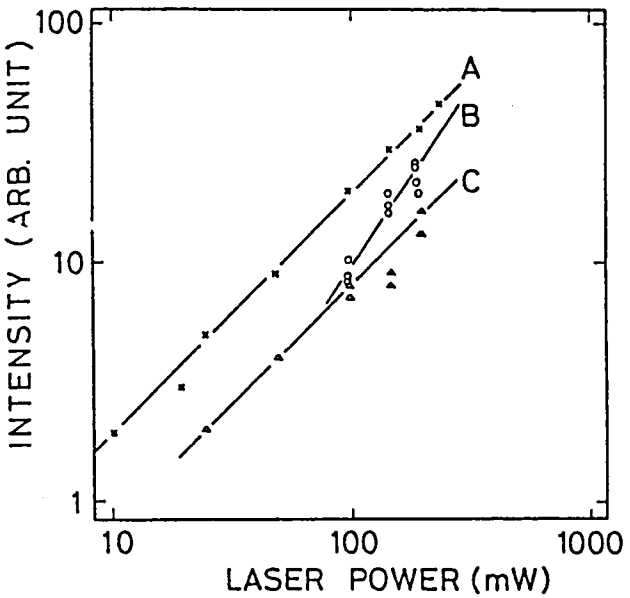

Fig. 3.23 Laser power dependence of the observed laser-induced fluorescence of Cs_2 at the cell C-2 (A), CsH at the cell C-1 (B), and CsH at the cell C-2 (C). The experimental conditions were as follows.

	Symbol	λ(nm)	Gas pressure (Torr)		T(°C)	R.P.(nm)	I vs. L.P.
			P_{H_2}	P_{He}			
A	x	520	4	550	300	1.5	$I \propto L.P.$
B	o	496.5	27	0	340	0.3	$I \propto (L.P.)^{3/2}$
C	Δ	496.5	4	550	340	1.5	$I \propto L.P.$

λ ; Wavelength of observed light

R.P.; Resolving power of monochromator

I ; Intensity of laser-induced fluorescence

L.P.; Laser power

A shows the fluorescence of Cs_2 observed in the cell C-2 and B and C show the fluorescence of CsH observed in the cells C-1 and C-2, respectively. In Fig. 3.23, the lines A and C can be expressed by the linear lines with a slope 1 and the line B has a slope 1.5. The experimental conditions for A, B, and C in Fig. 3.23 are as follows. The cell temperature was 300°C for the line A and 340°C for the lines B and C. The resolving power of the monochromator was 1.5 nm for the lines A and C,and 0.3 nm for the line B.

From the consideration of the excitation mechanism of Cs_2, we expected that the intensity of the fluorescence of Cs_2 is proportional to the excitation laser power, which has been confirmed by the fact that the line A has a slope 1. The intensity of the fluorescence of CsH had been reported to be proportional to the $\frac{3}{2}$ power of the incident laser intensity by Tam *et al.*[1,89] at the pressure between 3 Torr and 50 Torr of H_2 in the cell. They considered that the CsH molecules are produced by the laser light at a rate proportional to the laser intensity and are destroyed mainly by collisions with other CsH molecules. Such collisions lead to $(CsH)_2$ dimers, and hence the CsH concentration is proportional to the square root of the laser intensity. This implies that the intensity of the fluorescence from CsH* is proportional to the $\frac{3}{2}$ power of the laser intensity. This is consistent with the slope of the line B showing the intensity of the fluorescence of CsH shown in Fig. 3.23. But, for the case C, the intensity of the fluorescence of CsH, which was observed in the cell C-2,

was proportional to the incident laser power. This means that the density of molecules or atoms to be excited is independent of the incident laser power such as for the case of Cs_2. But this is not true for the case of CsH because CsH molecules are produced by the incident laser beam. We think this is explained as follows: The production of CsH particles consumes CsH molecules and make the density of CsH molecules constant, and hence the intensity of fluorescence of CsH becomes proportional to the incident laser power.

From these experimental evidences of existence of CsH molecules and the microscopic observation of existence of crystals, the laser-produced particles are considered now to be CsH crystals when the cell temperature is relatively low($T < 270°C$). However, at relatively high temperature $T > 330°C$, these laser-produced particles are considered to be mainly Cs droplets because CsH crystals may be decomposed into H_2 gas and Cs metal at this temperature.

III. 3. 5 Discussions

We have described the experiment of laser-production of CsH particles and its relevant experiments such as spectroscopy of excited Cs atoms, Cs_2 molecules, and CsH molecules. In this subsection, we discuss the chemical processes of laser-production of CsH molecules.

Detailes of chemical reactions may be different for the energies and states of excited Cs atoms reacting with H_2 molecules, and there are several excitation mechanisms as mentioned already. But it has been considered that these chemical reactions can be broadly classified as a direct reaction and an indirect reaction.

Tam *et al.*[1] proposed the direct reaction of Cs* and H_2 which is expressed as

$$Cs^* + H_2 \rightarrow Cs + H. \qquad (3.27)$$

Sayer *et al.*[10] proposed the indirect reaction of Cs* and H_2 or the reaction of Cs and $H_2(v)$, which is expressed as

$$\left.\begin{aligned} Cs^* + H_2 &\rightarrow Cs + H_2(v), \\ H_2(v) + Cs &\rightarrow CsH + H. \end{aligned}\right\} \qquad (3.28)$$

From quantitative experiments, Sayer *et al.* found that the rate coefficient of CsH formation is proportional to the densities of Cs(7P), H_2, and Cs in the ground state, and that the reactions can be summarized as follows:

$$Cs(7P) + H_2 + Cs \rightarrow CsH + \text{other products}. \qquad (3.29)$$

They guessed Reaction (3.29) is realized by the processes as

$$Cs(7P) + H_2 \rightarrow Cs(6S) + H_2(\nu), \tag{3.3}$$

$$Cs(6S) + H_2(\nu) \rightarrow CsH + H. \tag{3.4}$$

But we note the direct processes

$$Cs(7P) + H_2 \rightarrow CsH + H, \tag{3.1}$$

$$Cs(6S) + H + X \rightarrow CsH + X, \tag{3.2}$$

where X represents any atom or molecule in the ground electronic state, are also consistent with Reaction (3.29).

When the H_2 pressure is higher than a few Torr,[100,101] the quenching of Cs* by H_2 is faster than the lifetime of Cs(7P) ($\sim 10^{-7}$ sec) (see Table 3.4) so that Cs* decays mainly by quenching due to H_2. Moreover the lifetime of $H_2(\nu)$ is also long ($\sim 10^{-6}$ sec) as described in III.2.2, so that the density of $H_2(\nu)$ becomes high. But about only half of energy of electronic state is generally transferred to vibrational state by collisions,[102,103] and so most of $H_2(\nu)(\nu = 3,4)$ produced have not enough energy to produce CsH. Since the dissociation energy of CsH is 1.86 eV (D_e(CsH)), only few percent of $H_2(\nu)(\nu \geq 6)$ have the energy which can produce CsH by collisions between Cs(6S) and $H_2(\nu)$ (Eq. (3.4)). Anyway, since we have not known the reaction rates

for the processes (3.1) - (3.4), we cannot tell which process, direct or indirect, is predominant.

III. 4 NaH Laser Snow

We describe the laser-production of NaH particles (NaH laser snow) in this section. First of all, we describe the excitation of Na atoms and molecules by lasers. Next, we describe the NaH laser snow formation by the excitation of Na_2 molecules and Na atoms. We describe also the experimental evidence of the dissociation of the produced NaH laser snow by the collisions with Na atoms in the 3P states.

III. 4. 1 Excitation of Na Atoms and Molecules by Lasers

The aim of our experiment of the excitation of Na atoms and molecules by different wavelength laser beams is to know how Na atoms and molecules are excited by lasers and to know which excited states of atoms and molecules produce NaH molecules.

We used the Ar^+ laser and the Ar^+ laser pumped dye laser as the exciting light source, but the wavelength of the dye laser was different from the case of Cs. The experimental setup is shown in Fig. 3.24. The cell used was cylindrical with about 1.5 cm i.d. and about 5 cm length, which was made of alkali-resistant aluminosilicate (Corning 1720) glass. In order to fill the cell with the pure sodium, we distilled a small amount of sodium metal several times in a vacuum of about 10^{-5} Torr. The cell was baked at 650 ℃ in a vacuum of 10^{-6} Torr for about 24 hours before filling with Na vapor and with H_2

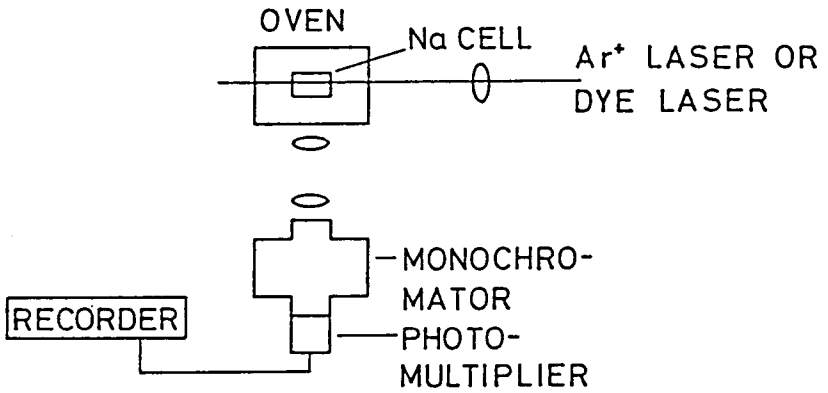

Fig. 3.24 Experimental setup of the excitation of sodium atoms and molecules.

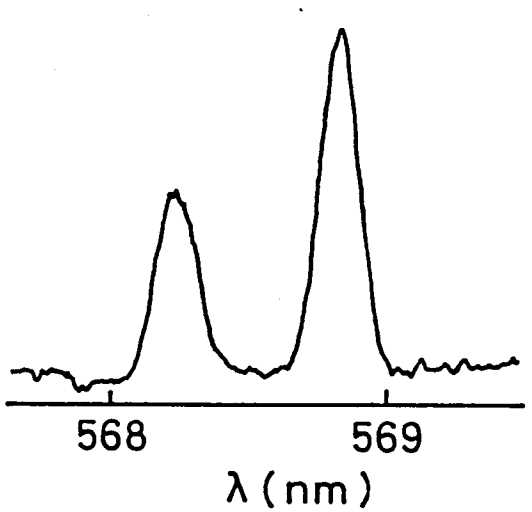

Fig. 3.25 Typical spectra of the fluorescence from the 4D states to the 3P states of Na ($\lambda = 568.3$ nm ($3P_{1/2} \leftarrow 4D_{3/2}$) and $\lambda = 568.8$ nm ($3P_{3/2} \leftarrow 4D_{3/2,5/2}$)). These fluorescence lines were observed when the cell temperature was 278°C and the cell, which was filled only with Na, was irradiated by the D_2 line ($\lambda = 589.0$ nm ($3S_{1/2} - 3P_{3/2}$)).

and/or He gases. The cell was placed in a transparent glass oven which was carefully designed so that the convection within the cell was minimized.

Let us consider the excitation of Na atoms by the dye laser tuned to one of the Na D lines. It is well known that the intense dye laser beam tuned to one of the Na D lines can excite Na atoms not only to one of the 3P states but also to the other 3P state and to highly excited states such as 5S and 4D.[73,104-107] The typical spectra of the fluorescence from the 4D states to the 3P states are shown in Fig. 3.25. One of the excitation mechanisms to the highly excited states were reported by Allegrini *et al.*[73] They considered that the excitation to the highly excited states is due to the collisions between the 3P state atoms, i.e.,

$$Na(3P) + Na(3P) \rightarrow Na(3S) + Na(nX) + \Delta E, \qquad (3.32)$$

where nX represents a highly excited state and ΔE is the energy defect or excess for the level nX with respect to twice the electronic energy of the colliding Na(3P) atoms (see Fig. 3.4). In this model, this ΔE is relatively large ($\Delta E \simeq +700$ cm^{-1} for the level 5S and $\Delta E \simeq -600$ cm^{-1} for the level 4D). Then, to remove the difficulty of the large energy defect or excess, Geltman[108] suggested another mechanism for this excitation, wherein he emphasized the importance of the laser-induced ionization or stimulated radiative Penning effect of the 3P state

atoms, i.e.,

$$Na(3P) + Na(3P) + h\nu \rightarrow Na(3S) + Na^{+} + e^{-}, \qquad (3.33)$$

But, recently, Kopystynska *et al.*[105] and Krebs *et al.*[106] have shown that the highly excited states of sodium atoms are produced by the energy transfer collisions between 3P state atoms and suggested that the mechanism shown by Allegrini *et al.*[73] is correct.

Next, let us consider the excitation of Na_2 molecules by the Ar^+ laser beam. It is well known that almost all of the Ar^+ laser lines can excite Na_2 molecules from the ground electronic state $X\,^1\Sigma_g$ to the $B\,^1\Pi_u$ state.[77,109-111] We made the experiments on the excitation of Na_2 molecules by using the several laser lines. The experimental setup is shown in Fig. 3.24. The Ar^+ laser lines used were 457.9, 465.8, 476.5, 488.0, 496.5, 501.7, and 514.5 nm lines. The laser-induced fluorescence from $Na_2(B\,^1\Pi_u)$ state could be observed at excitation by most of the Ar^+ laser lines except for 457.9 nm and 465.8 nm in our experiment. The typical spectra of fluorescence in the case of the excitation by the Ar^+ laser 488.0 nm line are shown in Fig. 3.26. The fact that we could not observe the fluorescence from $Na_2(B\,^1\Pi_u)$ molecules under the irradiation of the Ar^+ laser 457.9 nm and 465.8 nm lines is considered to be due to the low excitation efficiencies and the low intensities of these laser lines.

The density of the excited Na_2 molecules is considered to be directly proportional to the intensity of the Ar^+ laser beam. But, as we used the Ar^+ laser oscillating on multi-lines for particle formation and changed its total power by changing the discharge current of the Ar discharge tube, the relative intensities of the Ar^+ laser lines were probably changed. Moreover, the efficiencies of production of $Na_2(B\,^1\Pi_u)$ molecules are different in laser lines. Therefore, strictly speaking, the density of $Na_2(B^1\Pi_u)$ molecules is not proportional to the total Ar^+ laser intensity. Figure 3.27 shows the intensity of laser-induced fluorescence from excited state of $Na_2(B^1\Pi_u)$ (I_F; λ =504.4 nm), in which we see that the fluorescence is almost proportional to the Ar^+ laser power I_L.

We intended also to excite Na atoms to highly excited states by the dye laser beam, i.e., we applied the dye laser beam at λ =614.5 nm, which corresponds to the transition between the $3P_{1/2}$ state and the $5S_{1/2}$ state, or 578.7 nm, which has just a half energy of the transition between the 3S state and the 4D state. When the density of $Na(3P_{1/2})$ is high, the 614.5 nm light excites Na atoms in the $3P_{1/2}$ state to the $5S_{1/2}$ state. When the 578.7 nm laser light is strong, the transition between the 3S state and the 4D state may occur frequently by absorbing two photons of the 578.7 nm light simultaneously. Since these dye laser beams can excite Na_2 molecules to the $A^1\Sigma_u$ state, which produce Na(3P) by energy transfer collisions between $Na_2(A^1\Sigma_u)$ and Na(3S),[76] we could observe the strong D_1 and D_2 fluorescence . However, we could

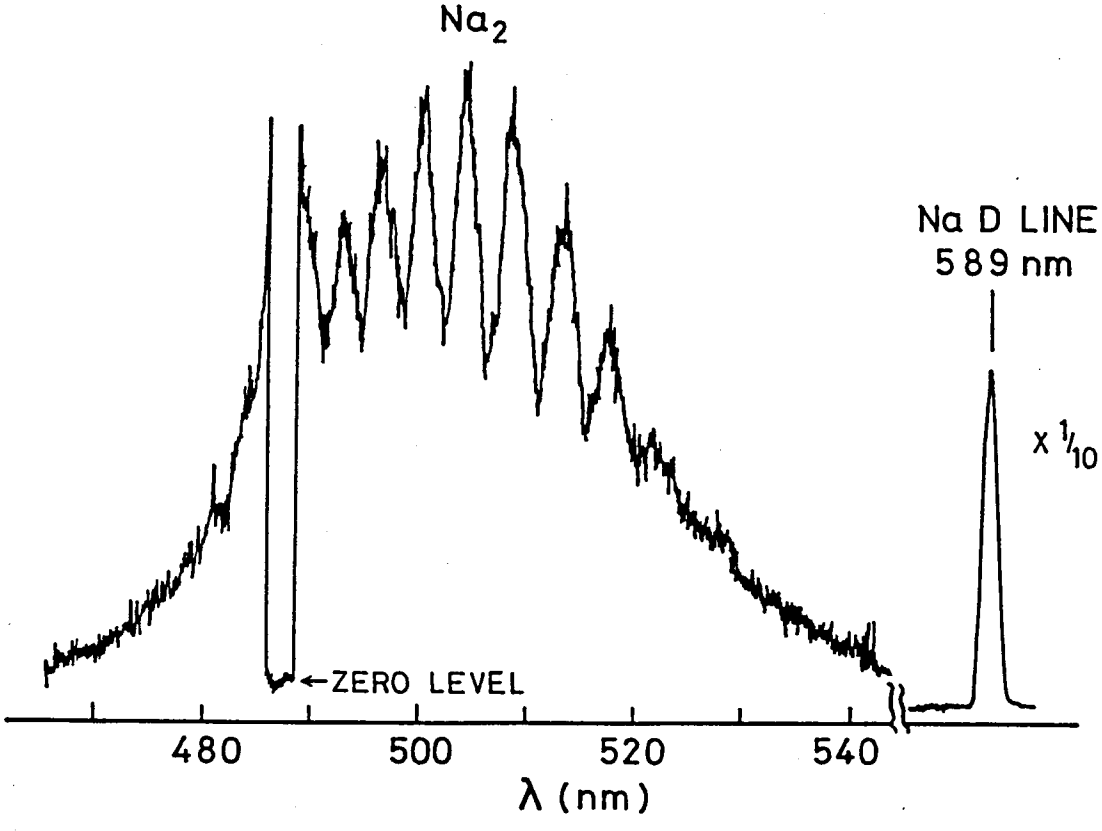

Fig. 3.26 Typical spectra of laser-induced fluorescence of Na_2 excited by the Ar^+ laser 488.0 nm line. The cell temperature is 230°C and the cell contains 620 Torr of He.

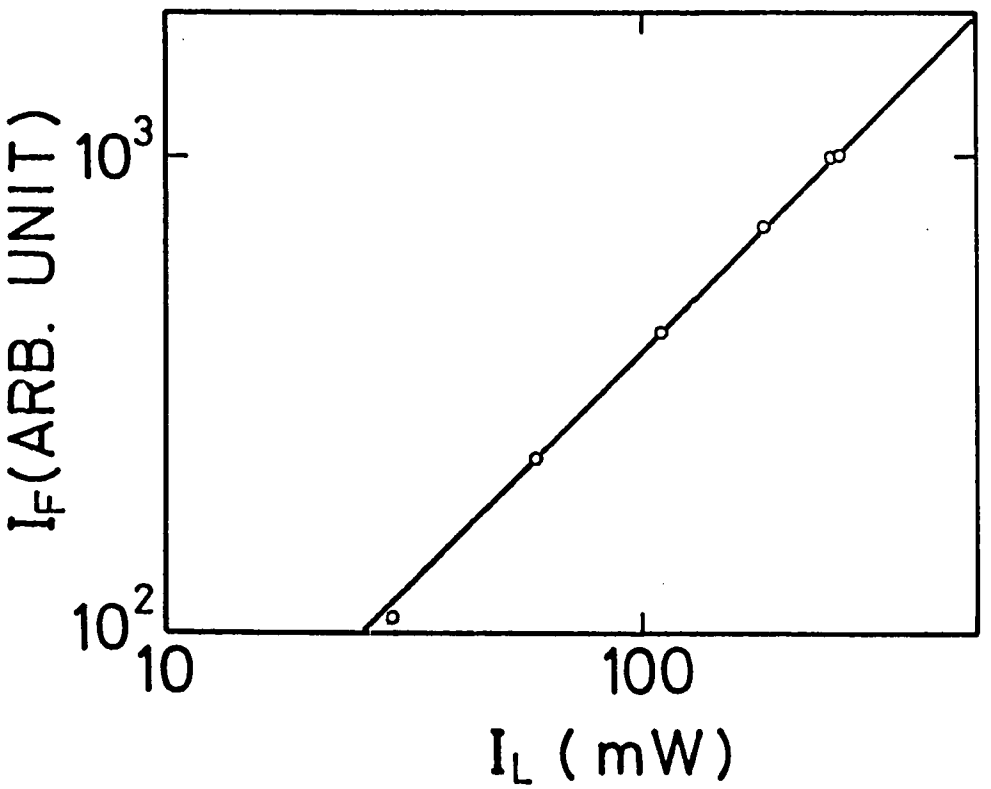

Fig. 3.27 Intensity of laser-induced fluorescence of $Na_2(B^1\Pi_u)$ (I_F; $\lambda = 504.4$ nm) vs. the Ar^+ laser power (I_L). The linear line in the figure has a slope 1.

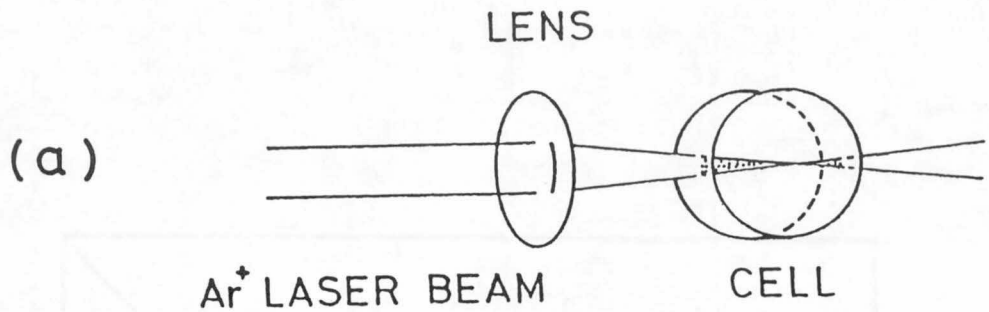

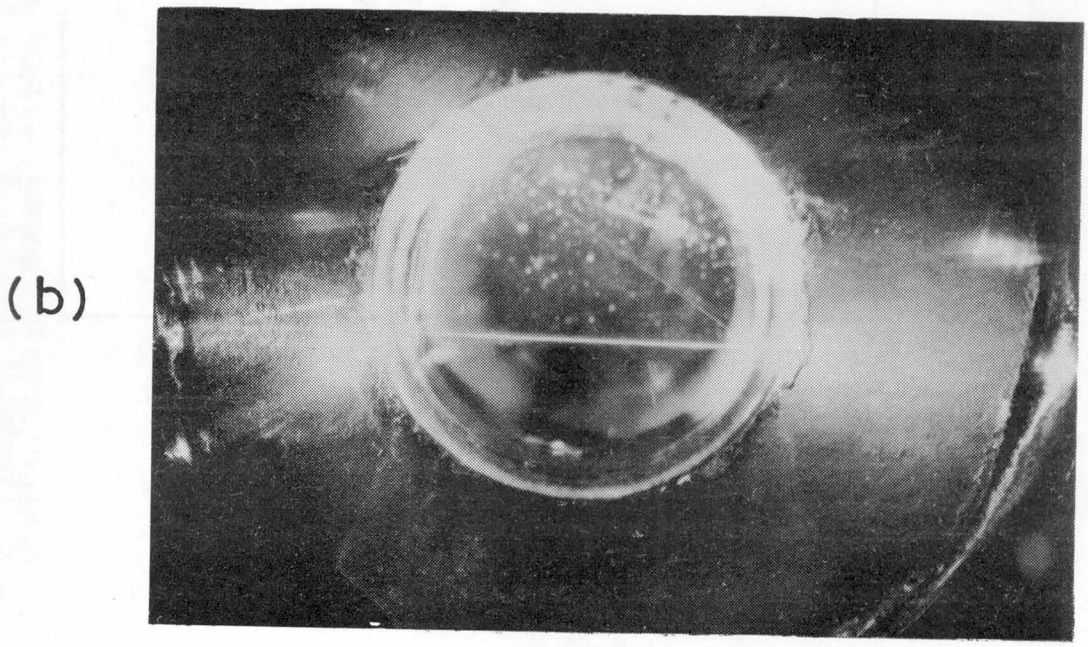

Fig. 3.28 (a) Experimental setup, and (b) a photograph showing the Mie scattering of the Ar^+ laser beam by the produced NaH particles.

not observe the fluorescence from the 5S and 4D states in our experiment.

III. 4. 2 Particle Formation by the Excitation of Na_2

Figure 3.28 (a) shows the simple experimental setup used to observe the NaH particle formation by the Ar^+ laser beam. In this experiment, we did not select a particular line of the Ar^+ laser lines, so that about six lines were simultaneously oscillating in the visible region. The Ar^+ laser beam was focussed by a lens (focal length ; 10 cm) and applied to the glass cell containing Na vapor mixed with H_2 gas of about 10 Torr and He gas of about 500 Torr, which was used as a buffer gas. We used the high pressure of He buffer gas to produce more particles and to make the movement of the produced particles slow enough to observe individual visible-size particles, although the particle formation could be observed in a cell without buffer gas as described later.

It is noted that the cell should be baked out at a temperature higher than 650 ℃, in a vacuum of about 10^{-6} Torr, for about 24 hours before filling with Na vapor and with H_2 and/or He gases. When the baking was not sufficient, we could not observe the particle formation. This fact must be due to the presence of Na_2O on the surface of the

walls, which reacts quickly with H_2 and results in a considerable decrease of H_2 pressure.

Figure 3.28 (b) is a photograph showing the strong Mie scattering of the Ar^+ laser beam by the produced particles, which was taken about 15 sec after the irradiation, in the case that the temperature of the cell was 280°C and the laser power was about 1 W. Within a few seconds after the laser irradiation, we could see the produced particles. The largest particles fell down from the laser beam through gravity with a velocity of about 1 mm/sec. By equating the force of gravity to the viscous retarding force of He buffer gas, we could estimate the size of the largest particles to be about 1 μm.

We measured the threshold Ar^+ laser power for the particle formation by varying the temperature of the cell from about 245°C to 285°C which corresponds to the Na_2 density from 1.4×10^{11} to $1.1 \times 10^{12} cm^{-3}$. Figure 3.29 shows the threshold Ar^+ laser power I_{Th} for particle formation as a function of Na_2 density n_{Na_2}, which was determined from the measured temperature. We see from Fig. 3.29 that the threshold condition for NaH particle formation can be expressed as

$$I_{Th}(T)\, n_{Na_2}(T) = \text{const.} \qquad (3.34)$$

When the saturation in absorption of the Ar^+ laser beam can be neglected, the density of sodium molecules in the $B^1\Pi_u$ state is thought

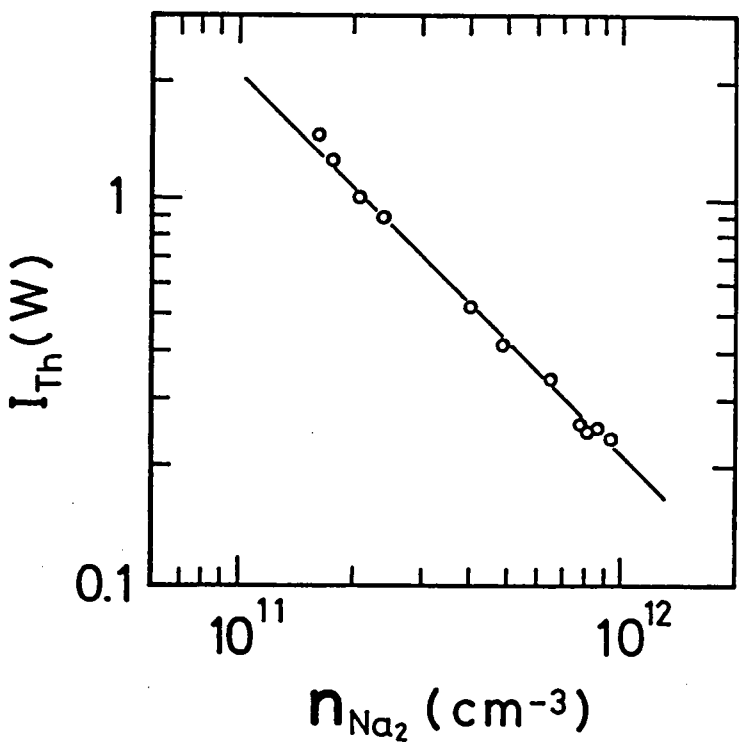

Fig. 3.29 Threshold Ar^+ laser power I_{Th} for particle formation as a function of Na_2 density n_{Na_2}.

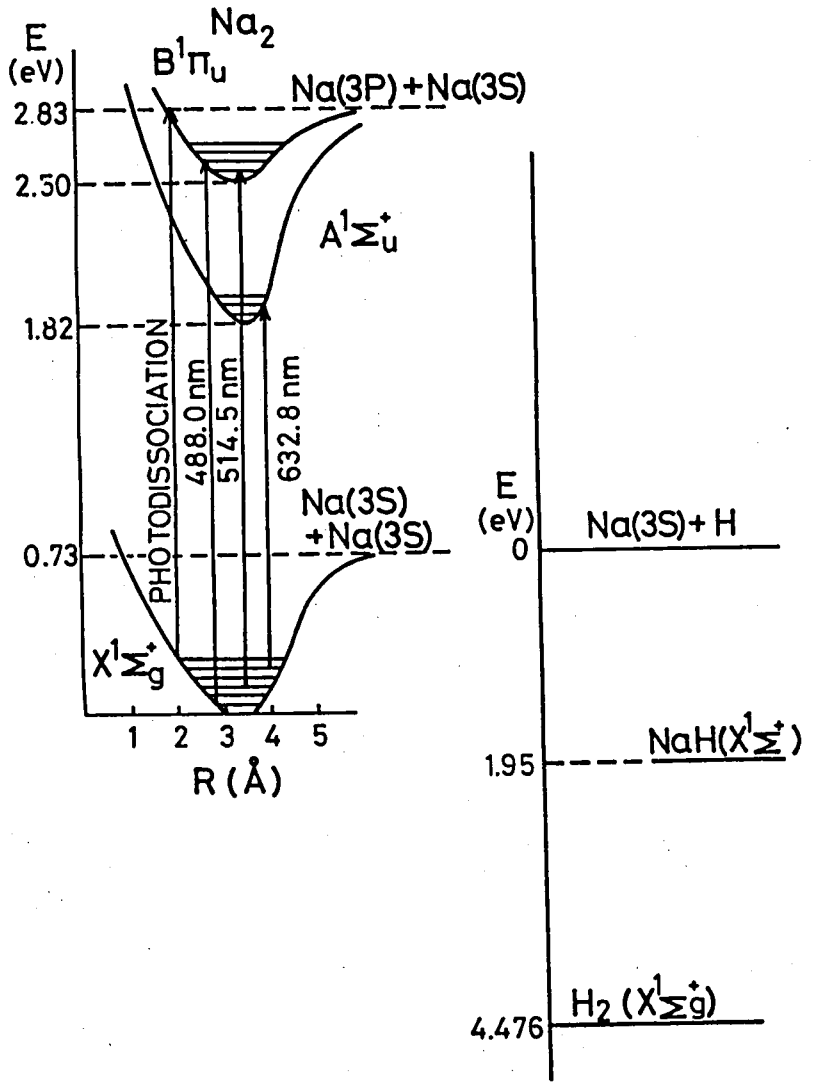

Fig. 3.30 Potential curves for Na_2 and the dissociation energies of NaH and H_2. The dissociation energies of the ground state of Na_2 ($D_0(Na_2) = 0.73$ eV),[70] NaH ($D_0(NaH) = 1.95$ eV),[112] and H_2 ($D_0(H_2) = 4.476$ eV)[70] are also shown.

to be proportional to the $I_{Th} n_{Na_2}$. Consequently, the threshold Condition (3.34) shows the fact that when the density of sodium molecules in the $B\,^1\Pi_u$ state reaches a certain value, the density of the produced NaH molecules become its critical value $n_{NaH,c}$ for condensation.

In the present stage, the most probable chemical reaction to produce the NaH molecules is considered to be

$$Na_2(B\,^1\Pi_u) + H_2 \rightarrow 2NaH, \tag{3.35}$$

which is energetically possible as described below. The energy relations are shown in Fig. 3.30. The energy of the Na_2 $B\,^1\Pi_u$ state at the bottom of the potential well is 2.52 eV[70] above the bottom of the Na_2 $X\,^1\Sigma_g$ state, and the dissociation energies of Na_2 and H_2 in the ground states are known to be $D_0(Na_2) = 0.73$ eV and $D_0(H_2) = 4.476$ eV.[70] The dissociation energy of NaH (D_e(NaH)) is not accurately known. In a few references, it has been calculated to be 1.79 eV[86] and 1.92 eV,[85] and it has been also estimated to 2.02 eV[71] by the extrapolation of the measured ground state vibrational levels. We will use the latest value of 2.02 eV as D_e(NaH) and 1.95 eV as D_0(NaH)[112] in this section. The energies required for the reactions between Na_2 and H_2 becomes

$$Na_2(B^1\Pi_u) + H_2 \rightarrow 2NaH + 1.21 \text{ eV}, \qquad (3.36)$$

$$Na_2(X^1\Sigma_g) + H_2 \rightarrow 2NaH - 1.31 \text{ eV}. \qquad (3.37)$$

Here, one may find also that Reaction (3.35) is consistent with the experimentally obtained relation between $I_{Th}(T)$ and $n_{Na_2}(T)$, which is given by Eq. (3.34).

Another possible mechanism to produce NaH molecules is the reaction of sodium atoms in the highly excited states, which may be created indirectly from $Na_2(B^1\Pi_u)$ through the process: $Na_2(B^1\Pi_u) \rightarrow Na(3P) \rightarrow Na(nX)$. The excitation of sodium atoms to the 3P states is possible partially by the dissociation of $Na_2(B^1\Pi_u)$ and partially by the energy transfer collisions of these excited molecules with ground state Na atoms. The energies of the 3P states of Na atoms ($E(Na(3P)) = 2.10$ eV) are not enough to produce NaH molecules by the direct reaction:

$$Na(3P) + H_2 \rightarrow NaH + H - 0.42 \text{ eV}. \qquad (3.38)$$

Therefore the excitation from the 3P states to some highly excited S and D states by (a) collisions between 3P state atoms as described in the preceding subsection, or (b) the laser excitation through the far wings of absorption lines broadened by He gas, is necessary for the direct reaction producing NaH molecules between Na atoms and H_2 molecules. It was found, however, that both of the processes (a) and (b) were not dominant for the production of NaH in the present experiment as follows.

To check the process (a), we excited Na atoms by the dye laser tuned at λ=614.5 nm and 578.7 nm as described in the preceding subsection and intended to observe the fluorescence from the highly excited states and the particle formation. However, we could only observe the strong D_1 and D_2 fluorescence instead of the fluorescence from the highly excited states and the particle formation. It should be noted that the D_1 and D_2 fluorescence for the dye laser excitation is a few times stronger than that for the Ar^+ laser excitation. These results indicate that the excitation of Na to the 3P state is not the main cause of the particle formation, in the case of the Ar^+ laser excitation.

As to the process (b), since the 514.5 nm line of the Ar^+ laser is very close to the transition frequencies from the 3P states to the 6S state ($\Delta\nu \simeq 13\ cm^{-1}$), we considered that this Ar^+ laser line may contribute to the excitation of Na to the 6S state and to the particle formation. However, if we assume that the process (b) is dominant, the threshold laser power as a function of Na_2 density must be given by $I_{Th}^2 n_{Na_2}$ = const., which disagrees with the experimental result given by Eq. (3.34). In this way we could ascertain that the Na_2 molecules in the $B^1\Pi_u$ state excited by the Ar^+ laser beam produce directly NaH by the process of (3.35).

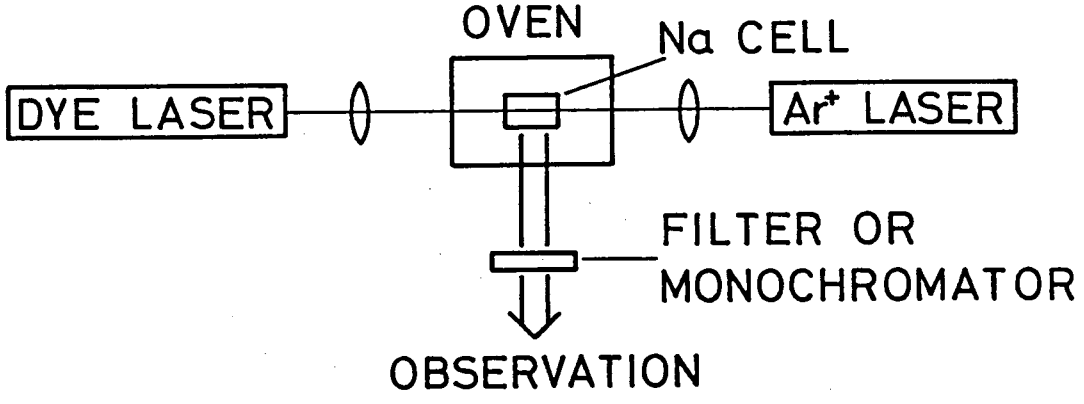

Fig. 3.31 Experimental setup for the observation of the NaH particles produced by the dye laser beam. The Ar^+ laser beam was used for the monitor beam for observing the light of the Mie scattering by the produced particles.

III. 4. 3 Particle Formation by the Excitation of Na

We applied the CW dye laser beam tuned at the Na D_1 or D_2 line onto the cell similar to that described before in order to know whether or not the particle formation takes place by the excitation of Na atoms. The experimental setup is shown in Fig. 3.31. When the dye laser beam tuned at one of the D lines is absorbed by Na atoms, the fluorescence at this resonance line is reemitted. Therefore we can not distinguish the light of the Mie scattering by the produced particles from the fluorescence at this resonance line. To observe snow formation by the Mie scattering, we must use the different setup from Fig. 3.28 (a). As shown in Fig. 3.31, the Ar^+ laser beam was used as a monitoring beam to observe the Mie scattering by the produced particles. This Ar^+ laser beam, which was weakened so as not to produce the NaH laser snow by itself, was applied from the opposite direction to the dye laser beam. Both of the beams were set so that they overlap to each other within the cell. Then, by using a proper filter or monochromator through which only the Ar^+ laser line can pass, we observed snow formation by monitoring the Mie scattering of the Ar^+ laser beam by the produced particles.

In the case of the excitation of Na atoms, the expected direct chemical reactions with H_2 molecules are

$$Na^* + H_2 \rightarrow NaH + H, \qquad (3.39)$$

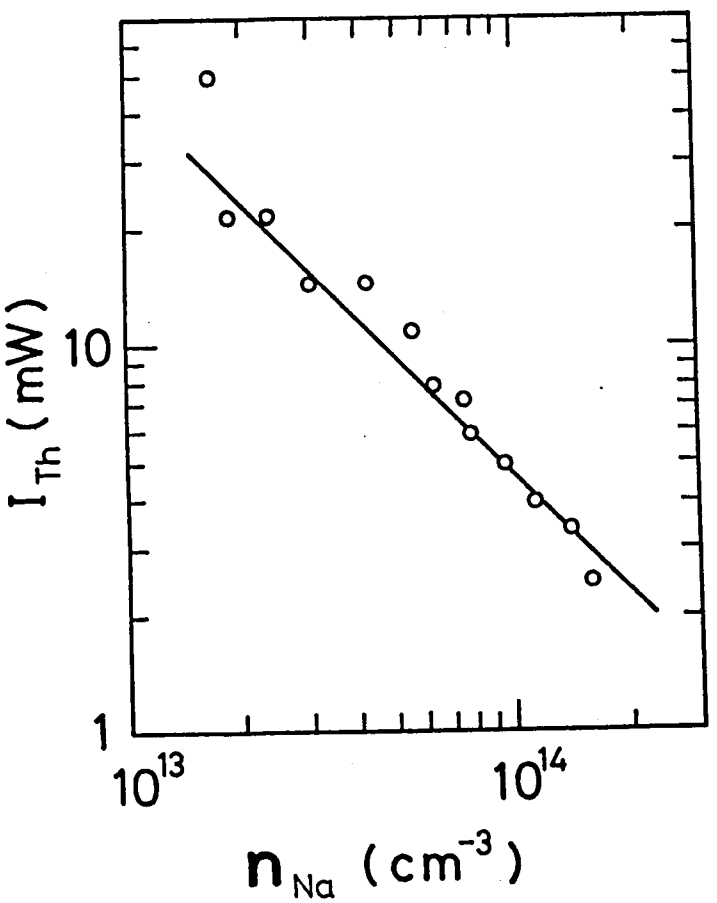

Fig. 3.32 Threshold power I_{Th} of the dye laser tuned at the D_1 line for particle formation as a function of Na density n_{Na}.

$$Na^* + H_2 \rightarrow Na + 2H, \tag{3.40}$$

$$Na + H + He \rightarrow NaH + He. \tag{3.41}$$

When we can neglect a small change in the kinetic energy of the system, we see, from the conservation of internal energies before and after the reactions, that the energy of Na*, i.e., E(Na*), required for Reactions (3.39) and (3.40) must satisfy the following conditions, respectively:

$$E(Na^*) > D_0(H_2) - D_0(NaH) = 2.53 \text{ eV}, \tag{3.42}$$

$$E(Na^*) > D_0(H_2) = 4.476 \text{ eV}. \tag{3.43}$$

From Conditions (3.42) and (3.43) we see that the Na atoms in the 3P states (E(Na(3P)) = 2.10 eV) have not enough energy for Reactions (3.39) and (3.40). However, as described in III.4.1, when the population of the 3P state atoms is large, the excitation to the higher energy states becomes possible. The atoms in the states 3D, 5S, and 4D satisfy Condition (3.42), and those in the states 6S and 5D satisfy Condition (3.43).

Similar to the experiment described in the preceding subsection, we have measured the threshold dye laser power I_{Th} for the formation of particles as a function of the cell temperature. Figure 3.32 shows I_{Th}, when the laser was tuned at the D_1 line, as a function of the sodium density n_{Na} calculated from the cell temperature.

We can see in Fig. 3.32 that I_{Th} is approximately proportional to the inverse of n_{Na} ; i.e., the threshold condition for the particle formation is given by

$$I_{Th}(T)\, n_{Na}(T) = \text{const.} \tag{3.44}$$

When the saturation of the transition from the 3S state to the $3P_{1/2}$ state can be neglected, $I_{Th} n_{Na}$ is approximately proportional to the population of Na atoms in the 3P states (the $3P_{1/2}$ and $3P_{3/2}$ states are completely mixed by the collisions with He atoms). Consequently, Eq. (3.44) implies that the particle formation begins when the population in the 3P states reaches a certain value. Since the 3P states do not have the energies required for Reactions(3.39) and (3.40), the threshold condition must be rewritten as

$$n_{Na(nX)} \propto (I_{Th} n_{Na})^{m} = \text{const.}, \tag{3.45}$$

where Na(nX) is a Na atom in the highly excited state satisfying Conditions (3.42) or (3.43), and m is an integer determined by the excitation mechanism to this state.

There is also another possibility of the indirect chemical reaction process similar to the process of the CsH production proposed by Sayer *et al.*[10)]

$$Na(3P) + H_2 \rightarrow Na(3S) + H_2(v), \tag{3.46}$$

$$Na(3P) + H_2(v) \rightarrow NaH + H. \tag{3.47}$$

These processes satisfy also Condition (3.44) and the energetical requirements. Here, let us recall the reaction between Na atoms in the 3P states and H_2 molecules,

$$Na(3P) + H_2 \rightarrow NaH + H - 0.42 \text{ eV}. \tag{3.38}$$

From the experiment, using a low-pressure sodium discharge lamp, Netten[113] showed that even though Reaction (3.38) is endothermic by about 0.4 eV, the rate of Reaction (3.38) is much faster than (3.47) in his experimental condition. But, in our experiment using the dye laser beam tuned to one of the D lines, the optical excitation density is about 10^7 times larger than that in his experiment, and hence the density of Na(3P) atoms is expected to be about 10^7 times larger than that in his experiment. By applying his theory to the case of large density of Na(3P), we obtain the opposite result that Reaction (3.47) is faster than Reaction (3.38). This means that the reaction mechanism is completely different when the laser beam is used as the exciting light source.
Then we can conclude that Reaction (3.47) is the

more probable reaction than Reaction (3.38) in our case. Here, we cannot conclude clearly which process, the direct reactions (3.39)-(3.40) or the indirect reactions (3.46)-(3.47), is predominant. But from the above discussions, we can write the chemical reaction globally as

$$Na(3P) + Na(3P) + H_2 \rightarrow 2NaH. \qquad (3.48)$$

In the present experiment, the dye laser was tuned at the Na D_1 or D_2 line and the spectral width at half-maximum of the dye laser beam was estimated to be about 10 GHz ($\Delta\lambda = 0.01$ nm). On the other hand, Since we used the cell containing He gas of about 500 Torr, the pressure broadenings of the D lines (full-width at half-maximum) are about 10 GHz. These are obtained by simple calculations from Table 3.5. These values are larger than the Doppler widths(~2 GHz) calculated from Eq. (3.7). Therefore both the dye laser and the pressure broadened D lines have almost the same width in our experiment, and frequency stabilized dye laser is required. If the dye laser is enough tuned to one of the D lines, the most of the longitudinal modes of the dye laser can contribute to the excitation of Na atoms. But, if the wavelength of the dye laser varies, the measurement of the threshold laser power becomes meaningless, because the excitation efficiency changes with the variation of the dye laser wavelength. Therefore we used the following procedure in order to minimize the

fluctuation of the dye laser wavelength. First of all, we tuned the dye laser wavelength at the D_1 line at each temperature and let the fluorescence of the D_2 line be maximum. Next, we changed the dye laser power by using two linear polarizers and by controlling the angle between the polarization directions of these two polarizers because the wavelength of the dye laser varies somewhat with the change of its power in general. We repeated this procedure at each temperature and obtained the results shown in Fig. 3.22. On the other hand, when we use the dye laser, whose wavelength is stabilized by a Faraday filter or other methods of using the spectral lines of atoms or molecules, the tuning and stabilization of the dye laser wavelength is expected to become extremely easy. Therefore, the experimental error could be reduced to a large amount when we use the wavelength-stabilized tunable lasers by the Faraday filter or by the saturated absorption etc.

Next, we changed the laser power in the experimental setup shown in Fig. 3.31, i.e., we applied the Ar^+ laser beam, whose power was set above the threshold value for the particle formation, and the dye laser beam, tuned at the D_1 line at above 10 mW, to the cell. We observed the disappearance of the particles in the region where two beams were overlapped as shown in Fig. 3.33. This phenomenon indicates probably the fact that both NaH particles and NaH molecules are dissociated by the collisions with the Na atoms in the 3P states. Because the Na atoms in the 3P states have energies, 2.10 eV,

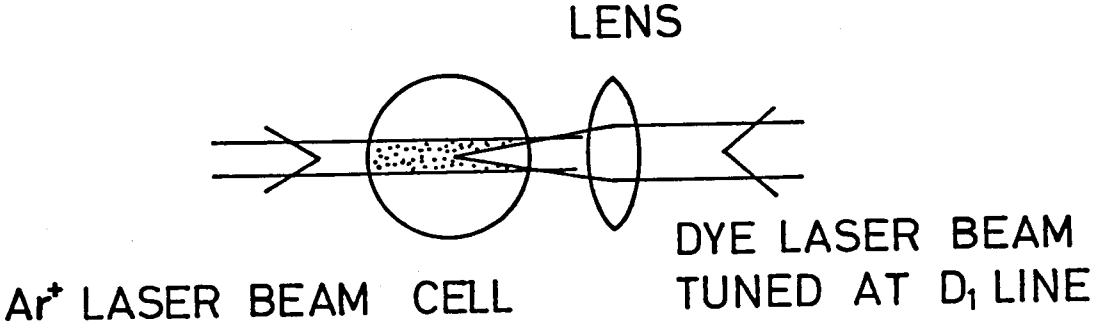

Fig. 3.33 Sketch showing the observed dissociation of NaH particles produced by the Ar^+ laser beam in the region where the dye laser beam tuned at the D_1 line is applied.

higher than the dissociation energy of the NaH, 1.95 eV, the 3P state atoms can dissociate the NaH molecules by collisions. But, in the case of laser-production of other alkali hydride molecules, such as CsH, RbH, and KH, which have been observed so far, the energies of the first P states of Cs, Rb, and K are lower than the dissociation energies of these molecules, so that the collisions with the atoms in the first P states cannot seriously affect the density of the produced alkali hydride molecules.

III. 4. 4 Discussions

We have measured the threshold laser power for particle formation at the range of temperature from 230°C to 290°C and obtained the relations

$$I_{Th}(T)\, n_{Na}(T) = \text{const.}, \tag{3.44}$$

$$I_{Th}(T)\, n_{Na_2}(T) = \text{const.} \tag{3.34}$$

From these results and the energy relations between Na, Na_2, and H_2, we found that NaH laser snow is produced not only by the excitation of Na atoms but also by the excitation of Na_2 molecules, although the experimental conditions were very limited in a small range of the cell temperature and in the filled gas pressure.

Table 3.7 Conditions of Na cells used in our experiment and results of the experiment of particle formation. The symbol "o" indicates that particle formation was observed, and the symbol "x" indicates that it has not been observed. The symbol "-" indicates that the experiment has not been made.

Serial cell No.	P_{H_2} (Torr)	P_{He} (Torr)	Exciting light source	
			Ar^+ laser	Dye laser
A-12	11	470	o	-
A-13	12	480	o	o
A-14	19	480	-	o
A-16	7	490	o	-
A-17	32	0	-	o
A-18	0	600	x	x
A-21	13	490	-	o
A-24	15	98	o	-
A-25	13	500	o	-

As the sodium easily reacts with the glass, even the alkali-resistant aluminosilicate glass cell becomes opaque at temperature higher than 290°C, whereas the ordinary pyrex cell becomes opaque at temperature higher than 260°C. Therefore we cannot measure the threshold laser power for producing particles quantitatively at temperature higher than 290°C. On the other hand, because of the limit of the laser power, the laser snow has not been observed at the temperature lower than 230°C for the dye laser and 245°C for the Ar^+ laser. Then the ranges of the densities of Na atoms and Na_2 molecules are about 1 order of magnitude.

The influences of the pressures of H_2 and He, must be checked. For this purpose, we have observed the particle formation by using several cells, though the filled gas pressures are not largely different. The conditions of the cells are listed in Table 3.7. In Table 3.7, we show also the results of the experiment of particle formation. The symbol "o" indicates that particle formation was observed, and the symbol "x" indicates that it has not been observed. The symbol "-" indicates that the experiment has not been made.

For observing the Mie scattering by the NaH laser snow produced by the dye laser beam, we used the Ar^+ laser beam in addition to the dye laser beam. It was necessary to reduce the Ar^+ laser power to avoid the influence on the snow formation by the dye laser beam at high temperature in this experiment. In the experiment of using only the Ar^+ laser beam, we used it for both producing and observing the NaH laser

snow. Therefore less amount of particles must have been observed when the higher Ar^+ laser beam intensity was needed for producing particles. However, we have not estimated these effects quantitatively.

We found the dissociation of the NaH laser snow by the collisions with the Na atoms in the 3P states, which have energies higher than the dissociation energy of NaH. In the case of other alkali hydride laser snows, such dissociation of the produced particles had not been observed so far.

III. 5 Summary and Conclusions

We have discussed the laser-production of CsH and NaH particles in this chapter. These particles have been produced by the irradiation of the laser beams with the particular wavelengths coincident with the spectral lines of Cs or Na atoms and/or molecules. We summarize the laser-production of CsH and NaH particles in this section and discuss the differences with other laser-produced particles.

The experimental requirements of the laser-production of CsH and NaH particles can be summarized in Table 3.8. Since the conditions of experiments at different wavelengths are not the same, it is difficult to discuss quantitatively. However, we can say that the particles are sometimes produced by only a few mW of the laser power and the densities of atoms and molecules are above 10^{13} cm^{-3} and 10^{11} cm^{-3}, respectively. This result might be applied to the laser-production of other particles, such as RbH particles. As seen in Table 3.8, higher laser power and higher densities of atoms and molecules are required for the laser-production of particles in the cell without He gas. This is considered to be due to the less pressure broadening of absorption lines and the higher diffusion velocity of produced alkali hydride molecules. Since these two effects decrease the densities of the produced alkali hydride molecules in the laser beam, it is needed to produce more alkali hydride molecules for the particle formation.

Table 3.8 Experimental requirements of laser-production of CsH and NaH particles.

(a) CsH

Wavelength(nm)	601.0	601.0	457.9
Temperature(°C)	≳175	300	240
Laser power(mW)	100	250	50
Filled gas(Torr)			
He	550	0	550
H_2	4	27	4
Cs density(cm^{-3})	$\gtrsim 5 \times 10^{14}$	4×10^{16}	8×10^{15}
Cs_2 density(cm^{-3})	$\gtrsim 9 \times 10^{11}$	2×10^{14}	2×10^{13}

(b) NaH

Wavelength(nm)	457.9 ~ 514.5	589.6	589
Temperature(°C)	≳245	≳230	280
Laser power(mW)	100 ~ 1500	2 ~ 50	400
Filled gas(Torr)			
He	470	480	0
H_2	11	12	32
Na density(cm^{-3})	$\gtrsim 3 \times 10^{13}$	$\gtrsim 2 \times 10^{13}$	1×10^{14}
Na_2 density(cm^{-3})	$\gtrsim 1 \times 10^{11}$	$\gtrsim 6 \times 10^{10}$	8×10^{11}

From the several experiments of the laser excitation of alkali vapor and of the particle formation, and from the consideration about energy relations, we have discussed the laser-induced chemical reactions to produce alkali hydrides. We have found that both the direct and indirect chemical reaction processes between excited alkali atoms and hydrogen molecules are possible in both cases of CsH and NaH. We have found also that NaH particles are produced directly through the reaction between the $Na_2(B^1\Pi_u)$ and H_2.

When the alkali hydride molecules are produced at high density, the small particles composed of these alkali hydride molecules become visible to the naked eye. We found also that the produced NaH particles are dissociated by the collisions with the Na(3P) atoms.

By comparing the alkali hydride laser snow with other laser-produced particles described in the preceding chapter, we can see the following differences. a) Typically a few seconds of laser irradiation is enough to produce the laser snow whereas it needs a few tens of seconds for $SO_2 - NO_2$ mixture and $CCl_4 - Cl_2$ mixture systems. b) The produced laser snow is composed of simple ionic crystal. c) It is possible to produce the laser snow by exciting alkali atoms so that the efficient excitation can be achieved. d) The processes of chemical reactions are comparatively simple.

We have described the laser-production of CsH and NaH particles and the formation mechanisms of CsH and NaH molecules in this chapter. Next, we must study the growth mechanisms of particles in order to understand the mechanisms of the laser-production of particles. For this purpose, we made another experiment of measuring the size distribution of the laser-produced CsH particles, which will be discussed in the next chapter.

CHAPTER Ⅳ

TEMPORAL CHANGES IN SIZE DISTRIBUTION OF CsH LASER SNOW

Ⅳ. 1 Introduction

Some studies have been reported on the laser snow and its formation mechanisms[1-6,10] as described in chapter Ⅲ. Particular attention has been placed in these works on the laser-induced chemical reactions to produce alkali hydride molecules, but the growth of particles has not been extensively studied so far. The size of the largest laser snow was estimated to be about 1 μm[2,6] from the falling velocity of the particles in a buffer gas of relatively high pressure, but the size distribution has not been measured yet.

In the natural world, there are many kinds of small particles produced in the air or other gases, but growth mechanisms of particles are not well known yet. The size distribution, especially its temporal changes, give us important informations to reveal the processes of growth of particles. The measurements of temporal changes of size distribution are quite few,[15,27] and most of the measurements have been done on the steady state or quasi-steady state size distributions of these natural particles,[21,114,115] although the temporal changes of the size distribution have been studied

theoretically by using simplified models.[28-30,116,117] A numerical study using optical data to yield a histogram distribution for the particle size distribution has recently been reported by Heintzenberg *et al.*[118] but they did not apply it to the realistic mesuarements of size distribution and its temporal changes.

In this chapter, we describe the measurements of the size distribution of the CsH laser snow and its temporal changes. The measurements of size distribution described in this chapter are based on the light scattering from the laser-produced particles. Under the production of CsH particles by applying an Ar^+ laser beam to a cell containing Cs vapor and H_2 gas, a linearly polarized white light beam is applied and the wavelength- and polarization-dependences of right-angle scattering from the laser-produced particles are measured. The measured dependences are compared with the theory, in which the scattered light intensity is given by the convolution of the scattered light intensity from each particle and the size distribution function assumed. For the scattering from each particle, we use the Mie theory assuming that the particle is spherical, and as to the size distribution, we use several test functions, each having three unknown parameters. By comparing the experimental results with the theory, we determine the best test function and the best values of its parameters, at each moment from the beginning of the laser-irradiation.

In the present work, we could succeed the first precise measurement of the size distribution of the laser-produced alkali hydride particles.

It must be noted that the temporal change of size distribution had not been measured precisely even for other particles.

Ⅳ. 2 Principle of Measurements of Size Distribution

Ⅳ. 2. 1 Mie Theory

In the paper published in 1908,[119] Mie obtained a rigorous solution for diffraction or scattering of a plane monochromatic wave by a homogeneous sphere of an arbitrary radius. The Mie theory can be applied to scattering by any number of spheres, provided that they have the same radius and composition and that they are distributed at random and separated from each other by distances larger than the wavelength. Under these circumstances there are no coherent phase relationships between the light waves scattered by the different spheres, and hence total scattered intensity is simply given by the multiplication of the intensity of light scattered by a spherical particle and the total number of particles.

First of all we recall the Mie theory and consider the scattering of the linearly polarized plane monochromatic light with a wavelength λ by a spherical particle with radius a and a complex refractive index $\tilde{n}$. It is convenient to use the normalized radius q defined as $q = 2\pi a/\lambda$. We take a Cartesian coordinates with the origin at the center of the sphere and with the x- and z-axes taken to the directions of polarization and propagation of incident light. The observation point is represented by $P(r, \theta, \phi)$, where r, θ, and ϕ are the quantities used in

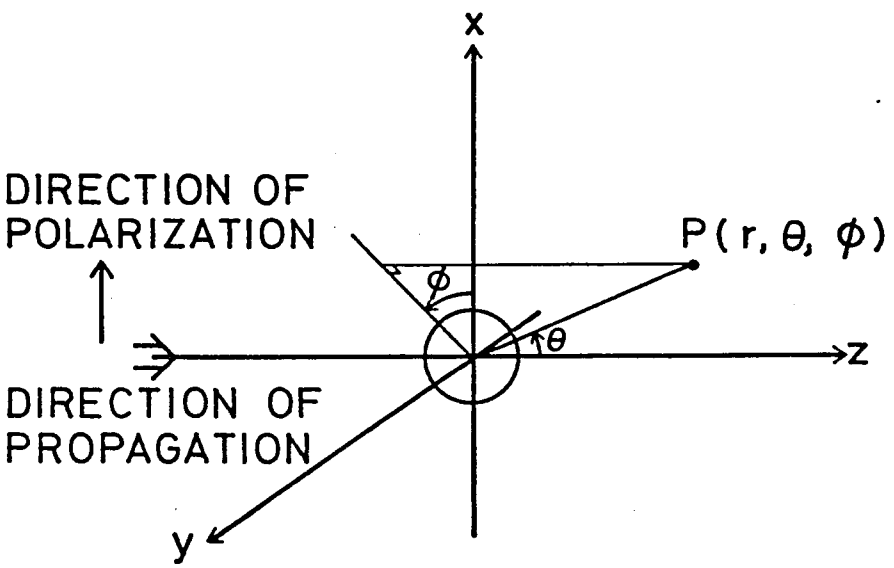

Fig. 4.1 Coordinates with the origin at the center of the sphere, the z-direction in the direction of the incident light propagation and the x-direction in the direction of the incident light polarization. The observation point is shown as $P(r, \theta, \phi)$.

ordinary polar coordinates:

$$\left.\begin{aligned} x &= r \sin\theta \cos\phi , \\ y &= r \sin\theta \sin\phi , \\ z &= r \cos\theta . \end{aligned}\right\} \qquad (4.1)$$

We define the plane of observation as that containing the direction of propagation of the incident light and the direction (θ, ϕ) of observation.

Our purpose here is to obtain the θ and ϕ components of scattered electric vector $\vec{E}^{(S)}$ and its intensity $I^{(S)}$ at the observation point. When we normalize the amplitude of the electric vector of the incident wave by unity, i.e. $|\vec{E}^{(i)}| = 1$, we can obtain $E_\theta^{(S)}$ and $E_\phi^{(S)}$ by solving the Maxwell's equation under the boundary condition that the tangential components of $\vec{E}$ should be continuous across the surface of the sphere [120]

$$\left.\begin{aligned} E_\theta^{(S)} &= -\frac{1}{k}\frac{\cos\phi}{r}\sum_{l=1}^{\infty}\Big\{ {}_e B_l \zeta_l^{(1)'}(kr)\, P_l^{(1)'}(\cos\theta)\sin\theta \\ &\qquad - i\, {}_m B_l \zeta_l^{(1)}(kr)\, P_l^{(1)}(\cos\theta)\frac{1}{\sin\theta}\Big\}, \\ E_\phi^{(S)} &= -\frac{1}{k}\frac{\sin\phi}{r}\sum_{l=1}^{\infty}\Big\{ {}_e B_l \zeta_l^{(1)'}(kr)\, P_l^{(1)}(\cos\theta)\frac{1}{\sin\theta} \\ &\qquad - i\, {}_m B_l \zeta_l^{(1)}(kr)\, P_l^{(1)'}(\cos\theta)\sin\theta\Big\}, \end{aligned}\right\} \qquad (4.2)$$

where $k = 2\pi/\lambda$. Scattering coefficients ${}^{e}B_{\ell}$ and ${}^{m}B_{\ell}$ are given as follows.

$$\left.\begin{aligned} {}^{e}B_{\ell} &= i^{\ell+1}\frac{2\ell+1}{\ell(\ell+1)}\frac{\hat{n}\psi_{\ell}'(q)\,\psi_{\ell}(\hat{n}q) - \psi_{\ell}(q)\psi_{\ell}'(\hat{n}q)}{\hat{n}\zeta_{\ell}^{(1)\prime}(q)\psi_{\ell}(\hat{n}q) - \zeta_{\ell}^{(1)}(q)\psi_{\ell}'(\hat{n}q)}, \\ {}^{m}B_{\ell} &= i^{\ell+1}\frac{2\ell+1}{\ell(\ell+1)}\frac{\hat{n}\psi_{\ell}(q)\psi_{\ell}'(\hat{n}q) - \psi_{\ell}'(q)\psi_{\ell}(\hat{n}q)}{\hat{n}\zeta_{\ell}^{(1)}(q)\psi_{\ell}'(\hat{n}q) - \zeta_{\ell}^{(1)\prime}(q)\psi_{\ell}(\hat{n}q)}. \end{aligned}\right\} \qquad (4.3)$$

The functions used in eqs. (4.2) and (4.3) are as follows:

$$\left.\begin{aligned} &\psi_{\ell}(q) = \sqrt{\frac{\pi q}{2}}\,J_{\ell+1/2}(q), \\ &\chi_{\ell}(q) = -\sqrt{\frac{\pi q}{2}}\,N_{\ell+1/2}(q), \\ &\zeta_{\ell}^{(1)}(q) = \psi_{\ell}(q) - i\chi_{\ell}(q) = \sqrt{\frac{\pi q}{2}}\,H_{\ell+1/2}^{(1)}(q), \\ &J_{\ell+1/2}(q)\ ;\ \text{the Bessel function}, \\ &N_{\ell+1/2}(q)\ ;\ \text{the Neumann functions}, \\ &H_{\ell+1/2}^{(1)}(q)\ ;\ \text{one of the Hankel function}, \\ &P_{\ell}^{(1)}(\cos\theta)\ ;\ \text{the associated Legendre polynomials}, \end{aligned}\right\} \qquad (4.4)$$

and the prime on ψ_{ℓ}, $\zeta_{\ell}^{(1)}$, and $P_{\ell}^{(1)}$ represents the differentiation with respect to their arguments. When the argument of $\zeta_{\ell}^{(1)}$ and $\zeta_{\ell}^{(1)\prime}$ is large, i.e., $|q| \gg 1$, we can use the following asymptotic formulae:

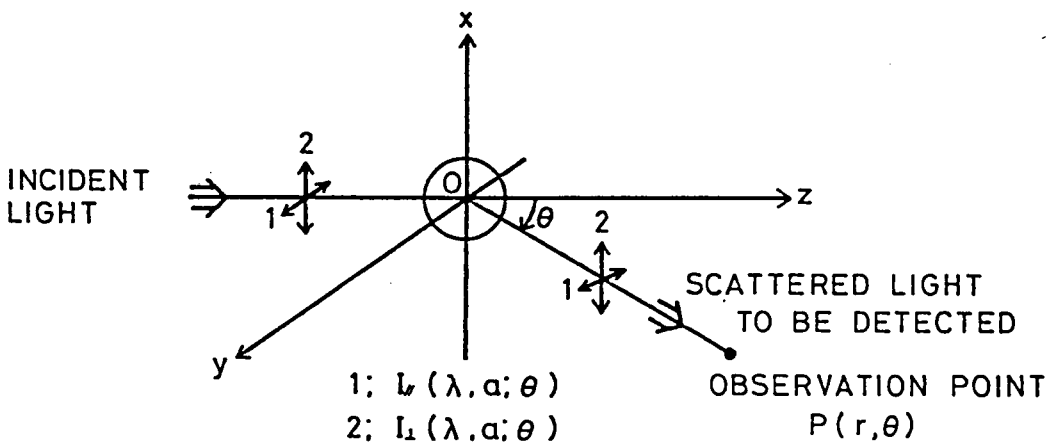

Fig. 4.2 Definition of the polarization of the scattered light. The origin is set at the center of the sphere and z-direction is chosen to the direction of the incident light propagation. The scattered light is observed from the direction on the y-z plane with the angle θ from the z-direction. $I_{//}(\lambda, a; \theta)$ is the scattered light intensity when the incident light is polarized to the y-direction and the polarization of detected light is on the y-z plane, and $I_{\perp}(\lambda, a; \theta)$ is the scattered light intensity when the incident light is polarized to the x-direction and the detected light has the same polarization.

$$\left.\begin{aligned} \zeta_l^{(1)}(q) &\sim (-i)^{l+1} e^{iq}, \\ \zeta_l^{(1)*}(q) &\sim (-i)^{l} e^{iq}. \end{aligned}\right\} \tag{4.5}$$

This is the case of a far field region ($kr \gg 1$). Using Eqs. (4.2)-(4.5), intensities of the scattered light become

$$\left.\begin{aligned} I_{//}^{(S)} &= \frac{\lambda^2}{4\pi^2 r^2}\left| \sum_{l=1}^{\infty} (-i)^l \left({}^{e}B_l P_l^{(1)*}(\cos\theta)\sin\theta - {}^{m}B_l \frac{P_l^{(1)}(\cos\theta)}{\sin\theta} \right) \right|^2, \\ I_{\perp}^{(S)} &= \frac{\lambda^2}{4\pi^2 r^2}\left| \sum_{l=1}^{\infty} (-i)^l \left({}^{e}B_l \frac{P_l^{(1)}(\cos\theta)}{\sin\theta} - {}^{m}B_l P_l^{(1)*}(\cos\theta)\sin\theta \right) \right|^2, \end{aligned}\right\} \tag{4.6}$$

$$|E_\theta^{(S)}|^2 = I_{//}^{(S)}\cos^2\phi, \quad |E_\phi^{(S)}|^2 = I_{\perp}^{(S)}\sin^2\phi,$$

where $I_{//}^{(S)}$ is the intensity of the scattered light polarized parallel to the plane of observation and $I_{\perp}^{(S)}$ is the intensity of the scattered light polarized perpendicular to the plane of observation.

For a practical experiment to be described later, it is convenient to use the new coordinate system shown in Fig. 4.2, where the origin is also set at the center of the sphere, z-direction is chosen to the direction of the incident light propagation, and the scattered light is observed at the distance r from the direction on

the y-z plane with the angle θ from the z-direction.

Along the experiment, we consider two cases of polarizations of incident light and detected light. The first case is such that the incident light is polarized to the y-direction and the polarization of detected light is on the y-z plane. In this case the incident and detected light intensities are defined as $I^0_{//}$ and $I_{//}$. The second case is such that the incident light is polarized to the x-direction and the detected light has the same polarization. In this case we write $I^0_{\perp}$ and $I_{\perp}$ as the incident and detected light intensities.

In the later coordinate system, the detected light intensities $I_{//}$ and $I_{\perp}$ are given by $I^{(S)}_{//}\cos^2\phi$ with $\phi = 0°$ and $I^{(S)}_{\perp}\sin^2\phi$ with $\phi = 90°$, respectively. We rewrite $I^{(S)}_{//}$ and $I^{(S)}_{\perp}$ as $I_{//}$ and $I_{\perp}$, which are functions of λ, a, and θ.

$$\left.\begin{aligned} I_{//}(\lambda, a;\theta) &= \frac{\lambda^2}{4\pi^2 r^2}\left| \sum_{\ell=1}^{\infty} (-i)^{\ell}\left(e_{B_\ell} P^{(1)}_{\ell}(\cos\theta)\sin\theta \right.\right. \\ &\qquad \left.\left. - m_{B_\ell}\frac{P^{(1)}_{\ell}(\cos\theta)}{\sin\theta}\right)\right|^2 I^0_{//}, \\ I_{\perp}(\lambda, a;\theta) &= \frac{\lambda^2}{4\pi^2 r^2}\left| \sum_{\ell=1}^{\infty} (-i)^{\ell}\left(e_{B_\ell}\frac{P^{(1)}_{\ell}(\cos\theta)}{\sin\theta} \right.\right. \\ &\qquad \left.\left. - m_{B_\ell} P^{(1)}_{\ell}(\cos\theta)\sin\theta\right)\right|^2 I^0_{\perp}, \end{aligned}\right\} \quad (4.7)$$

where $I^0_{//}$ and $I^0_{\perp}$ represent the incident light intensities.

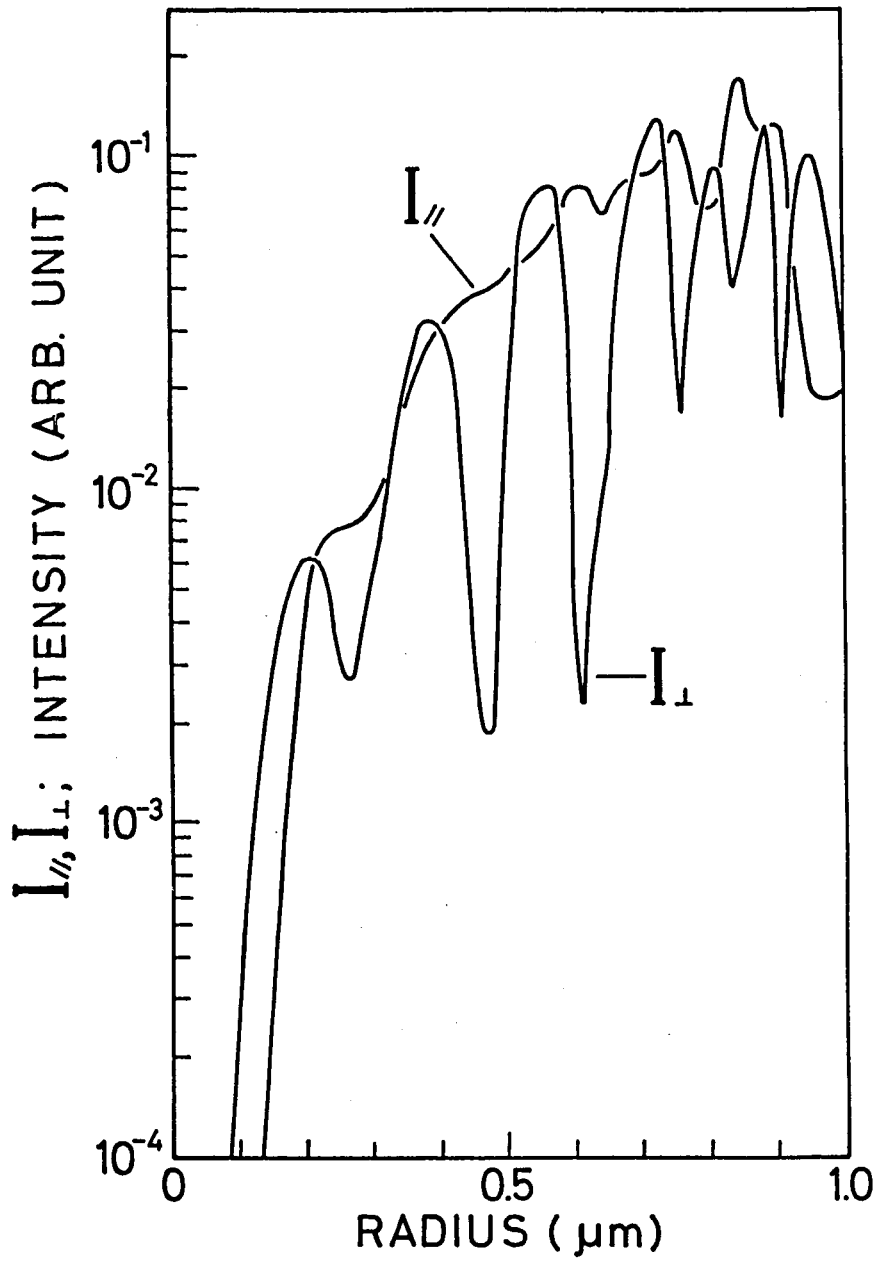

Fig. 4.3 Intensities $I_{//}(\lambda, a; \theta)$ and $I_{\perp}(\lambda, a; \theta)$ as functions of particle radius a in the case that $\lambda = 642.5$ nm, $\theta = 85°$, and $\hat{n} = 1.48$.

Ⅳ. 2. 2 Light Scattering from Particles with a Size Distribution and Requirements from Experiment

We consider here the light scattering by the ensemble of spherical particles with different radii. When the incident light is scattered by a large number of particles moving at random at different positions, the interference among the light waves scattered by particles must be smeared out,and hence the detected light intensity is approximately given by the sum of intensities of light scattered by particles. When we observe the scattered light with wavelength λ from the direction of angle θ, the light intensities for the two cases of the polarization described in Ⅳ.2.1 can be expressed as

$$\left.\begin{aligned} I_{//}(\lambda;\theta) &= \int_0^\infty \Psi(a)\, I_{//}(\lambda, a;\theta)\, da, \\ I_{\perp}(\lambda;\theta) &= \int_0^\infty \Psi(a)\, I_{\perp}(\lambda, a;\theta)\, da, \end{aligned}\right\} \qquad (4.8)$$

where $\Psi(a)$ is the size distribution of particles to be measured, and $I_{//}(\lambda, a;\theta)$ and $I_{\perp}(\lambda, a;\theta)$ are those given by Eq. (4.7). Figure 4.3 shows $I_{//}(\lambda, a;\theta)$ and $I_{\perp}(\lambda, a;\theta)$ as functions of a in the case that $\lambda = 642.5$ nm, $\theta = 85°$, and $\tilde{n} = 1.48$. In our experiment to be described in Ⅳ.3, we have observed the light scattered to the y-direction, i.e. $\theta = 90°$.

Expressions (4.7) are for an ideal case that the monochromatic light is observed from the direction defined strictly. However, in

the practical experiment, one may observe the light scattered by the ensemble of particles through a solid angle and the light to be detected has a spectral width. So, we have to average Eq. (4.7) over the sight of angle $\Delta\theta$ centered at θ and over the spectral width $\Delta\lambda$ centered at λ, and then insert them into Eq. (4.8) as $I_{//}(\lambda, a; \theta)$ and $I_{\perp}(\lambda, a; \theta)$. It must generally be necessary to average over the sight of angle $\Delta\phi$ centered at ϕ. However, in the practical case, we observe $I_{//} = I_{//}^{(S)} \cos^2\phi$, where the sight of angle $\Delta\phi$ is centered at 0°, and $I_{\perp} = I_{\perp}^{(S)} \sin^2\phi$, where the sight of angle $\Delta\phi$ is centered at 90°, as described in Ⅳ.2.1. This means that $I_{//}$ (or $I_{\perp}$) is a slowly varying function of ϕ, and the averaging with respect to ϕ may be unnecessary in the case of small sight of angle $\Delta\phi$.

In our experiment, the both angles of sight $\Delta\theta$ and $\Delta\phi$ were 16°, and the spectral width $\Delta\lambda$ of the detected light, which was determined by the resolving power of the monochromator, was about 2 nm. This value of $\Delta\lambda$ is much smaller than the spread of the size distribution of CsH particles to be measured, so that the effect of the spectral width can be considered not to give a significant difference from the case of monochromatic light. This was, in fact, verified in the experiment using some different values of $\Delta\lambda$. Thus, in our practical analysis of experimental data, we have used $I_{//}(\lambda, a; 90°)$ and $I_{\perp}(\lambda, a; 90°)$ which were averaged only over θ.

The important quantity in the data analysis is the refractive index of CsH particles, but the value has not been known as far as we

aware. So, we used the value $\hat{n}=1.48$, which was estimated from the refractive indices of crystals of NaH ($\hat{n}=1.470$) and KH ($\hat{n}=1.453$). It is, however, apparent from Eq. (4.3) that this uncertainty of $\hat{n}$ does not give a significant error in determination of the size distribution. We have assumed that $\hat{n}$ is constant over the wavelengths of the detected light (which are in the visible region).

In the present work, the integration with respect to the particle radius a in Eq. (4.8) is carried out from zero to 1 μm, because the size of the largest particles has been measured to be about 1 μm from the falling velocity.

Ⅳ. 2. 3 Test Functions Used to Determine the Size Distribution

If we can observe the light scattering from the laser snow for wide wavelength range, it must be possible to determine precisely the size distribution $\Psi(a)$ from the measured intensities $I_{//}(\lambda)$ and $I_{\perp}(\lambda)$ by using Eq. (4.8). But, in the present experiment, the light scattering has been observed for only several wavelengths in visible region, so that we have to make a relatively crude approximation. To obtain the approximate size distribution, we have used several test functions for $\Psi(a)$, each having three unknown parameters. We have inserted these test functions into Eq. (4.8) and calculated numerically $I_{//}(\lambda;90°)$ and $I_{\perp}(\lambda;90°)$ while changing the values of parameters.

By comparing these with experimentally obtained wavelength- and polarization-dependences, we could determine the best-fitted test function and its parameters, at each moment after the beginning of laser-irradiation, i.e. after the beginning of production of CsH molecules.

The test functions used in the present work are the Gauss, Stevenson, and Junge distribution functions, which are known to give approximate size distributions of particles produced in the natural world.

The Gauss distribution function is defined by

$$\Psi_G(a) = A_G \exp\left(-\frac{(a-\mu)^2}{2\sigma^2}\right), \tag{4.9}$$

where A_G is a positive constant, μ is a mean radius, and σ is a standard deviation. The Gauss distribution is known to give the approximate size distribution of raindrops.[18]

The Stevenson distribution function is defined by

$$\left.\begin{aligned} \Psi_S(a) &= A_S(a-a_0)\exp\left(-\left(\frac{a-a_0}{s}\right)^3\right), && a \geq a_0, \\ \Psi_S(a) &= 0, && a < a_0, \end{aligned}\right\} \tag{4.10}$$

where A_S is a positive constant and a_0 is the radius of the smallest particles. The value s determines the modal radius a_m, the full-width at half-maximum w, and the "half-spread" $(a_m - a_0)$ through relations

$$\left.\begin{aligned} w &= 0.9015\ \mathrm{s}, \\ a_m - a_0 &= 3^{-1/3}. \end{aligned}\right\} \tag{4.11}$$

Stevenson *et al.*[121] used this distribution function as an approximate representation of size distribution of emulsions.

The Junge distribution function is defined by

$$\left.\begin{aligned} \Psi_J(a) &= A_J a^{-p}, && a \geq a_c, \\ \Psi_J(a) &= 0, && a < a_c, \end{aligned}\right\} \tag{4.12}$$

where A_J and p are positive values. Junge *et al.*[21] found that this exponential distribution function gives well the size distribution of stratospheric aerosol particles in the size range of 0.1 μm to 1 μm in radius. The value p for stratospheric aerosol is about three. According to their definition, the Junge distribution function becomes infinite as the radius tends to zero. This is not natural, so that we have introduced a cut-off radius a_c, as in Eq. (4.12).

IV. 2. 4 Determination of the Best Test Function and Its Parameters

To estimate the deviation between $I_{/\!/}(\lambda)$ and $I_{\perp}(\lambda)$ obtained experimentally and those calculated theoretically for a test function

with given values of its parameters, we introduce the mean-square deviation E defined as

$$E = \sum_{\lambda,k} \left(\frac{I_k^{Obs.}(\lambda) - I_k^{Theor.}(\lambda)}{I_k^{Obs.}(\lambda)} \right)^2 , \qquad (4.13)$$

where $I_k^{Obs.}(\lambda)$ is the observed intensity of the scattered light at wavelength λ, $I_k^{Theor.}(\lambda)$ is the theoretically calculated intensity, and k represents a set of polarizations of incident light and detected light, i.e. $I_k = I_{//}$ or $I_{\perp}$. The summation is made over the observed wavelengths and the set of polarizations. The intensity $I_k^{Theor.}(\lambda)$ is calculated by substituting a test function $\Psi(a)$ with given values of parameters into Eq. (4.8). By finding the test function and its values of parameters, giving the minimum value of E, we can determine the best-fit size distribution.

When the experimental error is not very small, there is ambiguity in determination of the best-fit size distribution and its parameters. This is mainly due to the fact that the light scattering is observed at the wavelengths in the visible region, so that the particles much smaller than the wavelengths do not contribute significantly to the observed light intensity. With respect to the present experiment, we consider that the size distribution determined as described above may approximate well the real size distribution in the range of radius a between 0.1 - 1 μm, but it is quite ambiguous for particles smaller than 0.1 μm.

Ⅳ. 3 Experiments and Analyses

Ⅳ. 3. 1 Experimental Method

The experimental setup is shown in Fig. 4.4. We used the Cs cell "C-2", which was described in Ⅲ.3. The cell was made of alkali-resistant aluminosilicate glass and baked at 650°C in a vacuum of 10^{-6} Torr before filling Cs metal, 4 Torr of H_2, and 550 Torr of He.

The cell was placed inside an transparent glass oven, and the cell temperature was kept within ±1°C at 330°C or 300°C in the present experiment. These temperatures give the Cs vapor densities 8×10^{16} or 4×10^{16} cm^{-3}, respectively. In the experiment, a particular attention was paid on the temperature distribution within the cell to avoid the convection.

The Ar^+ laser beam at 457.9 nm was applied to the cell. This laser line excites Cs(6S) to Cs(7P) through the wing of the pressure broadened absorption line under the relatively high pressure of He. The laser power was set at 50 mW or 100 mW in the present experiment.

The light source used in the measurement of the size distribution of laser snow was a halogen lamp. We will call the light from the lamp "white light" although it has a relatively large wavelength dependence even in a visible region. The white light beam was applied to the cell from the opposite direction to the laser beam, and we adjusted optics so that these beams overlapped to each other. The white light beam diameter at the cell was set about 10 mm and the laser beam diameter was set 0.2 mm or 2 mm so that the laser beam was

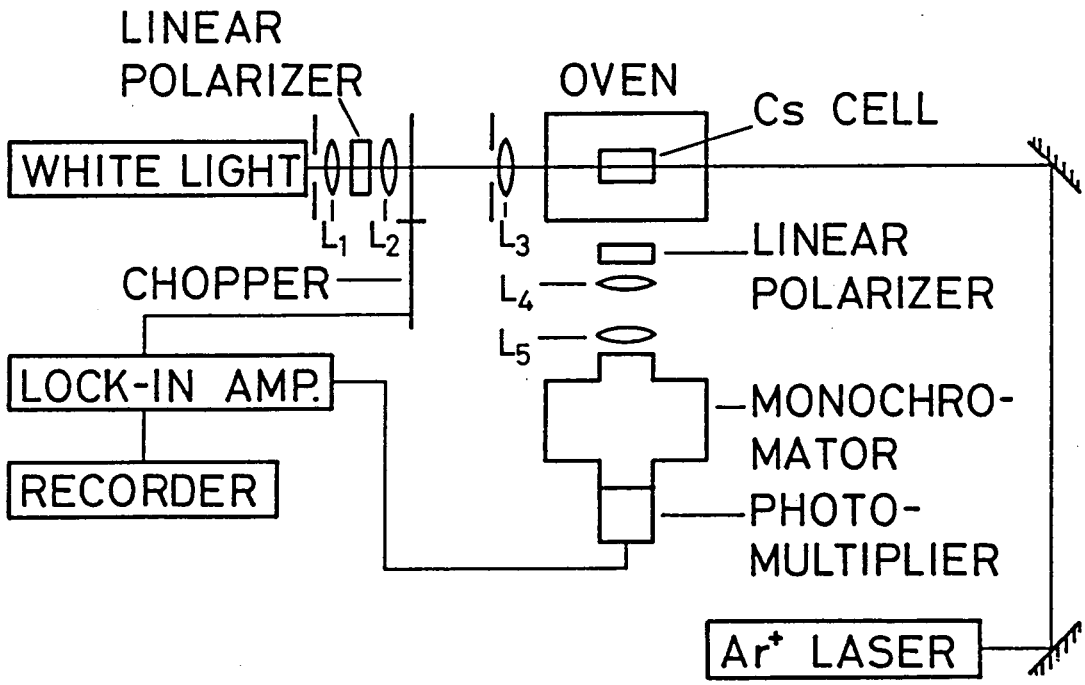

Fig. 4.4 Experimental setup. The Cs cell is made of alkali-resistant aluminosilicate (Corning 1720) glass and filled with a small amount of Cs metal, 4 Torr of H_2, and 550 Torr of He.

placed within the white light beam. The white light beam diameter at the cell was also set about 5 mm when the laser beam diameter was set 5 mm or 15 mm, in order to place the white light beam within the laser beam.

The light scattered by the laser snow was observed by the following observation system. The light scattered to the direction perpendicular to the light beam was collected by lenses and detected by a photomultiplier through a monochromator in order to select the wavelength to be observed. The resolving power of the monochromator or the spectral width of the detected light was about 2 nm. In order to improve signal-noise ratio, we chopped the incident white light by a mechanical chopper and the output of the photomultiplier was applied to a lock-in amplifier tuned at the chopping frequency. The time constant of the lock-in amplifier was set 0.3 sec throughout the present experiment. The incident white light and scattered light were linearly polarized in order to detect $I_{//}(\lambda)$ or $I_{\perp}(\lambda)$.

When the Ar^+ laser beam was applied to the cell, we could observe the production of particles, by eyes, within few seconds. The temporal change of the intensity of the white light scattered by the laser snow was recorded on a chart recorder, just after the beginning of the irradiation of the laser beam, i.e. after the beginning of production of CsH molecules. After taking the recorder trace for a particular wavelength and for a particular set of polarizations, we shut the laser

beam off until particles disappeared completely. Then, we repeated the same procedure as above for the different wavelength and/or for the different set of polarizations. In this way, we could measure the temporal changes of the scattered light intensities $I_{//}(\lambda)$ and $I_{\perp}(\lambda)$ for five wavelengths in the range 440 - 710 nm.

The size distribution at a given time T after the beginning of the laser-irradiation can be calculated through Eqs. (4.8) and (4.13) from the scattered light intensities $I_{//}(\lambda)$ and $I_{\perp}(\lambda)$ at T for several wavelengths. However, in the present case, these intensities were measured by repeating the procedure described above, and hence relatively high reproducibility was required in production of particles. So, we paid a particular attention to keep constant the conditions such as the cell temperature and the intensities of the laser light during the experiment.

Ⅳ. 3. 2 Experimental Results and Analyses

The photograph of the CsH laser snow irradiated by the white light is shown in Fig. 3.20. In Fig. 3.20, we can see not only the stripes of the scattered light intensity but also the changes of color or wavelength. This indicates clearly that there are not only spatial distributions of the particle density but also of the particle size. Therefore we must restrict our observation region so as not

to observe the size distribution averaged in spatial distribution. However, in the early stage of particle formation, we observe that there are no changes of color in whole space. This indicates the fact that there is no spatial distribution of particle size, and hence the following analyses are particularly useful in the early stage of particle formation.

We used seven different experimental conditions which are listed in Table 4.1. The experiments J1, J2, J3, and J4 are a series of experiments which were performed within 24 hours. The experiments J5, J6, and J7 are another series of experiments which were made on another day. But we discuss mainly five experiments J1, J2, J3, J4, and J6, because the series of experiments J5, J6, and J7 showed about the same results.

We first describe on the result of J6 (The Ar^+ laser beam is set 50 mW in power and 5 mm in diameter, the white light beam is set 5 mm in diameter, and the cell temperature is set 330°C.). Next we show the results of J1 - J4 and discuss the effects of the experimental conditions, such as the laser power density and temperature.

The obtained scattered light intensities at the experiment J6 are shown in Fig. 4.5 (a) and (b) as a function of time after the beginning of the laser-irradiation. Figure 4.5 (a) and (b) show respectively the scattered light intensities $I_{//}(\lambda)$ and $I_{\perp}(\lambda)$ at the wavelengths: 440 nm, 507.5 nm, 575 nm, 642.5 nm, and 710 nm. Hereafter, let us write T as the time after the beginning of the laser-irradiation. General feature of the change of scattered light intensity seen in.

Table 4.1 Experimental conditions for measurement of size distribution. The experiments J1, J2, J3, and J4 are a series of experiments which were performed within 24 hours. The experiments J5, J6, and J7 are another series of experiments which were performed on another day.

Experiment No.	J1	J2	J3	J4	J5	J6	J7
Ar^+ laser beam							
Power (mW)	50	50	100	50	50	50	100
Diameter (mm)	2	0.2	2	2	15	5	15
White light beam							
Diameter (mm)	10	10	10	10	5	5	5
Temperature (°C)	330	330	330	300	330	330	330

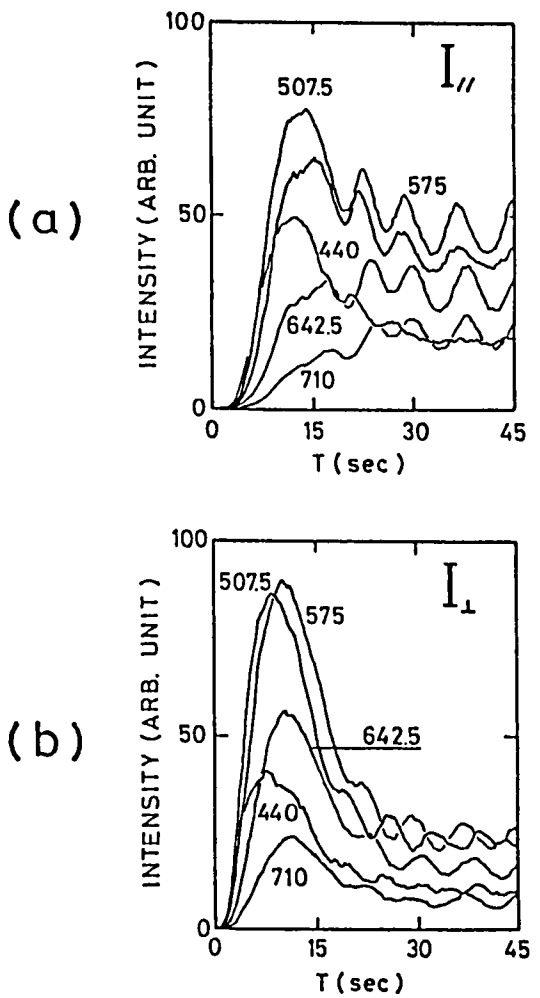

Fig. 4.5 (a) Recorder traces showing the changes of the scattered light intensities $I_{//}$ at five wavelengths, obtained in the experiment J6 (the Ar^+ laser: 50 mW and 5 mm i.d.; the white light: 5 mm i.d.; the cell temperature: 330°C). (b) The same as in (a), but for $I_{\perp}$.

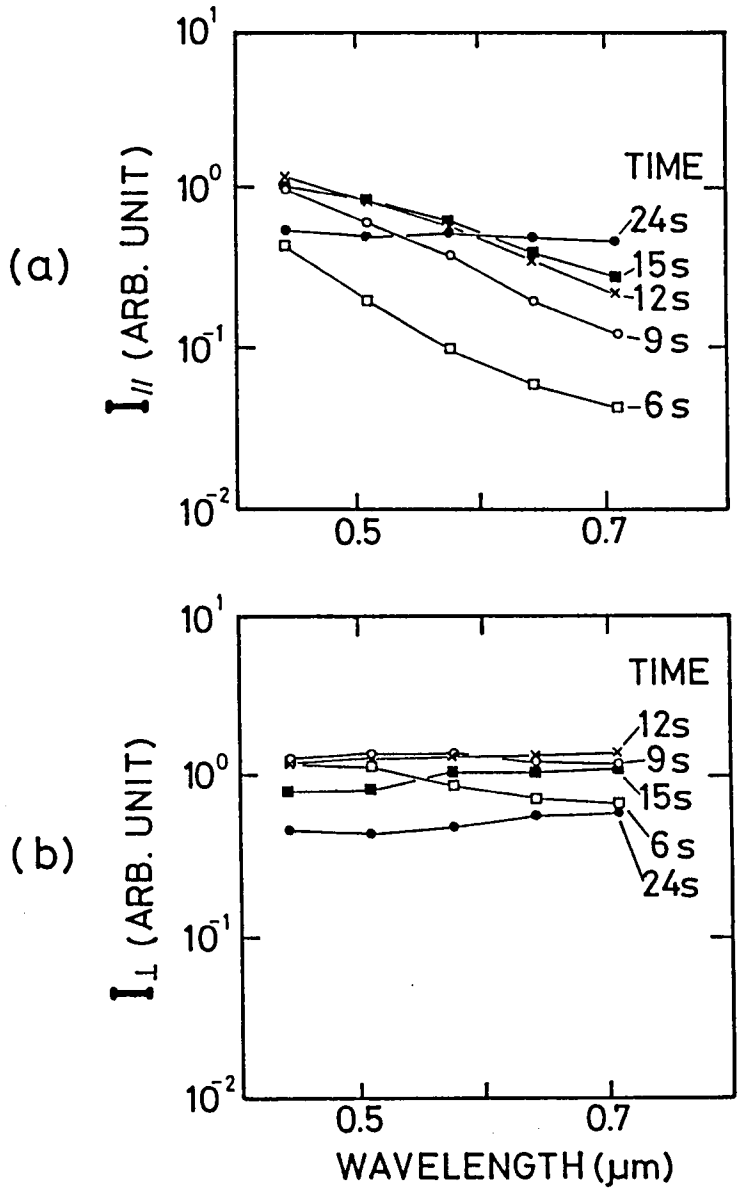

Fig. 4.6 Normalized scattered light intensities (a) $I_{//}(\lambda)/I^{0}_{//}(\lambda)$ and (b) $I_{\perp}(\lambda)/I^{0}_{\perp}(\lambda)$, as functions of wavelength λ. The time T after the beginning of the laser-irradiation is changed as a parameter. This figure shows the result of the experiment J6 (the Ar^{+} laser: 50 mW and 5 mm i.d.; the white light: 5 mm i.d.; the cell temperature: 330°C).

Fig. 4.5 (a) and (b) is such that, with the increase of T from zero, it increases rapidly and shows a peak, and then it decreases accompanied with an oscillation. Quantitative discussions on this oscillation have been given by Tam *et al.*[3] This oscillation may be explained by the following cyclic processes: (1) the increase of CsH density until it arrives at the critical value for condensation, (2) the production and growth of particles accompanied with the decrease of CsH density, (3) the falling down of large particles through gravity, and then going back to the process (1). Looking at Fig. 4.5 (a) and (b), we see that the time arriving at the first peak is delayed when the wavelength is increased, or when the polarization is switched from $I_{\perp}$ to $I_{//}$ for the same wavelength. These facts indicate apparently the increase of either or both of number density and size of particles with time T. Since the light source of the "white light", the photomultiplier, and other optical elements used in this experiment have the wavelength- and polarization-dependences. The results shown in Fig. 4.5 include these dependences of the optical system used. To eliminate these, we measured at first the wavelength- and polarization-dependences, $I_k^0(\lambda)$ with $k = //$ or $\perp$, of the total optical system, by replacing the cell by a small mirror. Then, we normalized the detected light intensities $I_k(\lambda)$ by $I_k^0(\lambda)$ to obtain the net wavelength- and polarization-dependences of the light scattered by particles. The normalized light intensities $I_k^{Obs.}(\lambda) = I_k(\lambda)/I_k^0(\lambda)$ as functions of λ are shown in Fig. 4.6 (a) and (b), where time T is varied as a parameter.

Table 4.2 The minimum values E of each test function and their best values of parameters.

	Gauss distribution				Stevenson distribution				Junge distribution			
T(sec)	E	μ(μm)	σ(μm)	A_G	E	a_0(μm)	s(μm)	A_S	E	p	a_c(μm)	A_J
3	0.8484	-0.07	0.05	2.60E5	1.7469	-0.10	0.12	2.03E6	0.8790	6.6	0.016	2.82E-4
6	0.3212	0.02	0.05	9.12E3	0.3599	-0.08	0.14	5.28E5	0.3887	7.8	0.096	3.23E-4
9	0.2031	0.13	0.03	9.74E2	0.1270	0.01	0.12	1.29E5	0.2198	7.8	0.120	1.13E-3
12	0.0818	0.13	0.04	9.14E2	0.1410	0.09	0.08	1.16E5	0.1106	7.8	0.136	2.09E-3
15	0.1507	0.15	0.04	5.11E2	0.1678	0.08	0.10	5.50E4	0.1341	7.8	0.152	2.80E-3
18	0.0714	0.16	0.05	3.02E2	0.0746	0.08	0.12	2.41E4	0.0815	6.2	0.152	3.13E-2
21	0.1577	0.16	0.05	2.57E2	0.1471	0.06	0.14	1.59E4	0.1045	5.2	0.144	1.11E-1
24	0.1745	0.20	0.04	1.71E2	0.1420	0.13	0.10	1.89E4	0.1121	3.4	0.136	1.09E 0
27	0.0692	0.03	0.17	1.56E2	0.0767	-0.09	0.34	1.47E3	0.2060	3.0	0.112	1.35E 0
30	0.2278	-0.10	0.32	6.59E1	0.3217	-0.08	0.54	1.47E2	0.1034	3.0	0.144	1.59E 0
33	0.0924	-0.04	0.20	1.61E2	0.1261	-0.10	0.34	1.36E3	0.1393	4.6	0.168	2.41E-1
36	0.2459	-0.09	0.26	1.09E2	0.3353	-0.10	0.46	3.08E2	0.1134	3.4	0.144	9.76E-1
39	0.2911	0.20	0.04	1.45E2	0.3192	0.11	0.12	1.12E4	0.1134	2.6	0.096	2.07E 0
42	0.0384	-0.09	0.21	2.15E2	0.0757	-0.10	0.36	9.94E2	0.1727	2.8	0.088	1.38E 0
45	0.1791	-0.10	0.29	9.04E1	0.2557	-0.10	0.50	2.30E2	0.0838	3.2	0.152	1.35E 0

By using these normalized scattered light intensities as $I_k^{Obs.}(\lambda)$ in Eq. (4.13), we determined the best values of the parameters of each test function by the method mentioned in Ⅳ.2. The minimum values of function E at each test function at time after the beginning of the laser-irradiation are shown with the values of parameters in Table 4.2. Next, we determine approximate size distribution functions by selecting the best test functions having the minimum value of function E at each moment T after the beginning of the laser-irradiation. Since the absolute values of scattered light intensities were not measured, we could not get the informations on the absolute size distribution, i.e. the absolute number density as a function of particle radius a.

Figure 4.7 shows the obtained temporal changes of the relative size distribution for the time T from 3 sec to 27 sec. As described already, the size distribution for the radius less than 0.1 μm is ambiguous because of the wavelengths of the light detected, and so we have not shown it in Fig. 4.7. For time T longer than about 20 sec, the oscillation in production of particles took place as seen in Fig. 4.5, but the reproducibility of the phase of oscillation was rather poor. So the error is considered to be relatively large for T> 20 sec. This is mainly due to the variation of the temperature of the cell ~1°C and that of laser power ~3 % during the experiment. As seen in Fig. 4.7, the size distribution for small T has a sharp peak at the small radius. With the increasing time T, the size distribution

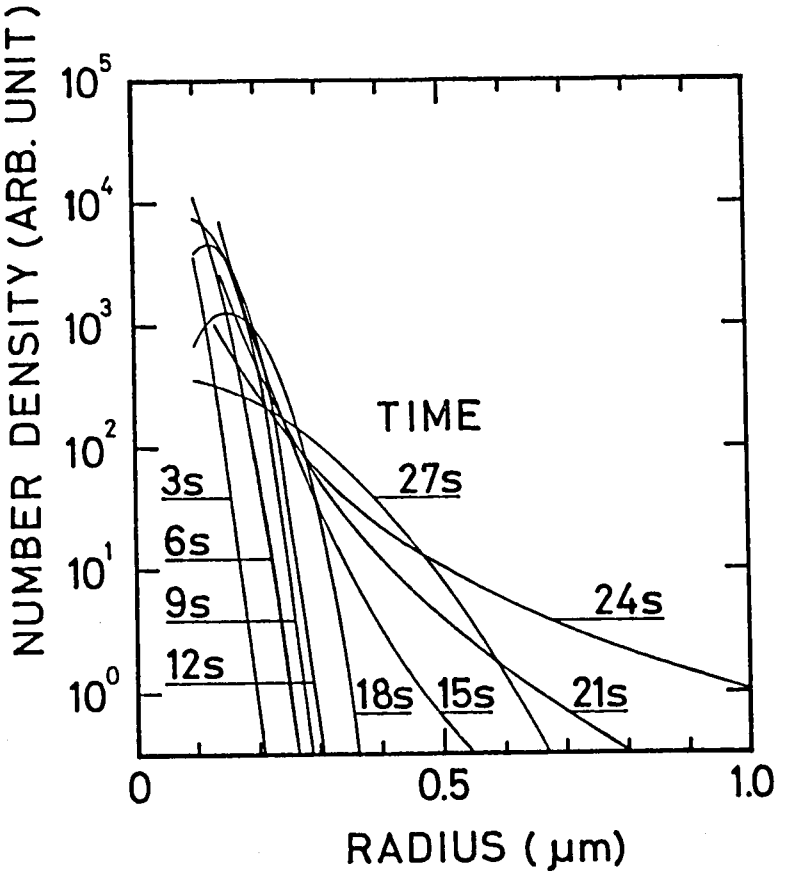

Fig. 4.7 Temporal changes of the size distribution, for the time T from 3 sec to 27 sec, obtained in the experiment J6 (the Ar^+ laser: 50 mW and 5 mm i.d.; the white light: 5 mm i.d.; the cell temperature: 330°C).

spreads toward the larger radius accompanied with decrease of the peak value. For T <12 sec, the best-fit test functions are those having peaks, namely the Gauss and Stevenson distribution functions. When time T exceeds about 20 sec, it turns mostly to the Junge distribution function. Although the determinations of parameters are considered to have relatively large error for T > 25 sec, for which we have not shown the result in Fig. 4.7, the best-fit functions were mainly the Junge distribution functions.

We calculated the number density N (arb. unit), the total radius a_t (arb. unit), the total volume V_t (arb. unit), the mean radius $\bar{a}$ (μm), and the mean volume $\bar{V}$ (μm^3), defined as

$$N = \int \Psi(a)\, da, \tag{4.14}$$

$$a_t = \int a\Psi(a)\, da, \tag{4.15}$$

$$V_t = \int a^3 \Psi(a)\, da, \tag{4.16}$$

$$\bar{a} = \frac{1}{N} \int a\Psi(a)\, da, \tag{4.17}$$

$$\bar{V} = \frac{4\pi}{3N} \int a^3 \Psi(a)\, da. \tag{4.18}$$

In the practical calculations, the integrations with respect to the radius a in Eqs. (4.14) - (4.18) were carried out from 0.1 μm to 1 μm. The obtained values of N, a_t, V_t, $\bar{a}$, and $\bar{V}$ as functions of T are shown in Fig. 4.8 (a). From Fig. 4.8 (a), we see that the number density N

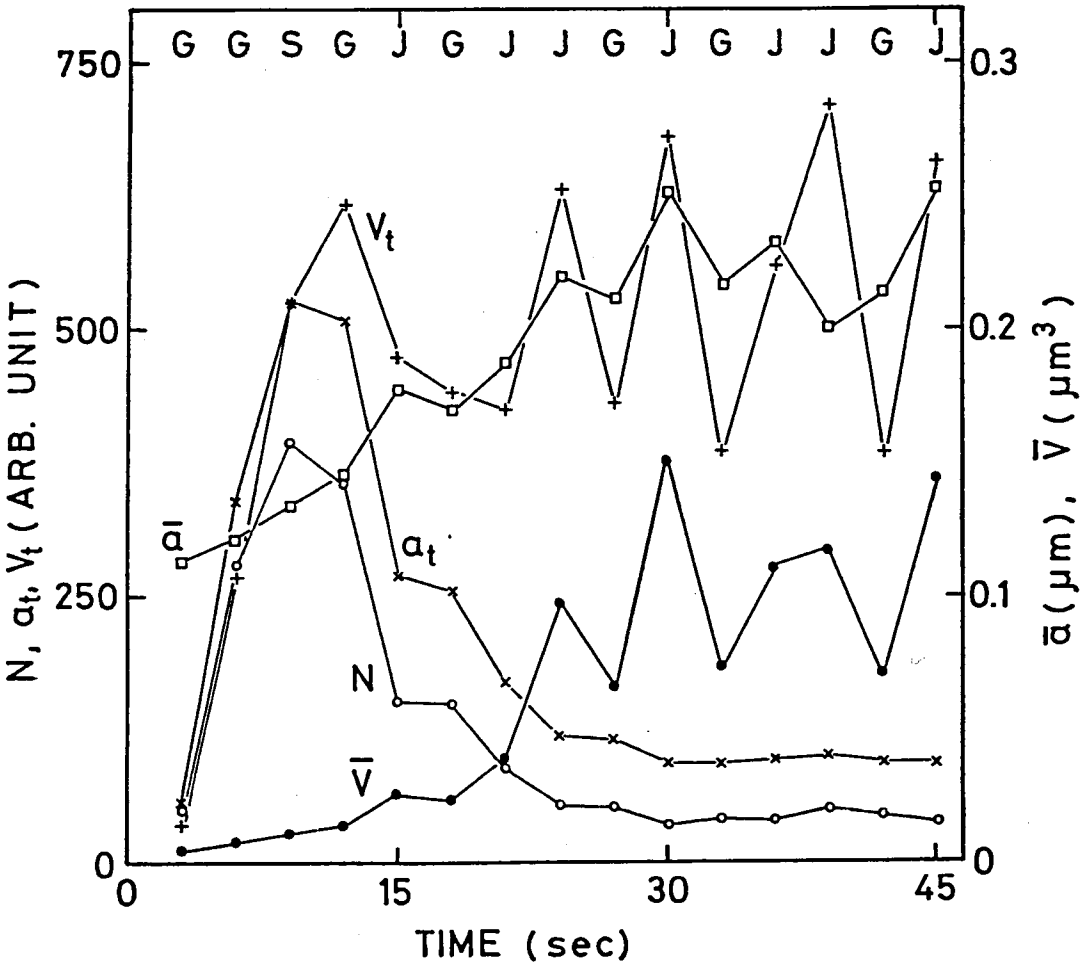

Fig. 4.8 (a) The temporal changes of the number density N (arb. unit), the total radius a_t (arb. unit), the total volume V_t (arb. unit), the mean radius $\bar{a}$ (μm), and the mean volume $\bar{V}$ (μm^3), obtained in the experiment J6 (the Ar^+ laser: 50 mW and 5 mm i.d.; the white light: 5 mm i.d.; the cell temperature: 330°C). The symbols G, S, and J indicate the best fit-test functions: G-Gauss, S-Stevenson, and J-Junge distribution functions.

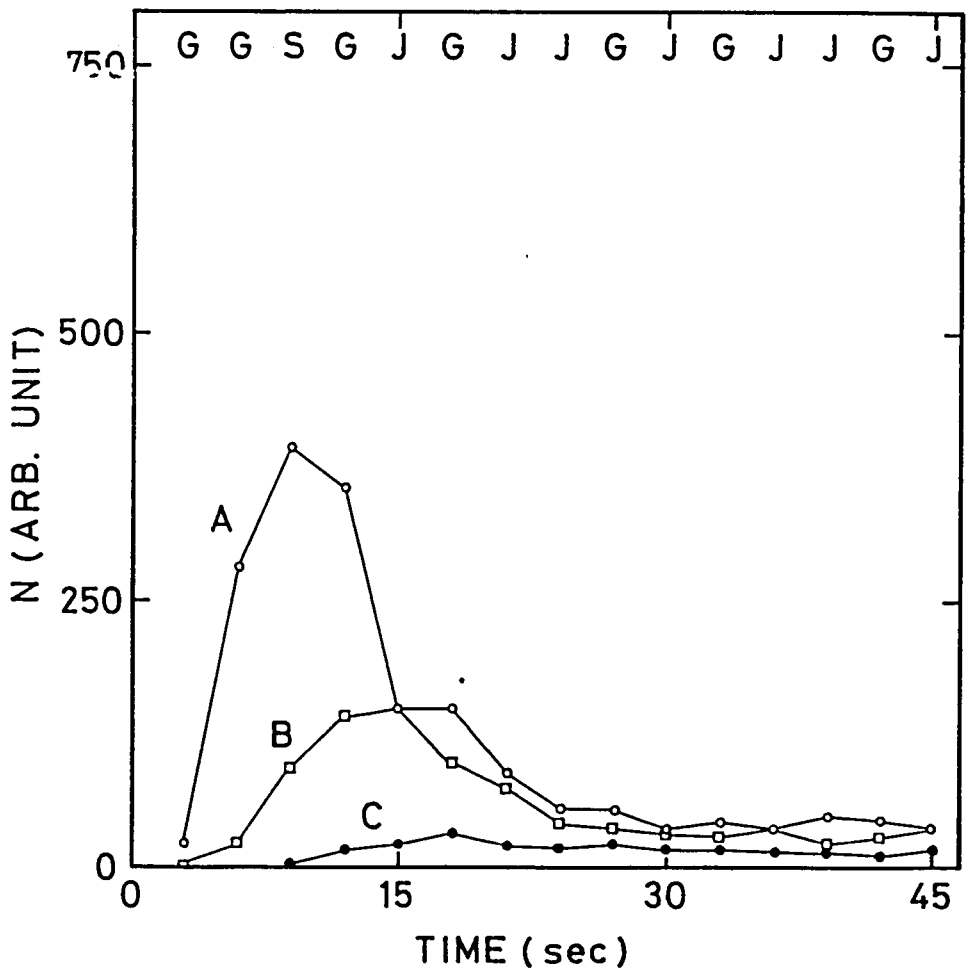

Fig. 4.8 (b) The number densities in the size range of 0.1 μm to 1 μm (A), 0.15 μm to 1 μm (B), and 0.2 μm to 1 μm (C) for the experiment J6 (the Ar^+ laser: 50 mW and 5 mm i.d.; the white light: 5 mm i.d.; the cell temperature: 330°C).

and the total radius a_t increase with T until T ≃ 9 sec and then they decrease, and that the total volume V_t increases with T until T ≃ 12 sec and decreases until 21 sec and then oscillates. On the other hand, the mean radius $\bar{a}$ and volume $\bar{V}$ increase with T until T ≃ 15 sec and then begin to oscillate. Generally the particle growth can be considered to be due to either or both of following two processes; the condensation by adsorbing molecules on the surface of particles, and the coalescence by sticking of particles. The values N and a_t decrease and V_t is constant when particles grow only by coalescence. The values N, a_t, and V_t increase when particles grow only by condensation. Therefore except for disappearing of particles from the observation region by falling through gravity and dissociation of particles, etc., V_t does not decrease at any time. The mean values $\bar{a}$ and $\bar{V}$ decrease only when the large particles disappear from the observation region or when the small particles are newly produced in the observation region.

When we apply the above mentioned consideration to Fig. 4.8 (a), we can see that the particles grow mainly by condensation within 9 sec but the particles grow mainly by coalescence of small particles after 9 sec to about 24 sec and that the effect of falling of particles through gravity begins to appear after 12 sec. This is also seen in Fig. 4.8 (b), where the number densities in the size range of 0.1 μm to 1 μm (A), 0.15 μm to 1 μm (B), and 0.2 μm to 1 μm (C) are shown. From the difference between A and B in Fig. 4.8 (b), we can see the change of small particle density in the size range of 0.1 μm to

0.15 μm radius and from the difference between B and C, we can see the change of the particle density in the size range of 0.15 μm to 0.2 μm. The characters G, S, and J, which are shown in the upper part of Fig. 4.8, indicate the best-fit functions among the Gauss, Stevenson, and Junge distribution functions.

The obtained scattered light intensities at the experiments J1, J2, J3, and J4 are shown in Figs. 4.9 - 4.12. These figures show the scattered light intensities $I_{//}(\lambda)$ and $I_{\perp}(\lambda)$ as functions of time T. The peaks of the scattered light intensities at five different wavelengths appear at about the same time in Figs. 4.9 - 4.12. This effect is considered to be resulted from the falling away of produced particles from the observed region almost the same time, because the Ar^+ laser beam is placed within the white light beam. On the other hand, as described already, the appearance of the peaks of the scattered light intensities is delayed for the longer wavelengths in the experiment J6 (See Fig. 4.5). This is considered to be resulted from the particle growth. Since the Ar^+ laser beam is larger than the white light beam in diameter in this case, the effect of the falling away of particles from the observed region is somewhat lessened by the falling into of particles from above, and hence the effect of particle growth becomes to appear more clearly in the experiment J6. This is also seen at the experiment J5 (Fig. 4.13) and J7 (Fig. 4.14).

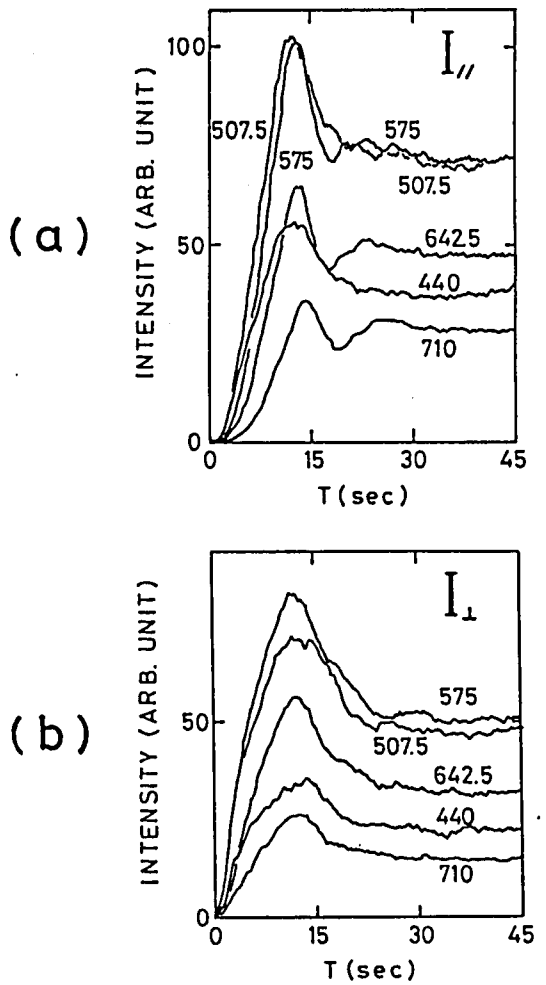

Fig. 4.9 (a) Recorder traces showing the changes of the scattered light intensities $I_{//}$ at five wavelengths, obtained in the experiment J1 (the Ar^+ laser: 50 mW and 2 mm i.d.; the white light: 10 mm i.d.; the cell temperature: 330°C). (b) The same as in (a), but for $I_{\perp}$.

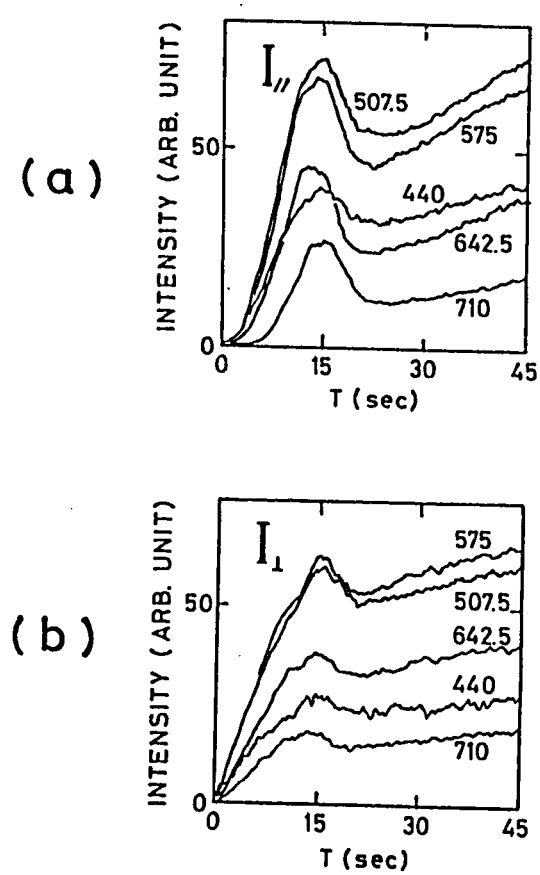

Fig. 4.10 (a) Recorder traces showing the changes of the scattered light intensities $I_{//}$ at five wavelengths, obtained in the experiment J2 (the Ar^+ laser: 50 mW and 0.2 mm i.d.; the white light: 10 mm i.d.; the cell temperature: 330°C). (b) The same as in (a), but for $I_{\perp}$.

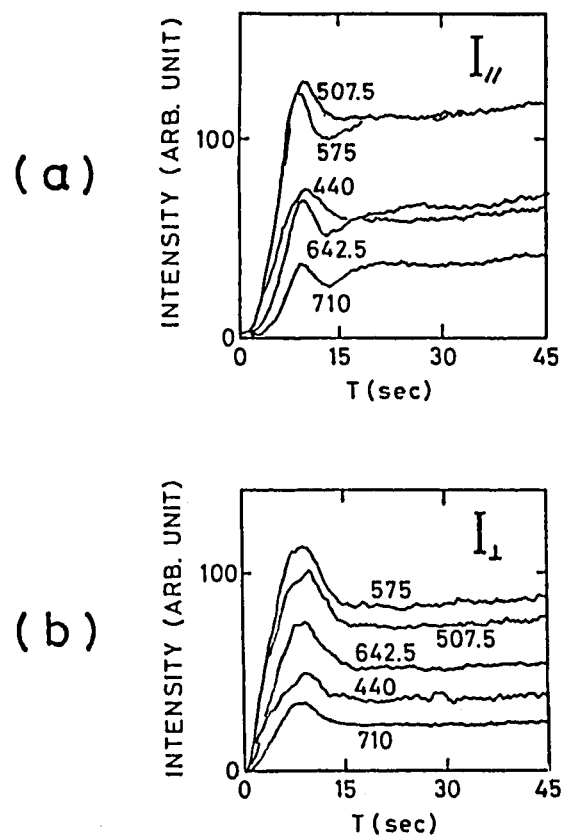

Fig. 4.11 (a) Recorder traces showing the changes of the scattered light intensities $I_{//}$ at five wavelengths, obtained in the experiment J3 (the Ar^+ laser: 100 mW and 2 mm i.d.; the white light: 10 mm i.d.; the cell temperature: 330°C). (b) The same as in (a), but for $I_{\perp}$.

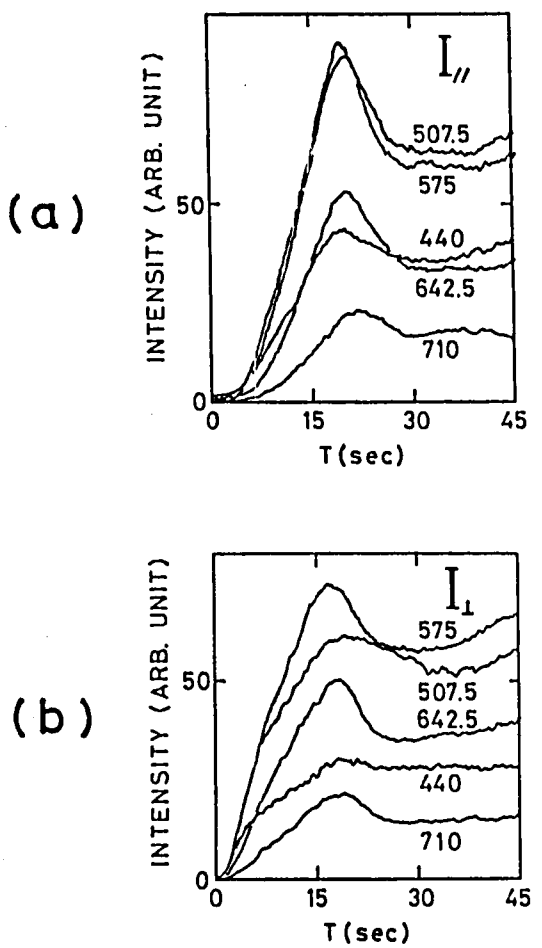

Fig. 4.12 (a) Recorder traces showing the changes of the scattered light intensities $I_{//}$ at five wavelengths, obtained in the experiment J4 (the Ar^+ laser: 50 mW and 2 mm i.d.; the white light: 10 mm i.d.; the cell temperature: 300 °C). (b) The same as in (a), but for $I_{\perp}$.

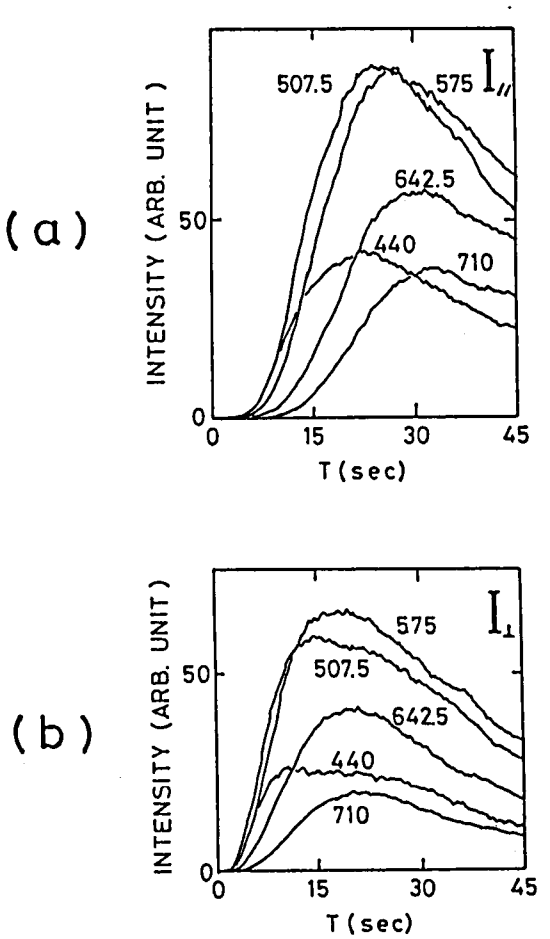

Fig. 4.13 (a) Recorder traces showing the changes of the scattered light intensities $I_{//}$ at five wavelengths, obtained in the experiment J5 (the Ar^+ laser: 50 mW and 15 mm i.d.; the white light: 5 mm i.d.; the cell temperature: 330 °C). (b) The same as in (a), but for $I_{\perp}$.

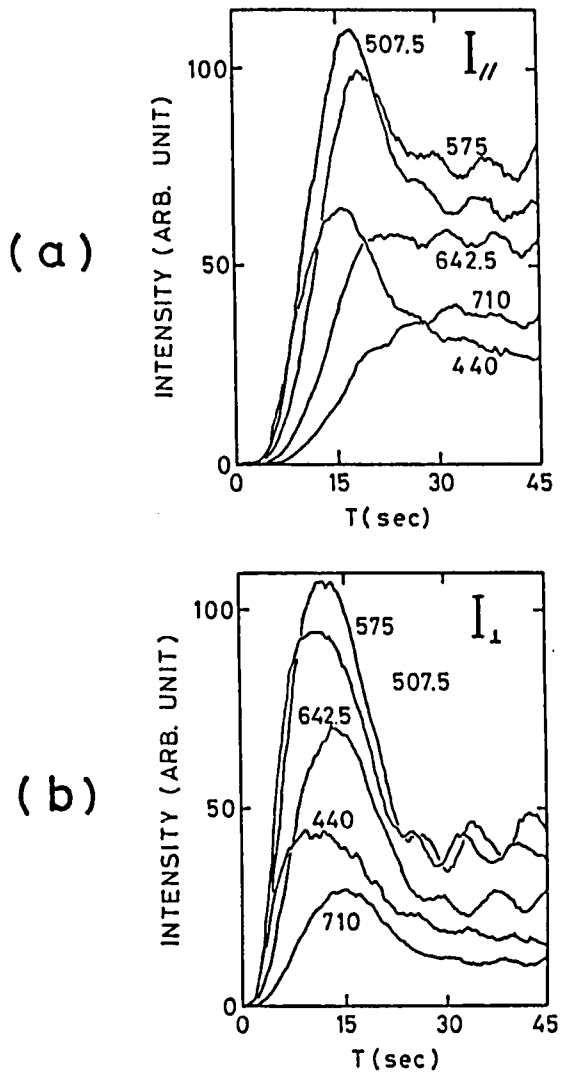

Fig. 4.14 (a) Recorder traces showing the changes of the scattered light intensities $I_{//}$ at five wavelengths, obtained in the experiment J7 (the Ar^+ laser: 100 mW and 15 mm i.d.; the white light: 5 mm i.d.; the cell temperature: 330°C). (b) The same as in (a), but for $I_{\perp}$.

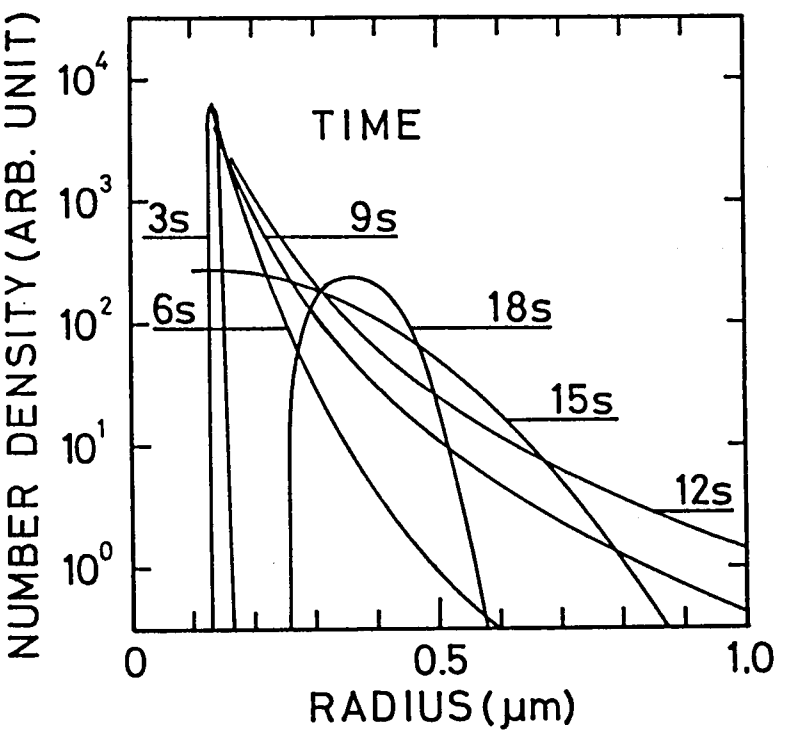

Fig. 4.15 Temporal changes of the size distribution, for the time T from 3 sec to 18 sec, obtained in the experiment J1 (the Ar^+ laser: 50 mW and 2 mm i.d.; the white light: 10 mm i.d.; the cell temperature: 330°C).

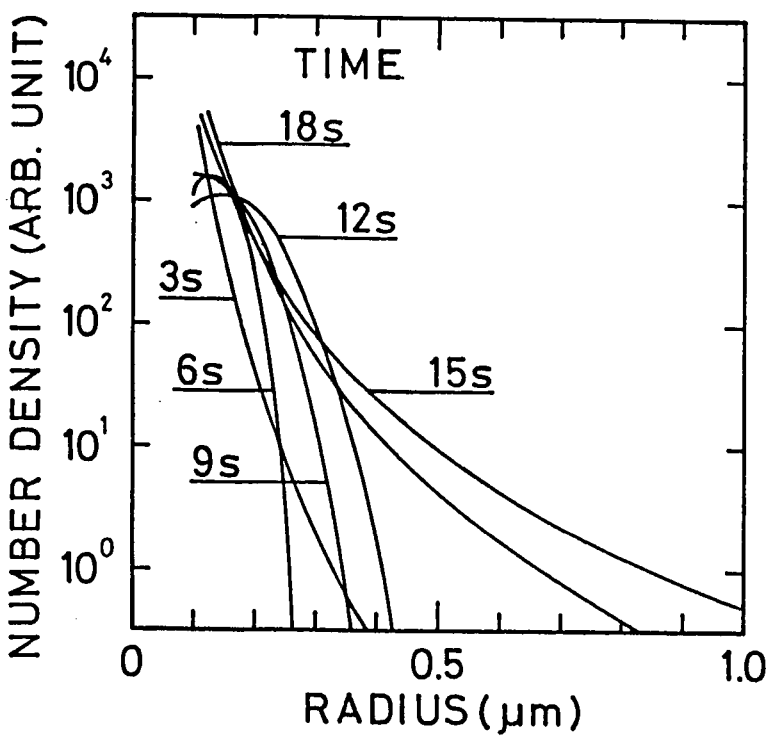

Fig. 4.16 Temporal changes of the size distribution, for the time T from 3 sec to 18 sec, obtained in the experiment J2 (the Ar^+ laser: 50 mW and 0.2 mm i.d.; the white light: 10 mm i.d.; the cell temperature: 330°C).

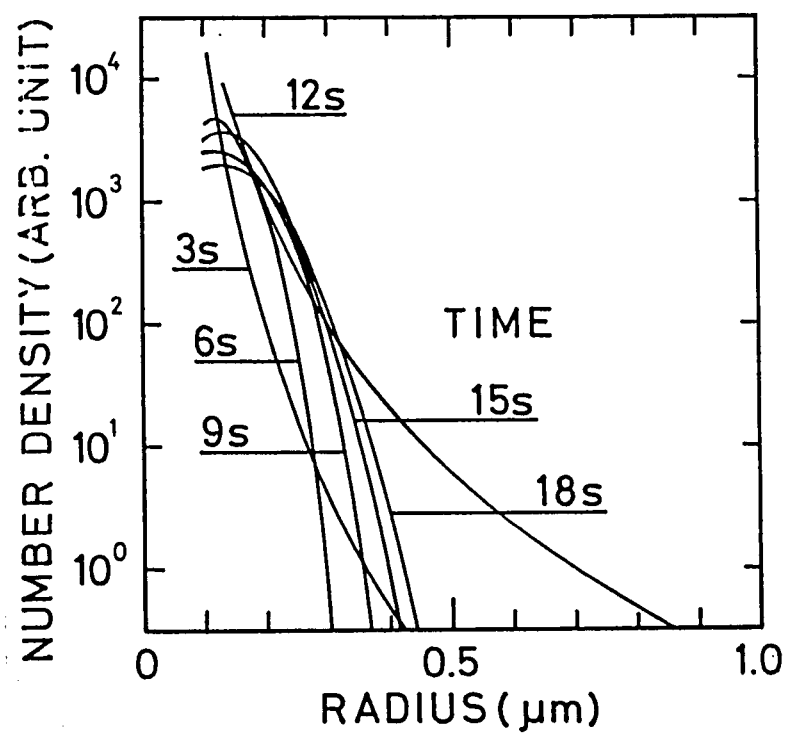

Fig. 4.17 Temporal changes of the size distribution, for the time T from 3 sec to 18 sec, obtained in the experiment J3 (the Ar^+ laser: 100 mW and 2 mm i.d.; the white light: 10 mm i.d.; the cell temperature: 330°C).

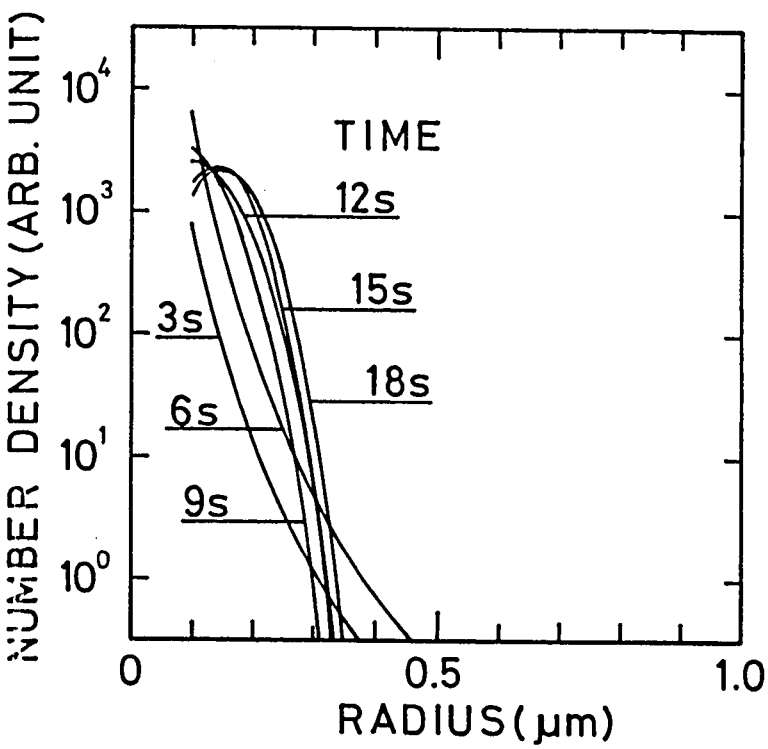

Fig. 4.18 Temporal changes of the size distribution, for the time T from 3 sec to 18 sec, obtained in the experiment J4 (the Ar^+ laser: 50 mW and 2 mm i.d.; the white light: 10 mm i.d.; the cell temperature: 300 ℃).

By using the normalized scattered light intensities obtained in a series of experiments of J1 - J4 as $I_k^{Obs.}(\lambda)$ in Eq. (4.13), we determined also the best-fit functions and its parameters. Thus approximated size distribution functions, namely number density (arb. unit) vs. radius (μm), at time after the beginning of the laser-irradiation are shown in Figs. 4.15 - 4.18.

We can also discuss the growth mechanisms from the calculated values of N, a_t, V_t, $\bar{a}$, and $\bar{V}$, which are shown in Figs. 4.19 - 4.22 (a) for J1 - J4, respectively. Figures 4.19 - 4.22 (b) show the number densities in the size range of 0.1 μm to 1 μm (A), 0.15 μm to 1 μm (B), and 0.2 μm to 1 μm (C) for J1 - J4, respectively. From these figures, we can see that only the small particles are produced within 3 sec and that these small particles grow mainly by condensation in this early stage. But both the growth rate and mechanisms are different in each experiment after 3 sec as described below.

From the result of J1 shown in Fig. 4.19, we can see the facts as follows:

1) Within 9 sec, particles grow by both the condensation and coalescence, because all quantities in Fig. 4.19 (a) increase with T, and both small and large particle densities increase.

2) From 9 sec to 12 sec, it is considered that particles grow mainly by coalescence, because only the value N and small particle density decrease.

3) After 12 sec, the values of N, a_t, and V_t, and particle densities

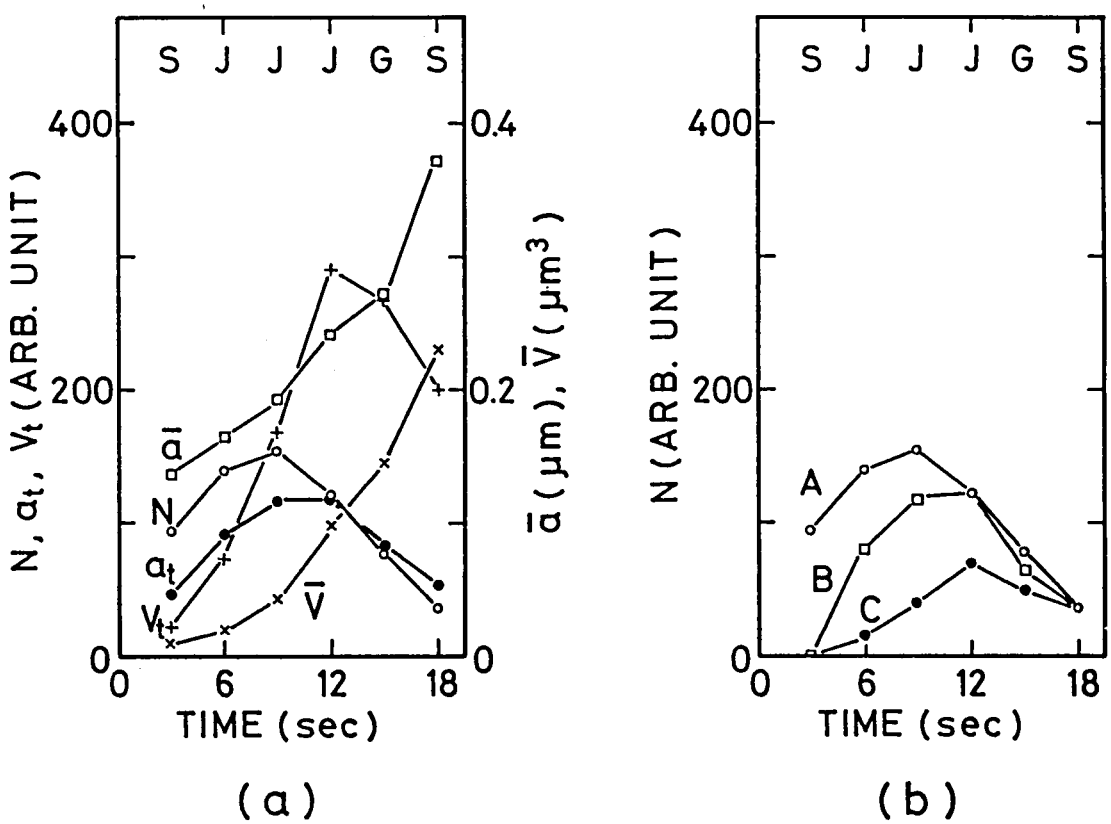

Fig. 4.19 (a) The temporal changes of the number density N (arb. unit), the total radius a_t (arb. unit), the total volume V_t (arb. unit), the mean radius $\bar{a}$ (μm), and the mean volume $\bar{V}$ (μm^3), obtained in the experiment J1 (the Ar^+ laser: 50 mW and 2 mm i.d.; the white light: 10 mm i.d.; the cell temperature: 330°C). The symbols G, S, and J indicate the best fit-test functions: G-Gauss, S-Stevenson, and J-Junge distribution functions. (b) The number densities in the size range of 0.1 μm to 1 μm (A), 0.15 μm to 1 μm (B), and 0.2 μm to 1 μm (C) for the experiment J1.

in all particle sizes decrease, probably because of the falling away of particles.

From the result of J2 shown in Fig. 4.20, we can see the facts as follows:

1) Because the values of N, a_t, and V_t increase and small particle density increase faster than larger one within 9 sec, particles grow mainly by condensation.

2) Because the laser power density is larger than that in J1, small particles are usually produced and so $\bar{a}$ and $\bar{V}$ are smaller than in J1.

From the result of J3 shown in Fig. 4.21, we can see the facts as follows:

1) Within 9 sec, because both the laser power and its density are larger than those in J1, particles are produced more quickly than in the case of J1, so that there exist more small particles. This makes $\bar{a}$ and $\bar{V}$ smaller than those in J1 but, of course, makes N, a_t, and V_t larger.

2) After 9 sec, because of the falling away of particles, the values of N, a_t, and V_t, and particle densities in all particle sizes decrease.

Form the result of J4 shown in Fig. 4.22, we can see the facts as follows:

1) Because the temperature of this experiment is 30°C lower than the other experiments, the particle production is slower than that in the other cases.

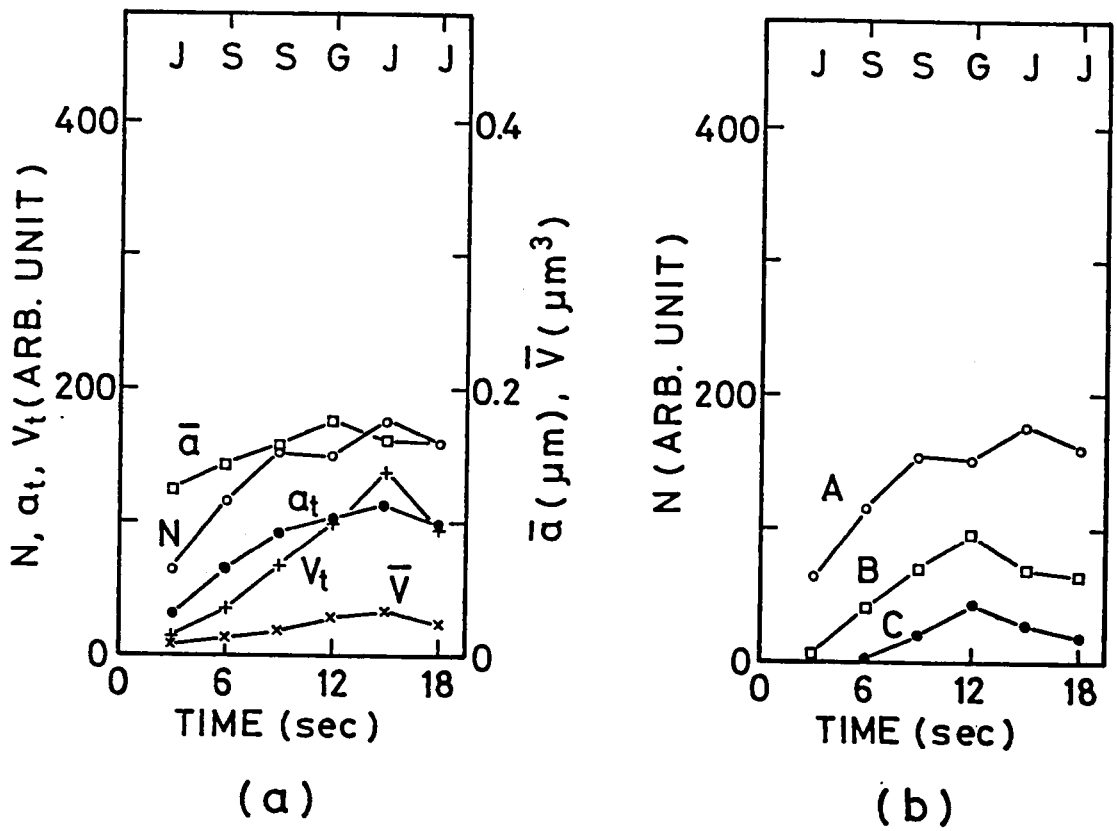

Fig. 4.20 The same as in Fig. 4.19, but for the experiment J2 (the Ar^+ laser: 50 mW and 0.2 mm i.d.; the white light: 10 mm i.d.; the cell temperature: 330°C).

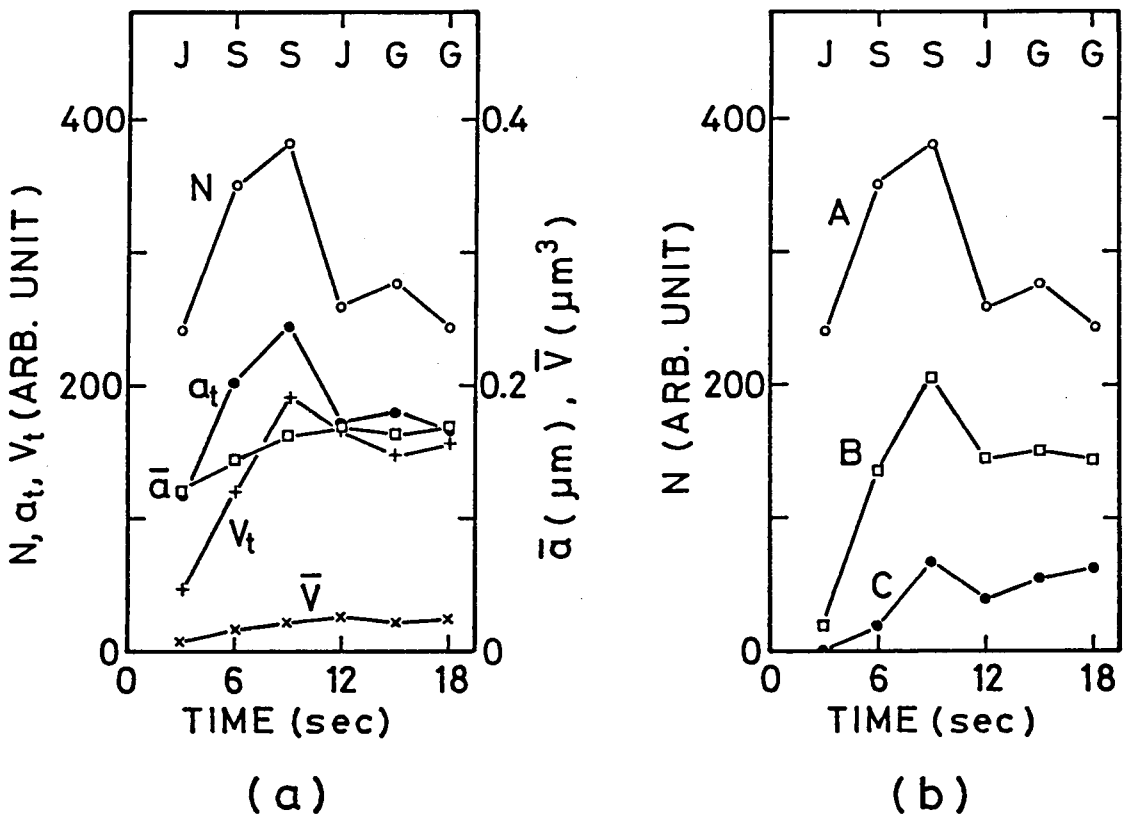

Fig. 4.21 The same as in Fig. 4.19, but for the experiment J3 (the Ar^+ laser: 100 mW and 2 mm i.d.; the white light: 10 mm i.d.; the cell temperature: 330°C).

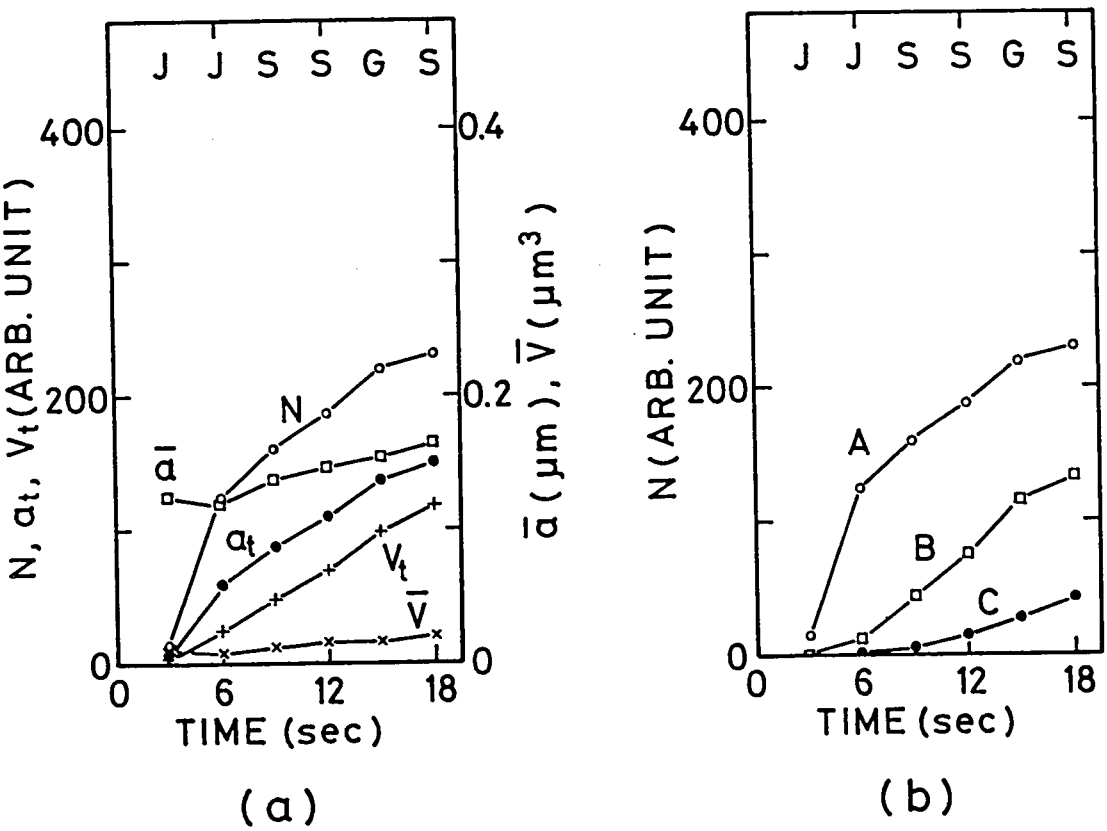

Fig. 4.22 The same as in Fig. 4.19, but for the experiment J4 (the Ar^+ laser: 50 mW and 2 mm i.d.; the white light: 10 mm i.d.; the cell temperature: 300°C).

2) Once the particles are produced, quantities N, a_t, and V_t increase monotonously. This indicates that particles are growing mainly by condensation and that particles are also produced successively.

3) The slight decrease of $\bar{a}$ and $\bar{V}$ from 3 sec to 6 sec are presumably resulted from the remained particles of the previous experiment. This is because the decomposition rate of particles is slower at 300 °C than at 330 °C and then, on repeating a series of experiments of observing wavelength- and polarization-dependences, we can not remove the produced particles in the previous experiment completely. But, at 3 sec, the produced and remained particles are not so many that only the weak scattered light can be detected. When the detected light itself is weak, our analysis is much influenced by experimental errors such as a reading error, a temperature deviation, and a laser power deviation. This error may cause the decreases of $\bar{a}$ and $\bar{V}$ from 3 sec to 6 sec.

Ⅳ. 4 Summary and Conclusions

In this chapter, we have described the first measurement of the size distribution of laser-produced CsH particles. The measurement is based on the wavelength- and polarization-dependences of light scattering by the produced particles. The results show that, just after the beginning of the production of CsH molecules by laser-irradiation, the size distribution is very narrow and has a maximum at the small particle radius, and the shape of distribution is well

expressed by the Gauss or Stevenson distribution function. As the time elapses, the size distribution spreads toward the larger radius with the decrease of peak value, and the shape of the distribution turns to the Junge distribution function $A_J a^{-p}$ with the value of p ranging between 2 and 4. It must be interesting to note that this steady-state size distribution is close to the size distribution of aerosol particles in the stratosphere. This is particularly seen in the experiment J6, in which the diameter of the Ar^+ laser beam is larger than that of the white light beam. But, in the experiments J1 - J4, in which the diameter of the Ar^+ laser beam is smaller than that of the white light beam, we cannot observe well the steady-state size distribution in particle growth because of the falling away of particles from the laser beam.

From the obtained temporal changes of the size distribution, we have calculated changes of the number density N, the total radius a_t, the total volume V_t, the mean radius $\bar{a}$, and the mean volume $\bar{V}$ of the produced particles with the radius between 0.1 μm and 1 μm.

In the experiment J6, we have found that particles grow mainly by coalescence of small particles after 9 sec because $\bar{a}$ and $\bar{V}$ are growing while N is decreasing. This seems to be contradictory to the experimental result of Tam *et al.*[1], which shows that the laser-produced CsH particles have large positive charges ($\lesssim 10^4$ electron charges). Since there exists strong repulsive force between charged particles,

we do not believe that these particles coalesce with each other. We think that this contradictory is due to the fact that the cell temperature is different between the present experiment and the experiment of Tam *et al.*,[1] although it is not explicitly noted in their paper. At relatively low temperature, typically lower than 280°C, the produced particles fall down through gravity without evaporation, and we can see the white powder lying on the bottom of the cell through a microscope. We found that the particles have a crystalline shape. The CsH crystal is known to have a large emissivity of photoelectrons, which may give a large amount of positive charges of produced particles within the laser beam. On the other hand, at the relatively high temperature, as in the present experiment, the produced particles are expected to evaporate by emitting mainly hydrogen atoms or molecules, and a small amount of cesium atoms. In fact at the temperature ~330°C, we could not see the white powder on the surface of the cell even at the long time after the beginning of the laser-irradiation. Unfortunately, we do not have the informations about the small particles produced quickly soon after the laser-irradiation. But, even though the small particles produced in the initial stage are crystals and have large amount of charges, they must turn into Cs droplet by evaporation at high temperature. Charge neutralization may be possible by emitting Cs ions simultaneously with the emission of neutral atoms or molecules Such Cs droplets are expected to grow by coalescence as seen in the present experiment.

We found also that particle production and growth are fast when the laser power is large but the mean radius $\bar{a}$ and the mean volume $\bar{V}$ are not always larger than the lower power experiment case. This is considered to depend whether or not the density of CsH molecules in the laser beam keeps its supersaturation ratio which is needed for nucleation of small particles. If the density of CsH molecules is lower than the critical density for nucleation, it becomes impossible to produce new particles. In the case of the experiment J3 (Ar^+ laser power $\simeq$ 100 mW), the density of CsH molecules is higher than the critical density, and so the nucleation is maintained. On the contrary, in the case of the experiment J1 (Ar^+ laser power $\simeq$ 50 mW), the density of CsH molecules is lower than the critical density, and so the condensation of molecules on the particles and the coalescence of small particles occur, and then particles grow bigger and bigger.

In our experiment at temperature 330°C, because the CsH particles decompose quickly into Cs and H_2 , the laser snow is expected to be neutralized by releasing Cs^+, and this makes the further growth of particles by coalescence possible. In fact, experimental results show the particle growth by coalescence at this temperature. On the other hand, we have known already that the particle growth by condensation was main process at J4, which was the experiment at 300° C. This is explained that because less neutralization by releasing Cs^+ is expected at 300°C, the coalescence must be difficult

under the strong electrostatic repulsive force between ionized particles.

Until the present work, there were no reports in the precise measurements of temporal changes of size distributions even for the production of many other particles, although they are known to be important to reveal the mechanisms of particle growth. In the present work, we could measure the temporal changes of the size distribution of laser-produced CsH particles with a relatively high accuracy, using the light scattering method. The error in the present case is mainly comes from the experimental procedure that the changes of the light scattering is measured by repeating the production of particles, under the assumption of high reproducibility. So, it is desirable to obtain the informations without repeating the experiment. It must be noted that the simultaneous measurements of the light scattering at two wavelengths and at two orthogonal polarizations are enough to determine the best-fit test function and its three unknown parameters.

We have used in the present work three simple test functions, each having three parameters. But, there are, of course, many other test functions to be considered. The modified gamma function[19,20,123-126] ($\Psi_g(a) = A\, a^p \exp(-B\, a^q)$, where A, B, p, and q are positive constants) may be particularly important because it is known to approximate the size distribution of many natural particles, especially the cloud particles in the atmosphere.[19,20]

CHAPTER V

CONCLUDING REMARKS

The invention of lasers, especially tunable lasers, have brought new possibilities of controlling chemical reactions and obtaining much knowledge about chemical reactions. The laser-production of particles is an example of laser use in chemistry. The chemical reactions and productions of particles by laser light have many advantages compared with those by ordinary light from a lamp. Important advantages are such that, i) light intensity is high, so that the rate of chemical reaction is very large and can easily be controlled, ii) state-selective and isotope-selective chemical reactions can be induced because of the sharp spectrum of laser radiation. The advantage i) may lead to the production of high densities of molecules and particles that cannot easily be produced by ordinary photochemical reactions induced by ordinary light. Because of the advantages ii), we can use laser light in precise studies of elementary processes of photochemical reactions, and in practical applications such as isotope separation.

In this thesis, we have reported on the laser-production of alkali hydride particles, giving particular attentions to (1) the fundamental processes of photochemical reactions to produce alkali hydride molecules,

(2) the first production of NaH particles, (3) the first measurement of size distribution of laser-produced particles and its temporal changes.

With respect to the chemical reactions of the alkali atoms in the excited states with hydrogen molecules to produce alkali hydride molecules, two possible processes were proposed by Tam *et al.*[1] and Sayer *et al.*[10] as described in chapter III. One is the direct reaction of the alkali atoms in the excited states with hydrogen molecules to produce alkali hydrides, and the other is the indirect reaction where energies of the excited state alkali atoms are transferred to the vibrational energies of hydrogen molecules by collisions, and the hydrogen molecules in the vibronic excited states react with the ground state alkali atoms. From the experimental results in the present work, we consider that both processes take place simultaneously more or less in the case of CsH, but we could not clearly determine which process is predominant. In the sodium vapor with hydrogen gas, we have found that NaH molecules are produced when sodium atoms are excited to the 3P states and also when sodium molecules are excited to the $B^1\Pi_u$ state. As described in III.4, the 3P states have not, however, energies enough to produce directly NaH molecules. So, we have proposed possible processes to produce NaH molecules; (a) collisions between two 3P state atoms excite one of those atoms to highly excited states, which react with H_2 molecules, and (b) the energies of the 3P state Na atoms are used to excite H_2 molecules to the high vibrational states, which react with

the 3P state Na atoms and produce NaH molecules. As to the production of NaH by the excitation of Na_2 molecules, we have proposed the process that Na_2 molecules in the excited state $B^1\Pi_u$ react directly with H_2 molecules in the ground electronic state.

With respect to (2), we could observe first the production of NaH particles by exciting Na atoms to the 3P states and by exciting Na_2 molecules to the $B^1\Pi_u$ state as described above. We found also that the produced NaH molecules and particles dissociate by the collisions with Na atoms in the 3P states. It must be noted that such dissociation do take place only in the case of sodium, since the first excited states of other alkali atoms have not energy to dissociate alkali hydride molecules. Among the production of alkali hydride particles, we are particularly interested in that of NaH particles, since relatively large amount of sodium and hydrogen are known to exist in the upper atmosphere of the earth and in the planetary atmosphere (for instance, Jupiter and its satellite Io), under the relatively strong solar radiation suitable to excite Na atoms.

As to (3), we could succeed the first measurement of the size distribution of the laser-produced CsH particles and its temporal changes after the beginning of the production of CsH molecules. Even for the production of other particles, there had no reports on such a precise measurement of temporal change of size distribution. By calculating the changes of number density, total radius, total volume, mean radius, and mean volume of the produced particles from the size

distributions obtained, we could get the informations of the growth of particles. In the relatively high temperature ($T = 330°C$), we found that the particles grow up by coalescence, i.e. by sticking of produced particles to each other. In the relatively low temperature ($T \lesssim 300°C$), we considered that the particle growth is mainly by condensation, because the number density of particles increase monotonously, and because the particles falling down from the laser beam and lying on the bottom of the cell were white crystalline particles.

It must be interesting to note a phenomenon observed when the laser intensity is changed. In the case of low laser intensity, once particles are produced, the number density of CsH molecules decreases and it becomes low not enough to produce new particles. As the result, the produced particles grow by collecting CsH molecules and by coalescence. But, in the case of very high laser intensity, even when the particles are produced, the CsH density is still higher than the critical value and new particles are successively produced. This results in the observed phenomenon that the total radius and total volume are increased with the increase of the laser intensity but the mean radius and mean volume are not always so.

In the present work, the temporal changes of size distribution have been measured by observing the scattered light intensities at five wavelengths and for two orthogonal polarizations, as repeating ten times the same procedures. So, the error of the measurement of the size distribution has been determined mainly by the reproducibility of production of

particles. When we use test functions with three unknown parameters to represent the shape of the size distribution, it is enough to determine the parameters by measuring the light scattering at two wavelengths and for two orthogonal polarizations. Such measurements can be done simultaneously without repeating the production of particles, so that more accurate informations about temporal changes in size distribution may be obtained.

In the present work, we have used three simple test functions to represent the shape of size distribution. But, there are many other test functions to be considered. One of the most important test functions might be the modified gamma function, which is known to approximate well the size distribution of cloud particles,[19,20] and we are now introducing it in our calculation.

REFERENCES

1) A. Tam, G. Moe, and W. Happer, Phys. Rev. Lett. 35, 1630 (1975).

2) T. Yabuzaki, S. Curry, J. Camparo, and W. Happer, Proc. Rep. Dept. Phys., Columbia Univ. (1978) No. 18 (unpublished).

3) A. C. Tam, W. Happer, D. Siano, Chem. Phys. Lett. 49, 320 (1977).

4) J. L. Picqué, J. Vergès, and R. Vetter, J. Physique. Lett. 41, L-305 (1980).

5) R. Omnès, J. Physique Lett. 41, L-63 (1980).

6) T. Yabuzaki, T. Sato, and T. Ogawa, J. Chem. Phys. 73, 2780 (1980).

7) K. Iwamoto, N. Presser, and J. Ross, J. Chem. Phys. 68, 663 (1978).

8) B. Cordier, P. Papon, and J. Leblond, J. Chem. Phys. 74, 3353 (1981).

9) A. M. Ronn and B. L. Earl, Chem. Phys. Lett. 45, 556 (1977).

10) B. Sayer, N. Ferray, J. Lozingot, and J. Berlande, J. Chem. Phys. 75, 3894 (1981).

11) J. Tyndall, Phil. Mag. 37, 384 (1869).

12) F. C. Wen, T. McLaughlin, and J. L. Katz, Science 200, 769 (1978).

13) A. W. Gertler, J. O. Berg, and M. A. El-Sayed, Chem. Phys. Lett. 57, 343 (1978).

14) M. Luria, R. G. de Pena, K. J. Olszyna, and J. Heicklen, J. Phys. Chem. 78, 325 (1974).

15) R. B. Husar and K. T. Whitby, Environ. Sci. Technol. 7, 241 (1973).

16) P. H. McMurry and S. K. Friedlander, J. Colloid Inteface Sci. 64, 248 (1978).

17) T. H. Maiman, Nature 197, 493 (1960).

18) H. Shimizu, T. Kobayashi, and H. Inaba, Oyo Buturi 47, 30 (1978).

19) D. Deimendjian, *The International Symposium on Radiation of the Radiation Commission*, IAMAP, Vienna, 1961, p. 171.

20) D. Deirmendjian, Appl. Opt. 3, 187 (1964).

21) C. E. Junge, C. W. Chagnon, and J. E. Manson, J. Meteor. 18, 81 (1961).

22) T. Takahashi, J. Atmos. Sci. 38, 347 (1981).

23) T. Takahashi, J. Atmos. Sci. 35, 1549 (1978).

24) S. Kinoshita, J. Meteorol. Res. (Tokyo) 4, 235 (1952).

25) N. Chodes, J. Warner, and A. Gagin, J. Atmos. Sci. 31, 1351 (1974).

26) A. M. Sinnarwalla, D. J. Alofs, and J. C. Carstens, J. Atmos. Sci. 32, 592 (1975).

27) R. Ferrara, G. Fiocco, and G. Tonna, Appl. Opt. 9, 2517 (1970).

28) E. X. Berry and R. L. Reinhardt, J. Atmos. Sci. 31, 1825 (1974).

29) E. X. Berry and R. L. Reinhardt, J. Atmos. Sci. 31, 1814 (1974).

30) E. H. C. Chin and M. Neiburger, J. Atmos. Sci. 29, 718 (1972).

31) D. T. Gillespie, J. Atmos. Sci. 32, 600 (1975).

32) V. S. Letokhov, Science 180, 451 (1973).

33) J. T. Knudtson and E. M. Eyring, Ann. Rev. Phys. Chem. 25, 255 (1974).

34) F. P. Schäfer, *Dye Lasers*, (Springer, Berlin, 1973) p. 66.

35) T. Endo, T. Yabuzaki, M. Kitano, T. Sato, and T. Ogawa, IEEE J. Quantum Electron. QE-13, 866 (1977).

36) T. Endo, T. Yabuzaki, M. Kitano, T. Sato, and T. Ogawa, IEEE J. Quantum. Electron. QE-14, 977 (1978).

37) T. Manabe, T. Yabuzaki, and T. Ogawa, Phys. Rev. Lett. 46, 637 (1981).

38) T. Kobayashi and T, Sueta, Oyo Buturi 50, 951 (1981).

39) S. Kobayashi, J. Yamada, S. Machida, and T. Kimura, Electron. Lett. 16, 746 (1980).

40) Y. Suematsu, Oyo Buturi, 51, 411 (1982).

41) T. Yabuzaki, A. Ibaragi, H. Hori, M. Kitano, and T. Ogawa, Jpn. J. Appl. Phys. 20, L451 (1981).

42) R. B. Heslop and K. Jones, *Inorganic Chemistry A Guide to Advanced Study*, (Elsevier, Amsterdam, 1976) Chap. 10.

43) T. Odiorne, P. Brooks, and J. V. V. Kasper, J. Chem. Phys. 55, 1980 (1971).

44) T. Mochizuki, Kagaku Sosetsu No. 26, 131 (1980).

45) U. Brinkmann, W. Hartig, H. Telle, H. Walther, Appl. Phys. Lett. 5, 109 (1974).

46) R. V. Ambartzumian, N. P. Furzikov, V. S. Letokhov, and A. A. Puretskii, Appl. Phys. 9, 335 (1976).

47) G. S. James, I. Itzkan, C. T. Pike, R. H. Levy, and L. Levin, IEEE J. Quantum Electron. QE-12, 111 (1976).

48) M. Yamashita, M. Kasamatsu, H. Kashiwagi, and K. Machida, Opt. Commun. 26, 343 (1978).

49) V. S. Letokhov and R. V. Ambartzumian, IEEE J. Quantum Electron. QE-7, 305 (1971).

50) P. Fettweis and M. N. de Mévergnies, J. Appl. Phys. 49, 5699 (1978).

51) S. W. Mayer, M. A. Kwok, R. W. F. Gross, and D. J. Spencer, Appl. Phys. Lett. 17, 516 (1970).

52) T. F. Deutsch, D. J. Ehrlich, and R. M. Osgood, Jr., Appl. Phys. Lett. 35, 175 (1979).

53) D. J. Ehrlich, R. M. Osgood, Jr., and T. F. Deutsch, Appl. Phys. Lett. 36, 698 (1980).

54) D. J. Ehrlich, R. M. Osgood, Jr., and T. F. Deutsch, Appl. Phys. Lett. 38, 1018 (1981).

55) D. J. Ehrlich, R. M. Osgood, Jr., and T. F. Deutsch, Appl. Phys. Lett. 36, 916 (1980).

56) D. J. Ehrlich, R. M. Osgood, Jr., and T. F. Deutsch, Appl. Phys. Lett. 38, 399 (1981).

57) T. F. Deutsch, D. J. Ehrlich, D. D. Rathman, D. J. Silversmith, and R. M. Osgood, Jr., Appl. Phys. Lett. 39, 825 (1981).

58) T. F. Deutsch, J. C. C. Fan, G. W. Turner, R. L. Chapman, D. J. Ehrlich, and R. M. Osgood, Jr., Appl. Phys. Lett. 38, 144 (1981).

59) D. J. Spencer, H. Mirels, T. A. Jacobs, and R. W. E. Gross, Appl. Phys. Lett. 16, 235 (1970).

60) R. A. Brown and F. H. Chaffee, Jr., Astrophys. J. 187, L125 (1974).

61) M. B. McElroy, Y. L. Yung, and R. A. Brown, Astrophys. J. 187, L127 (1974).

62) L. Trafton, T. Parkinson, and W. Macy, Jr., Astrophys. J. 190, L85 (1974).

63) T. D. Parkinson, J. Atmos. Sci. 32, 630 (1975).

64) T. P. Whaley, *Comprehensive Inorganic Chemistry*, Volume 1. Chap. 8, *Sodium, Potassium, Rubidium, Cesium, and Fransium*, ed. J. C. Bailar, H. J. Emeleus, Sir R. Nyholm, and A. F. Trotman-Dickenson (Permagon Press, Oxford, 1973).

65) A. N. Nesmeyanov, *Vapor Pressures of the Elements* (Academic, New York, 1963).

66) F. C. M. Coolen, L. C. J. Baghuis, H. L. Hagedoorn, and J. A. van der Heide, J. Opt. Soc. Am. 64, 482 (1974).

67) D. T. Hurd, *An Introduction to the Chemistry of the Hydrides* (Wiley, New York, 1956) Chap. 2 - Chap. 4.

68) T. B. Reed, *Free Energy of Formation of Binary Compound* (MIT Press, Cambridge, Massachusetts, 1971).

69) G. Herzberg, *Atomic Spectra and Atomic Structure* (Dover, New York, 1944) Chap. 6.

70) G. Herzberg, *Molecular Spectra and Molecular Structure*, Volume I. *Spectra of Diatomic Molecules* (Van Nostrand Reinhold, New York, 1950) 2nd ed., p. 501.

71) M. Giroud and O. Nedelec, J. Chem. Phys. 73, 4151 (1980).

72) W. Stwalley, S. C. Yang, Y. K. Hsieh, F. B. Orth, and K. C. Li, J. Chem. Phys. 69, 1791 (1978).

73) M. Allegrini, G. Alzetta, A. Kopystynska, and L. Moi, Opt. Commun. 19, 96 (1976).

74) A. C. Tam, T. Yabuzaki, S. M. Curry, M. Hou and W. Happer, Phys. Rev. A 17, 1862 (1978).

75) A. C. Tam and W. Happer, Opt. Commun. 21, 403 (1977).

76) E. K. Kopeikina and M. L. Yanson, Opt. Spectrosc. 41, 217 (1976).

77) W. Demtröder, M. McClintock, and R. N. Zare, J. Chem. Phys. 51, 5495 (1969).

78) E. Zouboulis, N. D. Bhaskar, A. Vasilakis, and Happer, J. Chem. Phys. 72, 2356 (1980).

79) O. S. Heavens, J. Opt. Soc. Am. 51, 1058 (1961).

80) G. Baumgartner, W. Demtröder, and M. Stock, Z. Physik 232, 462 (1970).

81) P. J. Dagdigian, J. Chem. Phys. 64, 2609 (1976).

82) S. C. Yang and Y. K. Hsieh, A. C. Tam, W. T. Zemke, K. K. Verma, and W. C. Stwalley, J. Chem. Phys. 75, 3679 (1981).

83) R. H. Chatham, A. Gallagher, and E. L. Lewis, J. Phys. B 13, L7 (1980).

84) T. Hori, Z. Physik, 71, 478 (1931).

85) R. E. Olson and B. Liu, J. Chem. Phys. 73, 2817 (1980).

86) A. M. Karo, M. A. Gardner, and J. R. Hiskes, J. Chem. Phys. 68, 1942 (1978).

87) E. S. Sachs, J. Hinze, and N. H. Sabelli, J. Chem. Phys. 62, 3367 (1975).

88) R. C. Pankhurst, Proc. Phys. Soc. (London) 62A, 191 (1949).

89) A. C. Tam and W. Happer, J. Chem. Phys. 64, 2456 (1976).

90) G. M. Almy and M. Rassweiler, Phys. Rev. 53, 890 (1938).

91) B. Laskowski and J. R. Stallcop, J. Chem. Phys. 74, 4883 (1981).

92) A. G. Gaydon and R. W. B. Pearse, Proc. R. Soc. London 173, 28 (1939).

93) A. G. Gaydon and R. W. B. Pearse, Proc. R. Soc. London 173, 37 (1939).

94) T. Hori, Z. Physik 62, 352 (1930).

95) A. G. Gaydon, *Dissociation Energy and Spectra of Diatomic Molecules* (Chapman and Hall, London, 1968) 3rd ed.

96) D. Jennings, W. Braun, and H. P. Broida, J. Chem. Phys. 59, 4305 (1973).

97) T. Yabuzaki, A. C. Tam, M. Hou, W. Happer, and S. M. Curry, Opt. Commun. 24, 305 (1978).

98) M. McClintock and L. C. Balling, J. Quant. Spectrosc. Radiant. Transfer. 9, 1209 (1969).

99) S. G. Leslie, J. T. Verdeyen, and W. S. Millar, J. Appl. Phys. 48, 4444 (1977).

100) D. A. McGillis and L. Krause, Phys. Rev. 153, 44 (1967).

101) I. N. Siara, R. U. Dubois, and L. Krause, Can. J. Phys. 60, 239 (1982).

102) G. Karl and J. C. Polanyi, J. Chem. Phys. 38, 271 (1963).

103) E. Bauer, E. R. Fisher, and F. R. Gilmore, J. Chem. Phys. 51, 4173 (1969).

104) M. Allegrini, G. Alzetta, A. Kopystynska, L. Moi, and G. Orriols, Opt. Commun. 22, 329 (1977).

105) A. Kopystynska and P. Kowalczyk, Opt. Commun. 25, 351 (1978).

106) D. J. Krebs and L. D. Schearer, J. Chem. Phys. 75, 3340 (1981).

107) V. S. Kushawaha and J. J. Leventhal, Phys. Rev. A 22, 2468 (1980).

108) S. Geltman, J. Phys. B 10, 3057 (1977).

109) W. Demtröder and M. Stock, J. Mol. Spectrosc. 55, 476 (1975).

110) W. Demtröder, W. Stetzenbach, M. Stock, and J. Witt, J. Mol. Spectrosc. 61, 382 (1976).

111) P. Kusch and M. M. Hessel, J. Chem. Phys. 68, 2591 (1978).

112) This value is claculated from the dissociation energy D_e(NaH) in Ref. 71 through the equation (III,94) of Ref. 70 (p. 100).

113) A. Netten, *International Conference on Phenomena in Ionized Gases* 11, 46 (1973).

114) E. de Bary and F. Rössler, J. Geophys. Res. 71, 1011 (1966).

115) J. P. Friend, Tellus 18, 465 (1966).

116) C. Hayashi and Y. Nakagawa, Prog. Theor. Phys. 54, 93 (1975).

117) R. C. Srivastava, J. Atmos. Sci. 28, 410 (1971).

118) J. Heintzenberg, H. Müller, H. Quenzel, and E. Thomalla, Appl. Opt. 20, 1308 (1981).

119) G. Mie, Ann. d. Phys. 25, 377 (1908).

120) M. Born and E. Wolf, *Principles of Optics* (Pergamon, Oxford, 1980) sixth ed., Chap. XIII, p. 611.

121) A. F. Stevenson, W. Heller, and M. L. Wallach, J. Chem. Phys. 34, 1789 (1961).

122) T. Sato, T. Yabuzaki, and T. Ogawa, to be published in Jpn. J. Appl. Phys. 21, No. 11 (1982).

123) E. K. Bigg, J. Atmos. Sci. 33, 1080 (1976).

124) Y. Mizutani, Y. Uga, and T. Nishimoto, Nihon Kikaigakkai Ronbunshu 37, 1746 (1971).

125) K. Chiba, Nihon Kikaigakkai Ronbunshu 40, 2236 (1974).

126) S. Nukiyama and Y. Tanasawa, Nihon Kikaigakkai Ronbunshu 5, 63 (1939).

127) M. Lapp and L. P. Harris, J. Quant. Spectrosc. Radiant. Transfer. 6, 169 (1966).